

Nucleon-nucleon correlations, short-lived excitations, and the quarks within

Or Hen

Massachusetts Institute of Technology, Cambridge, Massachusetts 02139, USA

Gerald A. Miller

Department of Physics, University of Washington, Seattle, Washington 98195, USA

Eli Piassetzky

School of Physics and Astronomy, Tel Aviv University, Tel Aviv 69978, Israel

Lawrence B. Weinstein

Department of Physics, Old Dominion University, Norfolk, Virginia 23529, USA

(published 13 November 2017)

This article reviews our current understanding of how the internal quark structure of a nucleon bound in nuclei differs from that of a free nucleon. The interpretation of measurements of the European Muon Collaboration (EMC) effect for valence quarks, a reduction in the deep inelastic scattering cross-section ratios for nuclei relative to deuterium, and its possible connection to nucleon-nucleon short-range correlations (SRCs) in nuclei are focused on. This review and new analysis (involving the amplitudes of non-nucleonic configurations in the nucleus) of the available experimental and theoretical evidence shows that there is a phenomenological relation between the EMC effect and the effects of SRCs that is not an accident. The influence of strongly correlated neutron-proton pairs involving highly virtual nucleons is responsible for both effects. These correlated pairs are temporary high-density fluctuations in the nucleus in which the internal structure of the nucleons is briefly modified. This conclusion needs to be solidified by the future experiments and improved theoretical analyses that are discussed herein.

DOI: [10.1103/RevModPhys.89.045002](https://doi.org/10.1103/RevModPhys.89.045002)

CONTENTS

I. Introduction: Short-range Correlations (SRCs) and Nuclear Dynamics	2	1. Mean field	23
A. The challenge of describing nuclei	3	2. Suppression of pointlike configurations	24
B. The need for short-range correlations: Beyond the nuclear shell model	4	3. Six-quark bags and the EMC effect	25
1. Spectroscopic factors	4	IV. The EMC-SRC Correlation	26
2. From the NN interaction to the shell model and beyond	6	A. Experimental overview	26
3. Short-ranged two-nucleon clusters	7	B. Theory overview	27
II. Hard Scattering and Short-range Correlations	9	1. High-momentum nucleons and PLC suppression	27
A. Hard reactions	9	2. Effective field theory	29
B. Exclusive scattering	10	3. The isovector EMC effect	30
C. Inclusive scattering	13	4. Summary	30
D. Universal properties of short-range correlations in nuclei	16	C. Are the nucleons in the correlated pair really nucleons?	30
III. Deep Inelastic Scattering and the EMC Effect	17	D. Determining the structure function of a free neutron	30
A. DIS and nucleon structure functions	17	1. The deuteron in-medium correction effect	30
B. The EMC effect	19	2. The free neutron structure function	31
C. Why conventional nuclear physics cannot explain the EMC effect	20	3. The d/u ratio at large x_B	32
1. Nucleons only	20	V. Existing Searches for Medium-modified Electromagnetic Form Factors	32
2. Nucleons plus pions	21	A. Polarization transfer in the $(\vec{e}, e' \vec{p})$ reaction	33
D. Beyond conventional nuclear physics: Nucleon modification	22	B. Polarization transfer in the $(\vec{e}, e' \vec{n})$ reaction	34
		C. The (e, e') reaction and the Coulomb sum rule (CSR)	34
		VI. Future Directions in Nuclear Deep Inelastic Scattering and Detecting Short-range Correlations	35
		A. Experiment	35
		1. Tagged structure function measurements	35
		2. Inclusive EMC and SRC measurements	36

3. Semi-inclusive and exclusive SRC measurements	37
4. Polarized EMC measurements	38
5. Parity violating deep inelastic scattering	38
B. Theory	39
VII. The Way We Think It Is and the Ways to Check	39
Acknowledgments	40
Appendix: Expanded Explanations	40
1. Understanding the np relative wave function	40
2. Basic terminology	41
3. Why center-of-mass and relative coordinates factorize	42
References	43

I. INTRODUCTION: SHORT-RANGE CORRELATIONS (SRCs) AND NUCLEAR DYNAMICS

Nuclear physics is one of the oldest fields in modern physics. Its history (Wong, 1998), separate from atomic physics, can be said to start with the discovery of radioactivity in 1896 by Henri Becquerel. Fifteen years later Rutherford used backward scattering of alpha particles to discover that the nucleus is a small object at the heart of the atom. In 1932 Chadwick discovered a neutral particle of about the same mass as the proton that he called the neutron. This discovery allowed scientists to understand that the binding energy accounted for less than 1% of the nuclear mass. Thus it is natural to say that the nucleus is made of neutrons and protons. In 1935 Yukawa suggested a theory of the strong force to explain how the nucleus holds together. In the Yukawa interaction a virtual particle, later called a meson, mediated a force between nucleons. This force explained why nuclei did not fall apart due to proton repulsion, and it also explained why the attractive strong force had a shorter range than the electromagnetic proton repulsion. Thus we may think of the stable nucleus as a tight ball of neutrons and protons (collectively called nucleons), held together by the strong nuclear force.

This basic picture has been studied for many years. Early models treated heavy nuclei, which could contain hundreds of nucleons, as classical liquid drops. The liquid-drop model can reproduce many features of nuclei, including the general trend of binding energy with respect to mass number, as well as nuclear fission.

The liquid-drop idea cannot explain more detailed properties of nuclei. Quantum-mechanical effects [which can be described using the nuclear shell model initially developed by Mayer (1950) and Haxel, Jensen, and Suess (1949)] explained that nuclei with certain numbers of neutrons and protons (the magic numbers 2, 8, 20, 28, 50, 82, 126, ...) are particularly stable because their shells are filled. Many studies were devoted to understanding how the liquid-drop model, with its collective features, could be consistent with the shell model.

Detailed studies of nucleon-nucleon scattering indicated that their interaction contains something like a hard core, making the origin of the shell model even more mysterious than its coexistence with the liquid-drop model. Brueckner and others (Gomes, Walecka, and Weisskopf, 1958) showed that in the nuclear medium the large, short-ranged effects of the strong nucleon-nucleon potential could be summed and treated in terms of a smoother object, defined as a G matrix.

This idea allowed much of nuclear phenomena to be understood (at least qualitatively) in terms of the fundamental nucleon-nucleon interaction. The nucleus was made of nucleons, with the occasional evanescent meson existing as it propagated from nucleon to nucleon.

After the single-particle shell model, the natural next step in describing nuclei is including the effects of two-nucleon correlations. The strong short-ranged nucleon-nucleon force that is averaged to make the mean-field G matrix also causes a significant nucleon-nucleon correlation function (see the Appendix for definitions). However, definitive experimental evidence for correlations had to await two kinds of high-energy reactions (Frankfurt and Strikman, 1981). These are the inclusive (e, e') scattering at values of Bjorken $x_B > 1$ (Egiyan *et al.*, 2003, 2006; Fomin *et al.*, 2012) and exclusive reactions that could isolate the effects of ground-state correlations from the various two-body currents and final state interactions that occur in nuclear reactions (Tang *et al.*, 2003; Piasetzky *et al.*, 2006; Shneor *et al.*, 2007; Subedi *et al.*, 2008; Baghdasaryan *et al.*, 2010; Hen *et al.*, 2014; Korover *et al.*, 2014; Monaghan *et al.*, 2014; Makek *et al.*, 2016).

Meanwhile, deep inelastic scattering (DIS) on nucleons led to the discovery that the nucleons are made of quarks. However, due to the small ($\leq 1\%$) nuclear binding energy and the idea of quark-gluon confinement, it was thought that quarks had no explicit role in the nucleus and that therefore nuclei could still be described in terms of nucleons and mesons. The simple and compelling nucleon-meson picture of the nucleus was shaken to its core by the 1982 discovery by the European Muon Collaboration (EMC) (Aubert *et al.*, 1983) of the nontrivial dependence of the per nucleon lepton deep inelastic scattering cross section on the specific nuclear target. The EMC initially reported incorrect results for $x_B < 0.15$. As a result many refer to the EMC effect as the reduction of the cross section per nucleon in the region $0.2 < x_B < 0.7$. This reduction has been observed many times and we use the term “the EMC effect” to refer to this region. The observation of this reduction, caused by the nucleus, showed that the quarks have a small but definite role in the nucleus. We need to understand this.

There are a number of fundamental unanswered questions about nuclear physics.

- (1) Is the nucleus really made of nucleons and mesons only?
- (2) How does the nucleus emerge from QCD, a theory of quarks and gluons?
- (3) How does the partonic content of the nucleus differ from that of N free neutrons plus Z free protons?

No one asked such questions before the discovery of the EMC effect.

At first glance there appears to be little relation between nucleon-nucleon correlations and the EMC effect. However, there is a strong phenomenological connection between them (Weinstein *et al.*, 2011) that occurs for the valence quarks that carry large momentum and that connection is the subject of this review. Indeed, the fundamental challenge for current explanations of the EMC effect is to explain also the inclusive and exclusive high-momentum transfer reactions dominated by short-range correlations which take up about 20% of the wave function. The data suggest that the non-nucleonic

admixture in these correlations is at most about 10%, leading to a 2% non-nucleonic contribution. However, the EMC effect is about 15%, so that one needs to find an enhancement mechanism.

We now summarize our most important conclusions for the benefit of the interested reader:

- There is much indirect and direct evidence for the existence of nucleon-nucleon SRCs).
 - (i) High-energy ($e, e'pN$) and ($p, 2pN$) reactions show that two-nucleon correlations exist in nuclei, dominate the high-momentum ($k \geq k_F$) tail of the nuclear momentum distribution, and are dominated, at certain nucleon momenta, by np pairs.
 - (ii) High-energy (e, e') reactions at large values of x_B (the Bjorken scaling variable) show that all nuclei have similar momentum distributions at large momentum, consistent with the direct observation that strongly correlated two-nucleon clusters exist in the nuclear ground state.
 - (iii) A consequence of the np -SRC dominance is the possible inversion of the kinetic energy sharing in nuclei with $N > Z$ (i.e., that protons might have more kinetic energy than neutrons in neutron-rich nuclei).
 - (iv) This leads to a dynamic model of nuclei where SRC pairs are temporary large fluctuations in the local nuclear density.
- Conventional (nonquark) nuclear physics cannot account for the EMC effect.
- Models need to include nucleon modification to account for the EMC effect. These models can modify the structure of any of the following:
 - (i) Predominantly mean-field nucleons, which are modified by momentum-independent interactions,
 - (ii) predominantly nucleons belonging to SRC pairs, or
 - (iii) both mean-field and SRC nucleons.
- There is a phenomenological connection between the strength of the EMC effect and the probability that a nucleon belongs to a two-nucleon SRC pair [$a_2(A)$]. This connection has also been derived using two completely different theories, so that it is no accident.
- In contrast to previous static models of the EMC effect, the association with SRCs implies that nucleons are temporarily modified only when they briefly fluctuate into an SRC pair.
- The influence of SRC pairs can account for the EMC-SRC correlation because both effects are driven by high-virtuality nucleons ($p^2 \neq M^2$).
- High-virtuality nucleons have an enhanced but still small amplitude for non-nucleonic configurations. Interference effects between nucleonic and non-nucleonic components (linear in the amplitudes) are responsible for the EMC effect.
- Modified nucleons, by definition, must contain a small fraction of baryons that are not nucleons. Amplitudes for such baryons, with effects enhanced in a coherent

manner, exist in the short-range correlations and are the source of the EMC effect.

We aim to critically discuss the reasons for these conclusions and provide enough details for one to appreciate the progress that has been made in recent years. The remainder of this review describes the experimental and theoretical evidence for the existence of two-nucleon short-range correlations and the properties thereof; the theoretical and experimental facts regarding deep inelastic scattering, nucleon structure functions, and the EMC effect; and the need for nucleon modification to explain the EMC effect. We then present the unexpected correlation between the strength of the EMC effect in a given nucleus and the probability that a nucleon in that nucleus belongs to an SRC pair. The ensuing discussion presents theoretical ideas connecting SRC and EMC physics and explores the idea that the SRC-EMC correlation can be used to determine the structure function of a free neutron. The final sections are concerned with other evidence that the nuclear medium modifies the structure of bound nucleons and future directions for experimental and theoretical research. The Appendix presents formal definitions of the terms we use and also explains some equations used in the main text. Specific locations of the various subjects are listed in the Table of Contents.

A. The challenge of describing nuclei

Nucleons bound in nuclei move under the influence of the strong interaction as effected by short-ranged two- and three-body potentials. Solving even the nonrelativistic A -body Schrödinger equation was initially an impossibly daunting challenge, so that understanding the vast array of relevant experimental data required the use of models.

The nuclear shell model was one of the earliest and perhaps most powerful models. In this model, each nucleon moves independently in the average field produced by the other nucleons. This shell model provides a reasonable description of many nuclear properties and is the fundamental starting point for all efforts to provide a theory of nuclei. Its explanation of the nuclear magic numbers is a major accomplishment in the history of physics. Despite this, early research involving collective degrees of freedom established that the single-particle picture of nuclei could not be complete. More generally, corrections to the shell model can be classified broadly in terms of the relevant distances needed to describe the various phenomena. There are both long-ranged (similar to the size of the nucleus) and short-ranged (similar to the size of the nucleon) phenomena.

The strong nucleon-nucleon force is known to bind medium and heavy nuclei, all with about the same average central density of $\rho_A = 0.16$ nucleon/fm³. Thus, the average distance between nucleons is about $1/\rho_A^{1/3} = 1.8$ fm. The radius of a nucleon is about $r = 0.86$ fm, so that most (but not all) of the time it does not overlap in space with other nucleons. The nucleon has a volume of $V = (4/3)\pi r^3 = 2.5$ fm³ and a corresponding density of $\rho_N = 0.4$ fm⁻³. Thus $\rho_N/\rho_A = 2.5$ and the maximum nuclear density, even without nucleons overlapping, is 2.5 times the average nuclear density.

The fact that a nucleon has about 2.5 times larger density than the nuclear central density and that nucleons move in the nucleus with about a quarter of the velocity of light opens up the possibility of large local density fluctuations. These also lead to large local momentum fluctuations via the uncertainty principle. The strong short-range repulsive force between nucleons restrains the size of these fluctuations, but since its range is smaller than a Fermi, the density and momentum fluctuations in nuclei can still be quite large.

The diverse features described indicate that understanding the broad range of nuclear phenomena requires the use of many experimental tools. Since electromagnetic interactions are well understood and presumably simple, electron scattering has long been used as a tool to investigate different aspects of nuclear structure. We examine the use of electron scattering to probe the validity of the single-particle shell model in the next section.

B. The need for short-range correlations: Beyond the nuclear shell model

1. Spectroscopic factors

Data from electroinduced proton knockout reactions on nuclei $A(e, e'p)$ provided early evidence for the validity of the shell model (Frullani and Mougey, 1984). These studies complemented the use of low-energy nuclear reactions, such as (d, p) and (p, pp) . Later on, more detailed studies using higher-energy electron beams explored the limits of the validity of the shell model. We next explain how this happened.

In the $(e, e'p)$ reaction the electron knocks out a nucleon so that an initial nuclear state $|i\rangle$ of A nucleons is converted to a final nuclear state $|f\rangle$ of $A - 1$ nucleons. The reaction can be analyzed in terms of spectroscopic factors (Macfarlane and French, 1960), which are probabilities that all but one of the nucleons will find themselves in the final state. More formally, if one considers a single-particle state of quantum numbers α , the spectroscopic factor S_α is given by the square of the overlap $S_\alpha = |\langle f|b_\alpha|i\rangle|^2$, where b_α destroys a nucleon. If the independent particle model were exact, then S_α would be unity for each occupied state α . Thus measuring S_α is a useful way to study the nuclear wave functions and the limitations of the independent particle model.

In the plane wave impulse approximation (PWIA), an electron transfers a single virtual photon with momentum \mathbf{q} and energy ν (sometimes written ω) to a single proton, then leaves the nucleus without reinteracting and can thus be described by a plane wave (see Fig. 1).

In PWIA the cross section factorizes in the form (Kelly, 1996)

$$\frac{d\sigma}{d\nu d\Omega_e dE_{\text{miss}} d\Omega_p} = K \sigma_{ep} S(E_{\text{miss}}, \mathbf{p}_{\text{miss}}), \quad (1)$$

where $K = E_p p_p / (2\pi)^3$ is a kinematical factor, E_p and p_p are the energy and momentum of the outgoing proton, σ_{ep} is the electron cross section (De Forest, 1983) for scattering by a bound proton, and S is the spectral function, the probability of finding a nucleon in the nucleus with momentum \mathbf{p}_{miss} and separation energy E_{miss} . The missing momentum and missing energy are given by

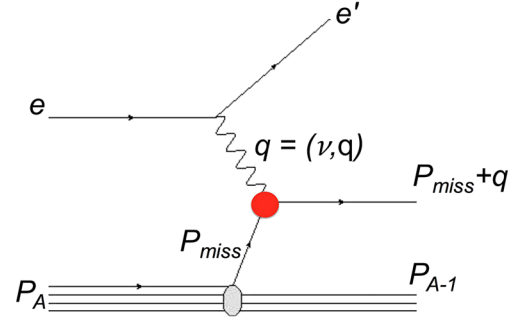


FIG. 1. The $A(e, e'p)$ reaction in the plane wave impulse approximation. A nucleus of four-momentum P_A emits a nucleon of four-momentum P_{miss} that absorbs a virtual photon of four-momentum q to make a nucleon of four-momentum $P_{\text{miss}} + q$, with $(P_{\text{miss}} + q)^2 = M^2$, where M is the nucleon mass. The blob represents the in-medium electromagnetic form factors.

$$\begin{aligned} \mathbf{p}_{\text{miss}} &= \mathbf{q} - \mathbf{p}_p, \\ E_{\text{miss}} &= \nu - T_p - T_{A-1}, \end{aligned} \quad (2)$$

where T_p and T_{A-1} are the kinetic energies of the detected proton and residual (undetected) $A - 1$ nucleus.

However, the knocked-out proton then interacts with other nucleons as it leaves the nucleus; these final state interaction (FSI) effects have been typically calculated either using an optical model at low momenta (Kelly, 1996) or using the eikonal or Glauber approximations at higher momenta (Ryckebusch *et al.*, 2003; Sargsian *et al.*, 2005). Calculations where the wave function of the knocked-out proton are distorted by FSI are referred to as distorted wave impulse approximation (DWIA) calculations. (Note that FSI effects mean that p_{miss} is no longer equal to the initial momentum of the struck nucleon.) In DWIA, the $(e, e'p)$ cross section does not exactly factorize as in the PWIA. However, factorization is a good approximation at $Q^2 \gg p_{\text{miss}}^2$ and the cross section is approximately proportional to a distorted spectral function S^D (Kelly, 1996). Neither PWIA nor DWIA calculations conserve current because the initial and final wave functions of the model calculations are not orthogonal and because the effective NN interactions used in the initial and final states are different. [Some models force current conservation by arbitrarily modifying kinematic variables such as q^μ (De Forest, 1983).] Relativistic DWIA models were developed by Van Orden and collaborators (Picklesimer, Van Orden, and Wallace, 1985; Picklesimer and Van Orden, 1989) and later elaborated by Udias *et al.* (1993, 1995, 1999), Kelly and Wallace (1994), and Kelly (1999).

Thus, $(e, e'p)$ measurements should be sensitive to the spectral function, i.e., to the momentum and energy distributions of nucleons in the nucleus. Figure 2 shows the $^{16}\text{O}(e, e'p)$ cross section at $Q^2 = 0.8 \text{ GeV}^2$ and $\nu = 0.439 \text{ GeV}$ plotted versus missing energy at several different missing momenta and plotted versus missing momentum for the two p -shell states. There are sharp peaks at $E_{\text{miss}} = 12$ and 18 MeV , corresponding to proton knockout from the $1p_{1/2}$ and $1p_{3/2}$ shells, a broad peak at $E_{\text{miss}} \approx 40 \text{ MeV}$ corresponding to proton knockout from the $1s$ shell (and other processes), and a long tail extending to large E_{miss} , especially at the largest missing momenta. The momentum

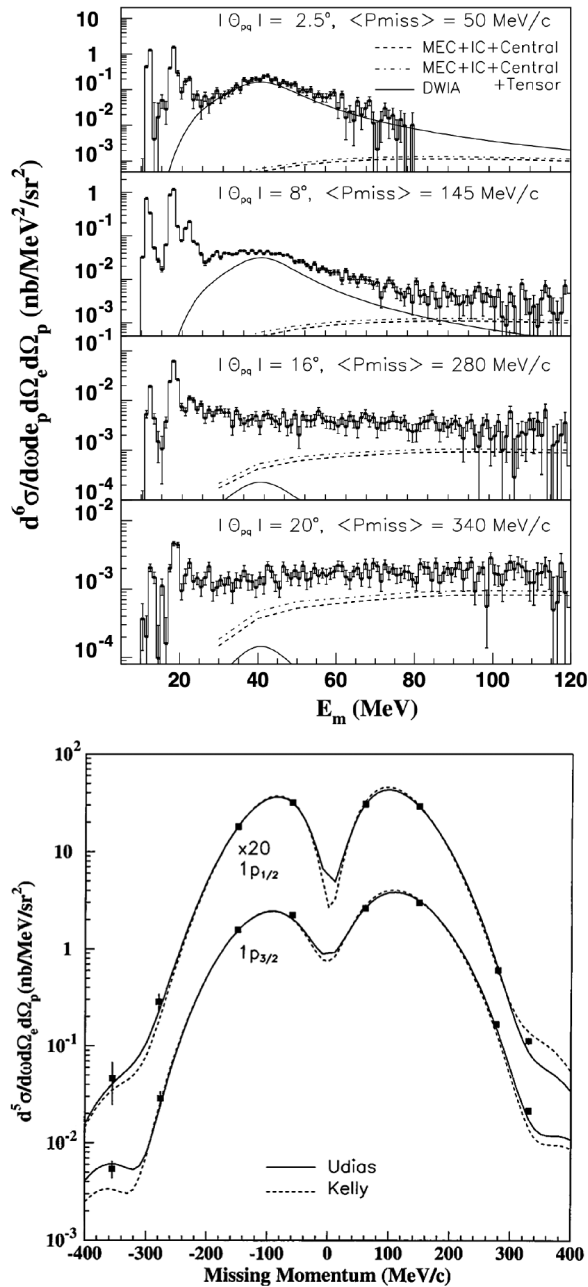


FIG. 2. (Upper) The $O(e, e'p)$ cross section plotted vs missing energy at $Q^2 = 0.8 \text{ GeV}^2$ and $\nu = 0.439 \text{ GeV}$ for different angles θ_{pq} between the proton spectrometer and \mathbf{q} . The curve labeled DWIA is a distorted wave impulse approximation calculation of s -shell knockout; the other curves are calculations of two-nucleon knockout including meson exchange currents (MEC), delta production (IC), and central and/or tensor correlations. From (Liyanage *et al.*, 2001). (Lower) The cross section plotted vs missing momentum for the $1p_{1/2}$ and $1p_{3/2}$ states. The curves show DWIA calculations. See Gao *et al.* (2000), Liyanage *et al.* (2001), and Fissum *et al.* (2004) for details. From Gao *et al.*, 2000.

distribution calculations shown in Fig. 2(lower) use an optical potential, a modern bound state wave function, and an off-shell cross section σ_{ep} and fit only the magnitude [see Gao *et al.* (2000) for details]. The calculations describe the data well, except for the fact that the ratio of data to theory (the spectroscopic factor) is approximately 0.7. This means that

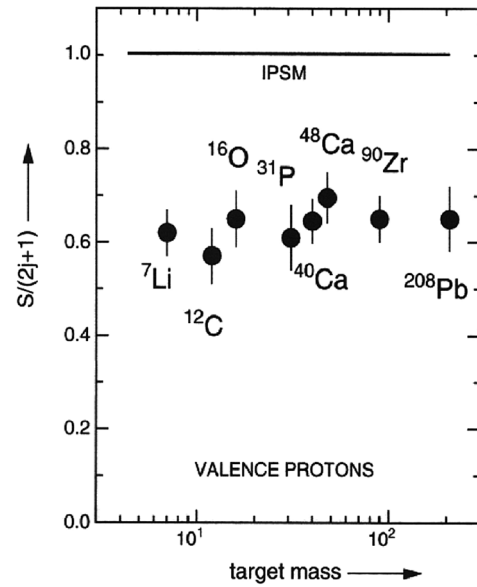


FIG. 3. The fractional spectroscopic factors (the ratio of measured cross sections to those calculated with the independent particle shell model) for valence nucleon knockout ($e, e'p$). Adapted from Lapikas, 1993.

the experiment measured only 70% of the expected number of p -shell protons.

This depletion of the spectroscopic factor was observed over a wide range of the periodic table at relatively low-momentum transfer (see Fig. 3) for both valence nucleon knockout using the ($e, e'p$) reaction (Lapikas, 1993) and stripping using the ($d, ^3\text{He}$) reaction (Kramer, Blok, and Lapikas, 2001). Only about 60%–70% of the expected valence nucleon strength was observed. The missing strength implies the existence of collective effects (long-range correlations) and short-range correlations in nuclei. The spectroscopic factors and the size of the collective effects depend on momentum transfer (Lapikas *et al.*, 2000; Frankfurt, Strikman, and Zhilov, 2001). In addition, the spectroscopic strength for valence proton knockout (e.g., $1p_{3/2}$ proton knockout from C) is distributed over many states and not all of these states are included when measuring the spectroscopic factor. The results in Fig. 3 cannot be directly related to the probability of short-range correlations in nuclei due to the effects of momentum transfer dependence, state splitting, and collective effects. Our focus will be on the short-range correlations as observed using high-momentum transfer probes.

In the DWIA independent particle shell model we expect that the spectroscopic factors are unity and that there is little cross section at large E_{miss} . The fact that spectroscopic factors are significantly less than unity for all nuclei and that there is significant cross section at large missing energy indicates that this simple model picture omits important physics. This is not surprising, since the short-ranged nature of the strong nuclear forces implies that nucleons must be influenced by nearby nucleons. There is no fundamental one-body potential in the nucleus, unlike the central one-body Coulomb potential that binds electrons to form the structure of the atom.

Indeed, since the NN forces are short ranged, the fact that the shell-model approximation has any relevance is somewhat

surprising. In the early days of nuclear physics, the fundamental question of nuclear physics was: how does the very successful shell model of the nucleus emerge in spite of the strong short-ranged interactions between nucleons?

We next answer this fundamental question and then examine the consequences of the answer.

2. From the NN interaction to the shell model and beyond

How can the mean-field shell model arise from a system made of nucleons interacting by strong short-ranged forces? An answer to this question was provided early on by Brueckner and Goldstone; see the review by [Bethe \(1971\)](#). The strong two-nucleon interactions encoded by the potential V , constructed to reproduce experimentally measured NN scattering observables and believed to include strong repulsion at short distance and attraction at longer ranges, are summed to form the T matrix of scattering theory and the G matrix for bound states. The operator G is obtained from T by modifying the propagator of the Lippmann-Schwinger equation to include the effects of the Pauli principle and to use the appropriate self-consistent (single) nucleon energies. The G matrix is considerably weaker than V . For example, even if the potential is infinitely strong, the product $V\Psi$ of the potential with the wave function obtained from the chosen Hamiltonian would be finite and well behaved. Schematically, one has $G\Phi = V\Psi$, where Φ is the shell-model two-nucleon wave function. Calculations show that G is reasonably smooth and can be used as input in higher-order calculations.

The theory proceeds by forming the nuclear mean field U through the Hartree-Fock method employing the G matrix, and the first approximation to the wave function is the antisymmetrized product of single-particle wave functions engendered by U . However, the complete nuclear wave function is obtained in a perturbative hole-line expansion that includes two-particle-two-hole excitations and other excitations which incorporate correlations. The presence of such correlations is demanded by the theory.

Later work formulated a relativistic version of Brueckner's theory in which the Dirac equation replaces the Schrödinger equation ([Anastasio *et al.*, 1983](#); [Brockmann and Machleidt, 1984](#)). There is also a light-front version ([Miller and Machleidt, 1999a](#); [Miller, 2000](#)).

The Brueckner theory approach presumes that the two-nucleon potential contains strong short-distance repulsion. Early attempts to construct soft potentials (i.e., lacking the strong repulsion) that also reproduce scattering data did not succeed in obtaining interactions that could be used perturbatively to calculate nuclear bound states ([Bethe, 1971](#)). This failure is now known to be caused in large measure by the omission of three-body forces. Relativistic G -matrix calculations include important three-body forces ([Anastasio *et al.*, 1983](#); [Brockmann and Machleidt, 1984](#); [Miller and Machleidt, 1999a](#); [Miller, 2000](#)). There are also fundamental three-nucleon forces, such as those involving an intermediate Δ resonance. In addition to true three-body forces, induced multinucleon forces occur as a result of using unitary transformations to produce soft, two-nucleon interactions ([Bogner, Furnstahl, and Schwenk, 2010](#)).

Much more has been learned since Bethe's 1971 review. (1) Our understanding of the connection through symmetries

between the NN interaction and the underlying theory of QCD is much improved. (2) Our ability to make fundamental first-principles calculations of nuclear energies is also much improved. (3) However, it is possible that improved treatments of nuclear energy levels decrease our ability to understand the nuclear high-momentum transfer interactions of interest in this review. (4) We now know that second-order interactions of the NN potential have a major effect on the density distribution and the correlation function in all existing approaches.

- (1) Chiral effective field theory provides a low-energy version of QCD, guided by chiral symmetry, in which one obtains the potential as an expansion in powers of Q/Λ_χ , where Q is a generic external momentum or the pion mass, and Λ_χ is the chiral symmetry breaking scale of about 1 GeV. Such approaches have the advantage of being systematically improvable for low-energy observables; see, e.g., [Bedaque and Kolch \(2002\)](#). In such theories the short-distance interaction can be treated as a contact interaction, modified by the inclusion of a cutoff, and the longer-ranged interactions are accounted for by one- and two-pion (or more) exchange interactions ([Machleidt and Entem, 2011](#)). The advantage gained is that different parts of the potential are divided between more easily understood long-ranged contributions and presumably unknown short-ranged contributions.
- (2) Modern first-principles calculations of nuclear spectra have been applied to an ever increasing mass range. One of the main tools is the use of soft potentials, which do not connect low relative momentum states to those of high relative momentum. This greatly simplifies the calculations by increasing the validity of perturbation theory and other approximation techniques.

The softness (involving low momentum) or hardness (involving higher momentum) of the potential is determined by the value of the cutoff; see, e.g., [Epelbaum, Hammer, and Meissner \(2009\)](#) and [Machleidt and Entem \(2011\)](#). Such potentials introduce a cutoff in momentum space at fairly low values of momenta. Typically, the momentum-space potential obtained from Feynman diagrams $V(\mathbf{p}, \mathbf{p}')$ is replaced:

$$V(\mathbf{p}, \mathbf{p}') \rightarrow V(\mathbf{p}, \mathbf{p}') e^{-(p'/\Lambda)^n} e^{-(p/\Lambda)^n} \quad (3)$$

with $p = |\mathbf{p}|$, $p' = |\mathbf{p}'|$, Λ ranges between 400 and 500 MeV, and n ranges between 2 and 4. These are very strong cutoffs in momentum that introduce significant nonlocality to the nucleon-nucleon interaction. This causes difficulties in maintaining conservation of the electromagnetic currents ([Gross and Riska, 1987](#)).

Another approach uses renormalization group methods to generate a soft NN potential from a hard interaction either by integrating out high-momentum components (in the case of $V_{\text{low-}K}$) or by using the similarity renormalization group ([Bogner, Furnstahl, and Schwenk, 2010](#)). This potential is perturbative in the sense that the Born series for scattering converges. Furthermore, many-body perturbation theory starting from a Hartree-Fock bound state can be applied to the nuclear bound state problem.

- (3) But there is another more general issue that arises in trying to understand high-momentum transfer nuclear reactions. The ability to originate and predict the results of experiments that probe short-range correlations [as was done by Frankfurt and Strikman (1981, 1988)] depends on the idea that the simple impulse approximation is the best way to think about the relevant kinematics and reaction physics. This simplicity may be lost if one uses dynamics generated by the different intent of simplifying nuclear spectroscopy. We now explain. Suppose that the renormalization group successfully eliminates matrix elements of the nucleon-nucleon (or internucleon) potential connecting low and high relative momentum states, leading to an accurate reproduction of nuclear binding energies and spectra. This procedure would also lead to wave functions without high-momentum components and truly short-range correlations. However, it would be necessary to consistently transform all other operators (Anderson *et al.*, 2010; Neff, Feldmeier, and Horiuchi, 2015) in order to calculate observables. For high-momentum transfer reactions, the renormalization group changes a known simple probe, described by a single-nucleon operator, into a more complicated probe describable by unknown (in practice) A -nucleon operators. This could prevent the efficient analysis of any high-momentum transfer experiment. The same remark holds for chiral potentials. The use of a cutoff, as in Eq. (3), leads to the violation of current conservation in electromagnetic interactions unless the currents are modified substantially. For example, one could use minimal substitution, which would introduce terms involving several powers of the electromagnetic potential A^μ . This means that the simplicity of using electromagnetic probes would be lost because of the need to use very complicated operators to analyze experiments. Again we reach the same conclusion: the use of potentials with strong momentum dependence is not optimum for the purpose of using high-momentum transfer electromagnetic processes to understand the short-range structure of nuclei.

It is worthwhile to put comments (1)–(3) into a broader perspective. The goal of effective field theory (EFT) is to obtain results that are independent of the chosen cutoff. In principle, this can be done. In practice, one chooses a given scale to simplify the problem at hand. The use of low-momentum scales simplifies nuclear structure calculations, but complicates the currents needed to understand high-momentum transfer reactions. The use of one-body currents of the impulse approximation simplifies the understanding of high-momentum transfer nuclear reactions, but involves NN potentials that do not have low-momentum cutoffs. Bjorken scaling (Bjorken, 1966) obtained via the use of the simple currents of the noninteracting quark model (impulse approximation) offers a useful historical example. If Bjorken had been overly concerned with issues of QCD evolution, Bjorken scaling and the existence of quarks might never have been discovered. Therefore, we take the experiment-based, discovery-based view that

we are using an implicit momentum scale at which the impulse approximation offers a reasonable first approximation to the physics at hand throughout this review.

- (4) Second-order effects of the tensor term of the one-pion exchange potential are common to all of these approaches, since the beginning (Brown, 1967; Bethe, 1971; Machleidt, 1989; Bogner *et al.*, 2005; Holt, Kaiser, and Weise, 2013) and through to the current days of effective field theory. These effects are large enough to cause convergence difficulties in the application of Brueckner theory (Vary, Sauer, and Wong, 1973) and also cause challenges in defining the power counting which defines any effective field theory (Bedaque and Kolck, 2002).

The effect of this on the relative s -wave function of two nucleons in nuclei can be characterized by the effective potential

$$V_{00} = V_T \frac{1}{E - H_0} Q V_T, \quad (4)$$

where V_T is the tensor potential, the subscript 00 indicates an s -wave to s -wave matrix element, H_0 is the Hamiltonian in the absence of V_T , and Q is a projection operator taking the Pauli principle into account. The operator V_{00} has a major effect on the density distribution and correlation function (as discussed in the Appendix). These effects occur in all existing approaches. A major purpose of this review is to show that the influence of the correlations induced by the tensor force is manifest in high-momentum transfer reactions.

To summarize, nuclear theorists have made tremendous progress in understanding the connections between NN potentials and QCD, as well as in calculating nuclear energies and states. High-momentum transfer experiments are easier to analyze using well-defined current operators, rather than using transformed A -nucleon operators with a renormalization-group-transformed potential. These well-defined current operators can be used if the effects of correlations are maintained in the nuclear wave function instead of being hidden in the current operators through the use of the renormalization group or very soft NN potentials. However, regardless of approach, the influence of the correlations induced by the tensor force is manifest in all theoretical approaches to date, and, as we shall see, is manifest in high-momentum transfer reactions.

3. Short-ranged two-nucleon clusters

As discussed in the previous sections, in the nucleus, nucleons behave approximately as independent particles in a mean field created by their average interaction with the other nucleons. But occasionally (20%–25% in medium or heavy nuclei) two nucleons get close enough to each other so that temporarily their singular short-range interaction cannot be well described by a mean-field approximation. These are the two-nucleon short-range correlations (2N-SRC), defined operationally in experiments as having small center-of-mass (c.m.) momentum and large relative momentum. These pairs are predominantly neutron-proton pairs. Colle *et al.* (2015) showed that it is predominantly nucleon-nucleon pairs in a nodeless relative- S state of the mean field that create these 2N-SRC. The force between the nucleons in the pair is predominantly a tensor force which creates a pair with the

quantum numbers of the deuteron ($S = 1$, $T = 0$), a neutron-proton system (Vanhalst, Cosyn, and Ryckebusch, 2011).

The two nucleons in $2N$ -SRC have a typical distance of about 1 fm which means that their local density is a few times higher than the average nuclear density. The relative momentum of the two nucleons in the pair can be a few times the Fermi momentum k_F , which is large. SRCs of more than two nucleons probably also exist in nuclei and might have higher density than that of the $2N$ -SRC. However, their probability is expected to be significantly smaller than the probability of $2N$ -SRC (Beth, 1971).

The $2N$ -SRC are isospin-dependent fluctuations. For example, the deuteron is the only bound two-nucleon system. We know now that density fluctuations involving one neutron and one proton occur more often than those involving like nucleons; see Sec. II.C. Therefore we examine the deuteron first.

The simplest nucleus, the deuteron, has spin $S = 1$, isospin $T = 0$, and $J^\pi = 1^+$. The relevant quantity for electron scattering is $n(k)$ which is the probability of finding a nucleon of momentum between k and $k + dk$. This function is the sum of two terms, one arising from the $l = 0$ (s wave), and the other from the $l = 2$ (d wave). At momenta of interest for short-range correlated pairs (i.e., p significantly greater than $p_F \approx 250$ MeV/ c , where p_F is the typical Fermi momentum for medium and heavy nuclei), the otherwise small d wave becomes important. This is especially true at $p \approx 400$ MeV/ c where there is a minimum in the s wave. In the Argonne V18 potential (Wiringa *et al.*, 2014) the d -wave component is due to the tensor force. The combination of d and s waves leads to a “broad shoulder” in the deuteron momentum distribution, which extends from about 300 to 1400 MeV/ c in the AV18 potential; see the Appendix for an explanation. This broad

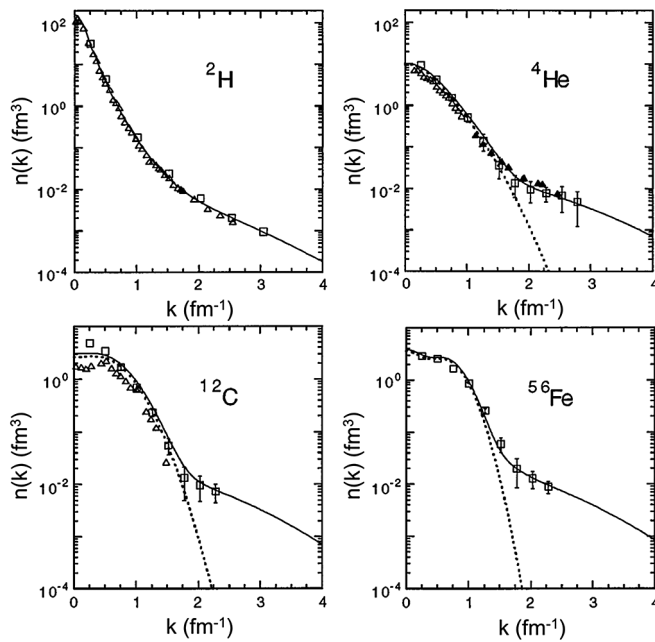


FIG. 4. The nucleon momentum distributions $n_0(k)$ (dashed lines) and $n(k)$ (solid lines) plotted vs momentum in fm^{-1} for the deuteron, ${}^4\text{He}$, ${}^{12}\text{C}$, and ${}^{56}\text{Fe}$. Adapted from Ciofi degli Atti and Simula, 1996.

shoulder is also a dominant feature in the tail of the single-nucleon momentum distributions computed with realistic internucleon interactions (see Fig. 4), in particular, with the AV18 potential for $A \leq 12$ (Wiringa *et al.*, 2014) and more effective approaches for heavier systems (Ciofi degli Atti and Simula, 1996; Ryckebusch, Vanhalst, and Cosyn, 2015).

We can also consider the spatial wave function of the nucleus. The short-range part of the NN interaction gives a correlation hole at small NN relative distances; see Fig. 5. Precise definitions are given in the Appendix. Calculations with various bare realistic interactions show that, apart from a normalization factor depending upon the different number of pairs in different nuclei, the relative two-nucleon density $\rho_{\text{rel}}(r)$ and its spin-isospin components $\rho_{ST}^{N_1 N_2}(r)$ at $r \leq 1.5$ fm exhibit similar correlation holes, generated by the interplay of the short-range repulsion and the intermediate-range tensor attraction of the NN interaction, with the tensor force governing the overshooting at $r \approx 1.0$ fm. The correlation hole is universal in that it is almost independent of the mass A of the nucleus (Ciofi degli Atti, 2015). The depth of the correlation hole depends on the short-distance behavior of the potential. The value of R_0 shown in Fig. 5 refers to the cutoff on the short-distance $N^2\text{LO}$ nucleon-nucleon potential, as defined by Gezerlis *et al.* (2014). A correlation hole is seen to occur for $R_0 = 1$ fm, but is much less deep for $R_0 = 1.2$ fm. The use of such a soft potential is not suitable in the present experiment-based high-scale context. Furthermore, this soft potential predicts erroneous nucleon-nucleon phase shifts for the 3D_1 partial wave and also for lab energies greater than 250 MeV.

In momentum space, the existence of this universal correlation hole translates into nucleon momentum distributions $n_A(p)$ that are significant at large momentum ($p \geq p_F$) and that are similar for all nuclei $n_A(p) \propto n_d(p)$ at these large momenta (Frankfurt and Strikman, 1981, 1988; Ciofi degli Atti and Simula, 1996; Alvioli *et al.*, 2013). Frankfurt and

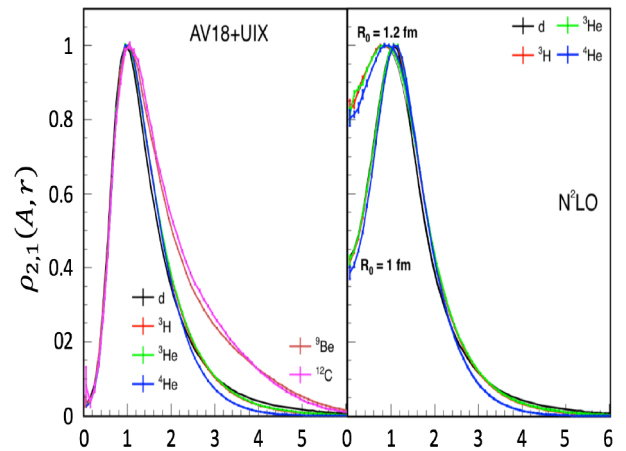


FIG. 5. Scaled two-body distribution function $\rho_{2,1}^A(r)/A$ [see Eq. (A11)] for nuclei with $A = 2, 3$, and 4. A correlation hole is seen for all of these nuclei. The two sets of curves are obtained with the (left) AV18 + UIX and (right) $N^2\text{LO}$ potentials. The meaning of R_0 is discussed in the text. Adapted from Chen *et al.*, 2016.

Strikman realized that these could be measured with hard probes (see Sec. II).

Ciofi degli Atti *et al.* (1991) and Ciofi degli Atti and Simula (1996) used this similarity to model the nucleon spectral function $P(\mathbf{p}, E)$ (the joint probability to find a nucleon in a nucleus with momentum \mathbf{p} and removal energy E) for all nuclei

$$P(\mathbf{p}, E) = \langle \Psi | b^\dagger(\mathbf{p}) \delta(E - H) b(\mathbf{p}) \Psi \rangle, \quad (5)$$

where $|\Psi\rangle$ represents the nuclear wave function, and spin, isospin, and nuclear (A) labels are suppressed for simplicity. The momentum density $n(\mathbf{p})$ is given by

$$n(\mathbf{p}) = \int dE P(\mathbf{p}, E). \quad (6)$$

They write

$$P(\mathbf{p}, E) = P_0(\mathbf{p}, E) + P_1(\mathbf{p}, E), \quad (7)$$

where the subscript 0 refers to values of E corresponding to low-lying intermediate excited states and the subscript 1 refers to high-lying continuum states that are caused by the short-range correlations. Therefore one also has $n(\mathbf{p}) = n_0(\mathbf{p}) + n_1(\mathbf{p})$, where $n_1(\mathbf{p})$ is associated with the high momentum caused by short-range correlations. $n_0(\mathbf{p})$ is typically dominant for $\mathbf{p} < 250$ MeV/ c or so and $n_1(\mathbf{p})$ becomes dominant for larger values. Furthermore, $n_1(\mathbf{p})$ is almost independent of A at $\mathbf{p} > 400$ MeV/ c . They attribute this to NN correlations; see Fig. 4. Note that for ${}^3\text{He}$ Ciofi degli Atti *et al.* (1991) showed that the proposed model spectral function agrees with the one obtained by direct calculation.

SRC pairs are conventionally defined in momentum space as a pair of nucleons with high relative momentum and low c.m. momentum, where high and low are relative to the Fermi momentum of medium and heavy nuclei. Thus the most prominent effects of SRCs will be to populate high-momentum states in the nuclear momentum distribution. As conventional mean-field theories predict only a very small high-momentum tail, the effect of SRCs there should be substantial. Formally, one needs the two-nucleon momentum density $n(\mathbf{p}_1, \mathbf{p}_2)$ (see the Appendix), where $\mathbf{p}_{\text{tot}} = \mathbf{p}_1 + \mathbf{p}_2$ and $\mathbf{p}_{\text{rel}} = 1/2(\mathbf{p}_1 - \mathbf{p}_2)$ are the center of mass and relative momenta of the two nucleons. Studies of spectral functions show that at large values of p_{rel} the two-nucleon momentum density factorizes

$$n(\mathbf{p}_{\text{tot}}, \mathbf{p}_{\text{rel}}) = n(p_{\text{tot}})n(p_{\text{rel}}). \quad (8)$$

A justification of this factorization is presented in the Appendix.

The coordinate-space correlation holes (Fig. 5) give similar NN relative (p_{rel}) momentum distributions (at large p_{rel}) in all nuclei. Exact calculations with the AV18 potential for ${}^4\text{He}$ show that at small p_{tot} there is a minimum in p_{rel} for pp pairs at $p_{\text{rel}} = 400$ MeV/ c . This is because, at small p_{tot} , the pp pair must be in a relative s state which has a minimum at $p_{\text{rel}} = 400$ MeV/ c , just as in deuterium. For np pairs, this minimum is filled in by the d wave caused by the short-range pion-exchange tensor force (Wiringa *et al.*, 2014).

Thus, the combination of the minimum in the s -wave momentum distribution at $p \approx 400$ MeV/ c and the filling in

of this minimum by the d -wave pion-exchange tensor force leads to the expected dominance of np correlated pairs over nn and pp pairs at $300 \leq p \leq 500$ MeV/ c . This ratio of np to pp pairs should decrease at relative momentum significantly greater than 400 MeV/ c , the s -wave minimum (as discussed Sec. II).

Short-range correlations in light nuclei have been theoretically examined recently from several points of view (Feldmeier *et al.*, 2011; Vanhalst, Cosyn, and Ryckebusch, 2011; Vanhalst, Ryckebusch, and Cosyn, 2012; Rios, Polls, and Dickhoff, 2014; Wiringa *et al.*, 2014; Ciofi degli Atti, 2015; Ryckebusch, Vanhalst, and Cosyn, 2015; Weiss, Bazak, and Barnea, 2015). One consistent finding of such work is the dominance of np deuteronlike pairs ($ST = 10$) over other pairs at high momentum.

These facts described in this section lead to an effective description of nuclei in momentum space as having two important regions: (1) a mean-field region ($k \leq p_F$), which accounts for about 80% of the nucleons, where the many-body dynamics result in single nucleons moving under the influence of an effective potential created by the residual $A - 1$ system and (2) a high-momentum region ($p \geq p_F$), which accounts for about 20% of the nucleons [but 70% of the kinetic energy (Benhar, Fabrocini, and Fantoni, 1989; Polls *et al.*, 1994)], where nucleons are predominantly in the form of pn -SRC pairs, having a very weak interaction with the residual $A - 2$ system. As noted, it is possible to use unitary transformations to derive a low-momentum effective interaction that weakens the strong short-range correlations present in the original interactions. However, the one- and two-body density operators also need to be transformed. It is necessary to include three or more body effects to obtain accurate results with these soft interactions (Feldmeier *et al.*, 2011). This approach complicates the analyses of experiments.

To summarize, the high-momentum nucleons in nuclei are mainly due to $2N$ -SRC and are therefore associated with high-density fluctuations in the nucleus. In what follows (see Sec. III.D) we will examine the hypothesis that these temporary high-density or large-momentum ‘‘hot spots’’ are the sites where the nucleon internal structure is modified and the EMC effect is created. First, we present the experimental evidence for short-range correlations.

II. HARD SCATTERING AND SHORT-RANGE CORRELATIONS

A. Hard reactions

In optics the resolving power is the minimum distance at which an imaging device can separate two closely spaced objects. This is normally proportional to the wavelength of the light. The smaller the wavelength, the better the resolution.

We often scatter particles to try to resolve the internal structure of a complex target. The sizes of the target and its constituents define the required resolving power. For example, to observe the nucleus of an atom one needs a spatial resolution of about 10 fm, to observe nucleons in nuclei one needs a resolution of about 1 fm, and to observe the partonic structure of a nucleon one needs sub-Fermi resolution.

The spatial resolution of a scattering experiment is determined by the de Broglie wavelength (λ) of the probe (scattering particle) and the momentum transfer of the reaction (q). We define as “hard” a process that fulfills the following conditions: $\lambda \ll R$ and $qR \gg 1$, where R is the size of the target or the structure to be studied. In practice, we see that the results of measurements can be interpreted as observing a hard reaction even though these kinematic conditions are not always rigorously met.

Another important lepton-scattering length scale is the coherence length, or Ioffe length (Gribov, Ioffe, and Pomeranchuk, 1966; Ioffe, 1969): $l_I = 2/Mx_B \approx 0.4 \text{ fm}/x_B$, where $x_B = Q^2/2M\nu$. Here M is the nucleon mass, Q^2 is the negative of the square of the virtual exchanged photon four-momentum, and ν is its energy. This length is the typical distance between the absorption and reemission of the virtual photon. This length must be short enough to resolve the relevant internucleon distance scales of the order of a Fermi. Thus, we focus on the region $x_B > 0.3$ where valence quarks are dominant and the sea is almost invisible.

In this review we are dealing with two reactions and the connection between them. DIS attempts to resolve the partonic structure of nucleons and quasielastic (QE) scattering attempts to resolve the nucleonic structure of nuclei. These reactions have different required resolutions and hence different kinematical conditions to achieve them.

For (e, e') DIS reactions, which are typically measured as a function of $x_B = Q^2/2M\nu$ for $x_B < 1$, there are two important parameters, the four-momentum transfer squared of the virtual photon Q^2 and the invariant mass of the virtual photon plus struck nucleon $W = \sqrt{M^2 + 2M\nu - Q^2}$. Since x_B , Q^2 , and W are all functions of the same two variables, only two are independent. For the inelastic scattering to be considered deep (the “D” in DIS), experiments typically require $W \geq 2 \text{ GeV}$. This allows the experiments to be sensitive to the internal structure of a proton or neutron and avoid the influence of individual nucleon resonances, which cause the cross section to fluctuate rapidly with W .

Early studies at high-energy facilities (SLAC and CERN) measured DIS for $5 \leq Q^2 \leq 50 \text{ GeV}/c^2$ and found that the ratios of DIS cross sections for $0.3 \leq x_B \leq 0.7$ are largely independent of Q^2 (Norton, 2003). The newer JLab experiments used lower lepton energies (typically 4–5 GeV) and therefore lower Q^2 , $4 \leq Q^2 \leq 6 \text{ GeV}^2$ (Seely *et al.*, 2009). The higher-energy SLAC and CERN measurements required $W \geq 2 \text{ GeV}$. However, the lower-energy JLab data required only $W \geq 1.4 \text{ GeV}$.

For inclusive (e, e') QE scattering, there are again only two independent kinematical variables, normally chosen to be Q^2 and x_B . However, in addition to making sure that the resolving power is sufficient, we also need to optimize the kinematics to select scattering from high-momentum nucleons in the nucleus and to reduce the effects of non-single-nucleon currents. In order to resolve nucleons in SRC pairs, measurements are typically made at $Q^2 > 1.5 \text{ (GeV}/c)^2$. Large ($p > p_F$) minimum initial momentum of the struck nucleon (assuming no final state interactions) can be selected at $Q^2 > 1.5 \text{ (GeV}/c)^2$ by choosing either $x_B \geq 1.5$ or $x_B \leq 0.6$ (see Sec. II.C). $x_B \geq 1$ is preferred, so that the energy transfer is

smaller, inelastic processes [resonance production, meson exchange currents (MEC), and isobar configurations (IC)] are suppressed, and the reaction is more sensitive to the nuclear momentum distribution. Increasing Q^2 further suppresses MEC contributions. The inclusive QE scattering data discussed in Sec. II.C were measured at $x_B \geq 1.5$.

In exclusive and semiexclusive reactions, ($e, e'p$) and ($e, e'pN$), large initial nucleon momenta can be directly selected and the x_B restrictions can be relaxed (see Sec. II.B).

B. Exclusive scattering

The study of SRCs using exclusive reactions has a long history that extends beyond the scope of this review. Here we focus only on exclusive measurements performed with high-energy probes and large-momentum transfer (hard reactions). See Kelly (1996) and references therein for a review of the older measurements. We use the term exclusive to refer to measurements in which, in addition to the scattered probe particle, two knocked-out nucleons are measured in the final state.

In the context of SRC studies, exclusive reactions are hard processes in which a probe scatters from one nucleon in an SRC pair and all particles emitted in the final state (e.g., the scattered probe and both nucleons of the pair) are detected. The energy of the probe and the momentum transfer must be large enough so that the probe interacts with a single, high-momentum ($p_i > p_F$) nucleon in the pair. If the pair was at rest ($p_{\text{c.m.}} = 0$) and neither nucleon rescattered as it left the nucleus, then the struck nucleon’s correlated partner would recoil with momentum $\mathbf{p}_2 = -\mathbf{p}_1$. This back-to-back angular correlation between the initial momentum of the knocked-out nucleon and the momentum of the recoil nucleon is a clear experimental signature for exactly two nucleons being involved in the interaction. We note that these reactions can be analyzed in terms of the decay function introduced by Frankfurt and Strikman (1988).

However, other reaction mechanisms can also involve two nucleons, leaving the residual $A - 2$ nucleus almost at rest. The probe can scatter from one nucleon, which can rescatter from a second (FSI), the probe can scatter from a meson being exchanged between two nucleons (MEC), or the probe can excite the first nucleon which can then deexcite via interaction with a second nucleon (IC). Disentangling these competing and interfering effects can be difficult. It is important to realize that the effects of MEC and IC are dramatically decreased by choosing kinematics with $x_B > 1$ and with larger values of Q^2 . The effects of FSI can also be dramatically decreased by (a) choosing kinematics where the relative momentum of the two final state nucleons is large and (b) avoiding kinematics where the opening angle between the two outgoing nucleons is 70° – 90° . (Nonrelativistically, when one billiard ball scatters from a second billiard ball at rest, the opening angle in the final state is 90° .)

The detection of the outgoing nucleons in exclusive reactions provides complementary information to the inclusive reactions discussed later. By detecting the struck nucleon at large p_{miss} and looking for the recoil partner nucleons, exclusive measurements can measure the fraction of high-momentum nucleons belonging to SRC pairs. They can also

extract information on the SRC-pair isospin structure and $p_{c.m.}$ distribution, as well as their A and momentum dependence.

This additional information, however, comes at the price of increased sensitivity to FSI. FSI can be generally split into two main contributions: rescattering between the nucleons of the pair, and rescattering between the nucleons of the pair and the residual $A - 2$ system. Rescattering between the nucleons of the pair will alter the measured relative momentum but leave $p_{c.m.}$ unchanged. Rescattering between the nucleons of the pair and the residual $A - 2$ system will change the momentum of the outgoing nucleons and “attenuate” them. The attenuation of the nucleons as they traverse the nucleus is usually referred to as the “nuclear transparency” and limits the spatial region probed in the experiment to the outer part of the nucleus. It can be calculated in the Glauber approximation (for large enough nucleon momentum). The momentum changes also affect the measured kinematical distributions. Here the use of high-momentum transfer, as required for hard reactions, also allows using the Glauber approximation to calculate the effects of FSI and to select kinematics to minimize their effects, in either the measured cross sections or the kinematical distributions.

Specifically, at $Q^2 \geq 1.5-2$ (GeV/c)² and $x_B \geq 1$ (or proton scattering experiments at $|t|, |u|, |s| \geq 2$ GeV/c²) Glauber calculations show that the outgoing nucleons predominantly rescatter from each other and not from the residual $A - 2$ system (Frankfurt and Strikman, 1981, 1988; Frankfurt *et al.*, 1993; Ciofi degli Atti and Simula, 1996; Arrington, Higinbotham *et al.*, 2012). This implies that certain quantities such as the total pair momentum $p_{c.m.}$ and pair isospin structure are insensitive to rescattering while other quantities like the pair relative momentum p_{rel} are very sensitive to rescattering and thus cannot be reliably extracted from the experimental data; see Frankfurt, Sargsian, and Strikman (1997) and Shneor *et al.* (2007) for details. The contributions of MEC and IC are also minimized at high Q^2 and $x_B \geq 1$.

The first exclusive hard two-nucleon knockout experiments, measuring the $^{12}\text{C}(p, 2pn)$ and $^{12}\text{C}(e, e'pN)$ reactions, were done at BNL and JLab, respectively (Tang *et al.*, 2003; Piasetzky *et al.*, 2006; Shneor *et al.*, 2007; Subedi *et al.*, 2008). These experiments scattered 5–9 GeV/c protons (BNL) and electrons (JLab) off high initial momentum ($300 \leq p_i \leq 600$ MeV/c) protons in ^{12}C and looked for a correlated recoil nucleon emitted in the direction of the missing momentum. The JLab experiment measured both proton and neutron recoils, whereas the BNL experiment measured only recoiling neutrons. Both experiments measured at large-momentum transfer [$Q^2 \approx 2$ (GeV/c)²], which suppressed competing reaction mechanisms and largely confined FSI to be between the nucleons of the pair.

The main results of the ^{12}C measurements are shown in Figs. 6, 7, and 8. Figures 6 and 7 show the angular correlation between the momentum vector of the recoil nucleons and the reconstructed initial momentum of the knocked-out proton. For the BNL data, the angle is shown as a function of the recoil neutron momentum. Two distinct regions are visible: below the Fermi momentum where no angular correlation is observed, and above the Fermi momentum where a clear back-to-back correlation is seen. The width of the recoil nucleon

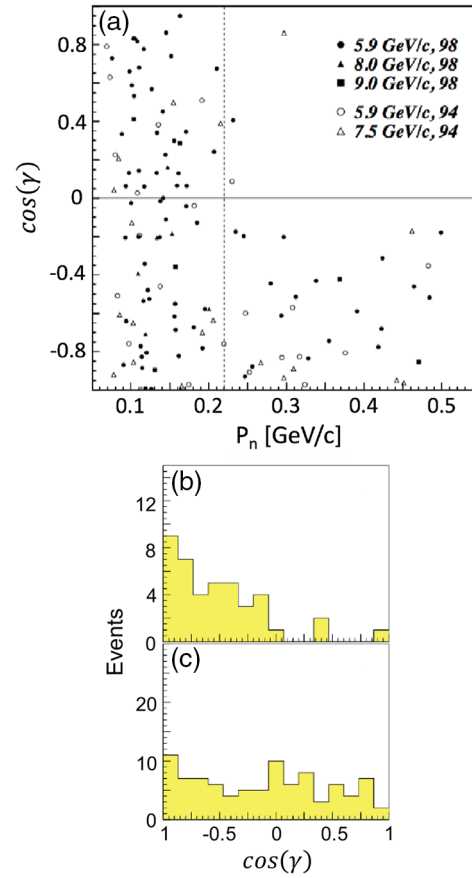


FIG. 6. Distributions of the relative angle (γ) between the reconstructed initial momentum of the knockout proton and the recoil neutron. Results for $^{12}\text{C}(p, 2pn)$ events from BNL, shown as a function of the momentum of the recoil neutron (a) and for events with recoiling neutron momentum greater than (b) and less than (c) $k_F = 225$ MeV/c. Note the transition from an isotropic distribution to a correlated one at about $k_F = 225$ MeV/c. Adapted from Tang *et al.*, 2003 and Piasetzky *et al.*, 2006.

opening angle distribution allowed extracting the pair c.m. motion; this motion can be described by a Gaussian distribution in each direction, with $\sigma = 143 \pm 17$ (BNL) and $\sigma = 136 \pm 20$ (JLab). These values are also in overall agreement

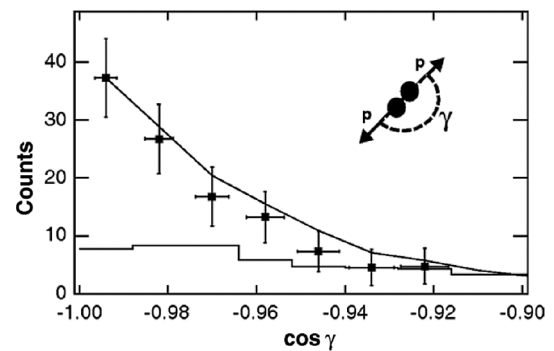


FIG. 7. Distributions of the relative angle (γ) between the reconstructed initial momentum of the knockout proton and the recoil nucleon. Results for $^{12}\text{C}(e, e'pp)$ events from JLab at kinematics corresponding to scattering off ~ 500 MeV/c initial momentum protons. From Shneor *et al.*, 2007.

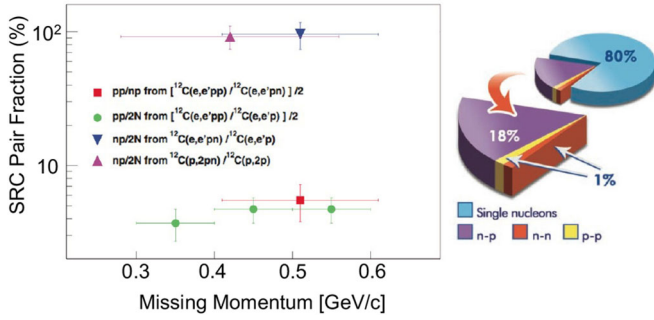


FIG. 8. The ratio of $^{12}\text{C}(e, e' pN)$ double knockout events to $^{12}\text{C}(e, e' p)$ single knockout events, shown as a function of the reconstructed initial (missing) momentum of the knocked-out proton from the $^{12}\text{C}(e, e' p)$ reaction. Triangles and circles mark $^{12}\text{C}(e, e' pN)$ and $^{12}\text{C}(e, e' pp)$ events, respectively. The square shows the $^{12}\text{C}(e, e' pp)/^{12}\text{C}(e, e' pn)$ ratio. A clear dominance of the $^{12}\text{C}(e, e' pn)$ events is observed, evidence of the tensor nature of the nucleon-nucleon interaction in the measured momentum range. The pie chart on the right illustrates our understanding of the structure of ^{12}C , composed of 80% mean-field nucleons and 20% SRC pairs, where the latter is composed of $\sim 90\%$ np -SRC pairs and 5% pp and nn SRC pairs each. Adapted from Subedi *et al.*, 2008.

with theoretical calculations (Ciofi degli Atti and Simula, 1996; Colle *et al.*, 2014). The electron and proton reactions are characterized by completely different operators and FSI mechanisms; therefore the agreement of their c.m. momentum distributions validates the consistent treatment of FSI in these measurements.

For example, for proton induced reactions the effective nuclear density is smaller than for electron induced reactions due to absorption effects that prefer scattering from the edge of the nucleus. The overall agreement between the results obtained using different high-energy hadronic and leptonic probes at very different momentum transfer (2 and 5 GeV^2) strongly supports the interpretation that in these reactions the projectiles interact with one nucleon of the SRCs. Note also that the saturation of the recoil channels by neutron and protons puts a strong limit on the admixture of non-nucleonic degrees of freedom in SRCs.

Figure 8 shows the extracted ratio of two-nucleon knockout (proton-neutron and proton-proton) to single proton knockout events and the ratio of proton-neutron to proton-proton two-nucleon knockout events. The ratios are all corrected for finite acceptance effects and shown as a function of p_{miss} , the reconstructed initial momentum of the knocked-out protons for $300 \leq p_{\text{miss}} \leq 600$ MeV/c . The ratio of two-nucleon knockout to single proton knockout is directly related to the fraction of high-momentum protons that are in SRC pairs. As can be seen, within statistical uncertainties of about 10%, all single-nucleon knockout events at $300 \leq p_i \leq 600$ MeV/c were accompanied by the emission of a recoil nucleon. The proton-to-neutron recoil ratio was found to be approximately 1 : 10, which corresponds to 20 times more np -SRC pairs than pp -SRC pairs in ^{12}C (Subedi *et al.*, 2008). This observed proton-neutron pair dominance was associated with the dominance of the tensor part of the nucleon-nucleon interaction at these initial moments (Sargsian *et al.*, 2005; Schiavilla *et al.*, 2007).

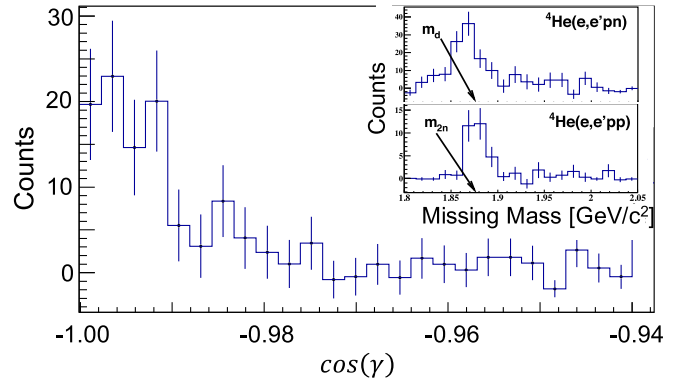


FIG. 9. The distribution of the cosine of the opening angle γ between \mathbf{p}_{miss} and $\mathbf{p}_{\text{recoil}}$ for the $^4\text{He}(e, e' pn)$ reaction. The solid curve is a simulation of scattering off a moving pair with a c.m. momentum distribution having a width of 100 MeV/c . The insets show the missing mass distributions. Adapted from Korover *et al.*, 2014.

A follow-up measurement of $^4\text{He}(e, e' pn)$ in similar kinematics set out to better constrain the importance of the tensor part of the NN interaction at short distance and extend the experimental data to larger initial momenta $400 \leq p_i \leq 800$ MeV/c (Korover *et al.*, 2014). At these higher momenta, the scalar repulsive core of the nucleon-nucleon interaction is expected to dominate over the tensor part, increasing the fraction of pp -SRC pairs. The ^4He nucleus was chosen to further reduce FSI and allow for comparisons with detailed *ab initio* few-body calculations. The results of this measurement are shown in Figs. 9 and 10.

The two-nucleon opening angle distribution for ^4He (see Fig. 9) is very similar to that for C (see Fig. 7). The reconstructed missing mass distribution peaks at small missing mass for both pp - and np -SRC pair knockout.

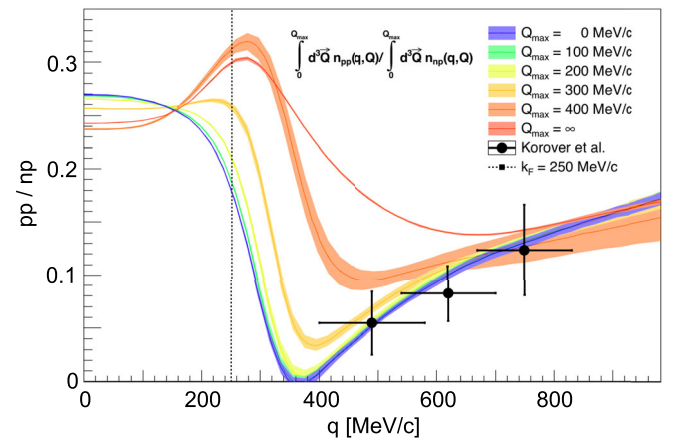


FIG. 10. The measured pp to pn ratio as function of the proton missing momentum (labeled q) (Korover *et al.*, 2014) compared to calculations of the two-nucleon momentum distribution (Wirringa *et al.*, 2014) integrated over various ranges of the c.m. momentum from zero (bottom curve) to infinity (top curve) (Weiss *et al.*, 2016). The data are shown as a function of the nucleon momentum and the calculations are shown as a function of the pair relative momentum. The two are equivalent for low c.m. momentum of the pair but differ at large c.m. momentum. Adapted from Weiss *et al.*, 2016.

As can be seen, there is a peak at back angle, associated with a breakup of ${}^4\text{He}$ into a SRC pair and a residual $2N$ system with low excitation energy. As with the ${}^{12}\text{C}$ measurements, the width of the opening angle distribution is due to the c.m. motion of the SRC pairs which was found to be consistent with a Gaussian in each direction with a width of 100 ± 20 MeV/ c .

The extracted ${}^4\text{He}$ pp/np SRC pairs ratio increases with p_{miss} for $p_{\text{miss}} > 400$ MeV/ c (see Fig. 10). The measured ratios are consistent with *ab initio* variational Monte Carlo calculations of Wiringa *et al.* (2014) integrated over c.m. momentum up to about 300 MeV/ c , which is consistent with the measured width of the c.m. momentum distribution. At higher c.m. momentum, the two-body momentum distribution is dominated by large contributions from uncorrelated pairs (Weiss *et al.*, 2016). Similar results were also obtained by different calculations (Ryckebusch, Vanhalst, and Cosyn, 2015; Alvioli, Atti, and Morita, 2016).

The importance of tensor correlations was further shown by measurements of the pp to pn ratio in ${}^3\text{He}(e, e'pp)n$ measured using the CEBAF Large Acceptance Spectrometer (CLAS) detector at JLab (Baghdasaryan *et al.*, 2010). They measured the relative and total momentum distribution of pp and pn pairs in ${}^3\text{He}$ by detecting events where the virtual photon was absorbed on one nucleon and the other two (spectator) nucleons were also detected. Figure 11 shows the ratio of pp to pn pairs in ${}^3\text{He}$ as a function of the pair total (e.g., center-of-mass) momentum for two pair relative momentum ranges $300 \leq p_{\text{rel}} \leq 500$ and $400 \leq p_{\text{rel}} \leq 600$ MeV/ c . The first range is centered at the s -wave minimum at 400 MeV/ c where the effects of tensor correlations are expected to dominate; the second is not. For p_{rel} centered at 400 MeV/ c , the pp to pn ratio is very small at $p_{\text{tot}} \leq 100$ MeV/ c and consistent with the ${}^{12}\text{C}(e, e'pN)$

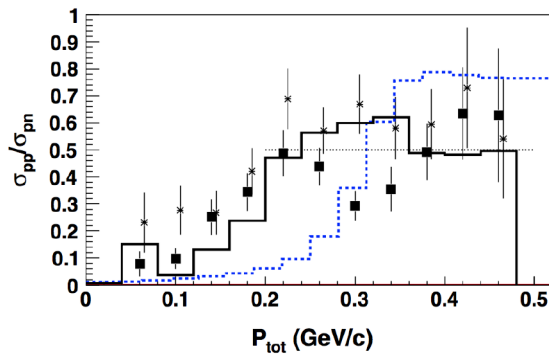


FIG. 11. The ratio of pp to pn pairs in ${}^3\text{He}(e, e'pp)n$. The solid and star points show the ratios for $300 \leq p_{\text{rel}} \leq 500$ and $400 \leq p_{\text{rel}} \leq 600$ MeV/ c , respectively, as a function of the total (e.g., center-of-mass) momentum of the pair. The pp/pn ratio is much less than 1 for small p_{tot} , increasing to the pair-counting ratio of 0.5 at large p_{tot} . The ratio at small p_{tot} is about 0.1 for $300 \leq p_{\text{rel}} \leq 500$ MeV/ c , and about 0.25 for $400 \leq p_{\text{rel}} \leq 600$ MeV/ c . The solid line shows a calculation by Golak for $300 \leq p_{\text{rel}} \leq 500$ MeV/ c which neglects rescattering of the struck nucleon but includes the reinteraction of the two nucleons in the SRC pair. The dashed line (blue) shows the ${}^3\text{He}$ momentum distribution integrated over the experimental acceptances. From Baghdasaryan *et al.*, 2010.

measurements already discussed. For p_{rel} centered at 500 MeV/ c , the pp to pn ratio at $p_{\text{tot}} \leq 100$ MeV/ c is significantly larger, consistent with the expected decreased dominance of tensor correlated pairs at this higher relative momentum. At large p_{tot} , the pp to pn ratio is 0.5, consistent with simple pair counting. The points at $300 \leq p_{\text{rel}} \leq 500$ MeV/ c are consistent with a calculation by Golak *et al.* (1995) which neglects rescattering of the struck nucleon but includes the reinteraction of the two nucleons in the SRC pair.

The combined results of the ${}^3\text{He}$, ${}^4\text{He}$, and ${}^{12}\text{C}$ measurements indicate that for $300 \leq p_i \leq 500$ MeV/ c nucleons are predominantly part of pn -SRC pairs as predicted by dominance of the tensor part of the NN interaction at short distances. At higher initial momentum, the contribution of pp -SRC pairs seems to increase by a factor of 2–3, possibly due to larger contributions from the scalar repulsive core of the NN interaction.

Encouraged by these results, the latest exclusive measurements extended to medium and heavy nuclei (${}^{12}\text{C}$, ${}^{27}\text{Al}$, ${}^{56}\text{Fe}$, and ${}^{208}\text{Pb}$), where the persistence of np -SRC dominance was still unproven (Hen *et al.*, 2014). In this experiment, the $A(e, e'pp)$ and $A(e, e'p)$ reactions were measured at similar kinematics to the previous ${}^4\text{He}$ and ${}^{12}\text{C}$ measurements, covering a reconstructed initial proton momentum range of $300 \leq p_i \leq 600$ MeV/ c . The analysis assumed that, in these nuclei, the reaction is still dominated by scattering off SRC pairs and extracted the relative fraction of np - and pp -SRC pairs. Figure 12 shows that SRC pairs are predominantly np -SRC pairs even in heavy neutron-rich nuclei.

C. Inclusive scattering

Inclusive quasielastic electron scattering allows probing the momentum distribution of nucleons in the nucleus. Elastic scattering from a nucleon at rest occurs at fixed kinematics $\nu = Q^2/2M$. This corresponds to $x_B = 1$. If all of the struck nucleons in a nucleus were at rest, the cross section would show a pronounced narrow peak—the quasielastic peak.

This peak is broadened by nucleon motion for electron scattering from bound nucleons. In order to study nuclear momentum distributions, experiments typically focus on the low-energy transfer side of the QE peak, or $x_B \geq 1$. In this case the initial momentum of the struck nucleon must be in the opposite direction from the momentum transfer so that the final momentum of the struck nucleon $\mathbf{p}_f = \mathbf{q} + \mathbf{p}_{\text{miss}}$ (in the absence of final state interactions or FSI, $\mathbf{p}_{\text{rmiss}} = \mathbf{p}_{\text{rinit}}$) is less than the momentum transfer. As the energy transfer decreases, the final momentum of the struck nucleon must

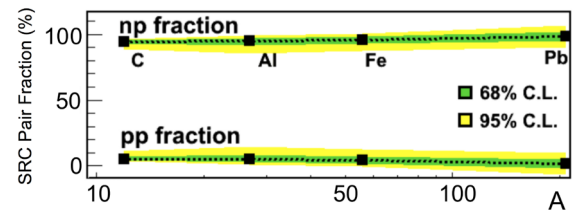


FIG. 12. The relative fraction of np and pp SRC pairs (excluding nn pairs) derived from $A(e, e'p)$ and $A(e, e'pp)$ measurements on a range of nuclei. From Hen *et al.*, 2014.

decrease and therefore the minimum initial momentum of the struck nucleon must increase.

The quasielastic inclusive electron scattering (e, e') cross section can be written in terms of a function F that depends on (Q^2, y) rather than (Q^2, ν) (Day *et al.*, 1987):

$$\frac{d^2\sigma(q, \nu)}{d\nu d\Omega} = F(y, Q^2)(Z\sigma_p + N\sigma_n) \frac{q}{\sqrt{M^2 + (y+q)^2}}, \quad (9)$$

where $\sigma_{p,n}$ are the elastic electron scattering cross sections from a bound nucleon, the last term is the Jacobian $dy/d\nu$, and $y = y(Q^2, \nu)$ is the minimum momentum of the struck nucleon (assuming that the residual $A-1$ system is unexcited) (Day *et al.*, 1990; Arrington, Daniel *et al.*, 2012).

Nonrelativistically, y is the component of the struck nucleon's initial momentum (\mathbf{p}_{miss}) in the direction of \mathbf{q} . The cross section at fixed y then includes an integral over the perpendicular components of \mathbf{p}_{miss} . Relativistically, it is a little more complicated. y is determined from energy conservation, assuming no FSI and that the $A-1$ nucleus recoils with momentum y :

$$\nu + M_A = [M^2 + (q+y)^2]^{1/2} + (M_{A-1}^2 + y^2)^{1/2}. \quad (10)$$

At the QE peak, $\nu = Q^2/(2M)$, $x_B = 1$, and $y = 0$. As ν decreases, x_B increases and y decreases. By selecting x_B or y (at fixed Q^2), we can select the minimum initial momentum of the struck nucleon (see Fig. 13). At large enough Q^2 the function $F(y, Q^2)$ scales and depends only on y (Ciofi degli Atti, Pace, and Salmè, 1991). The nucleon momentum distribution $n(p = y)$ can be calculated from the derivative of the scaling function $dF(y)/dy$ at large Q^2 :

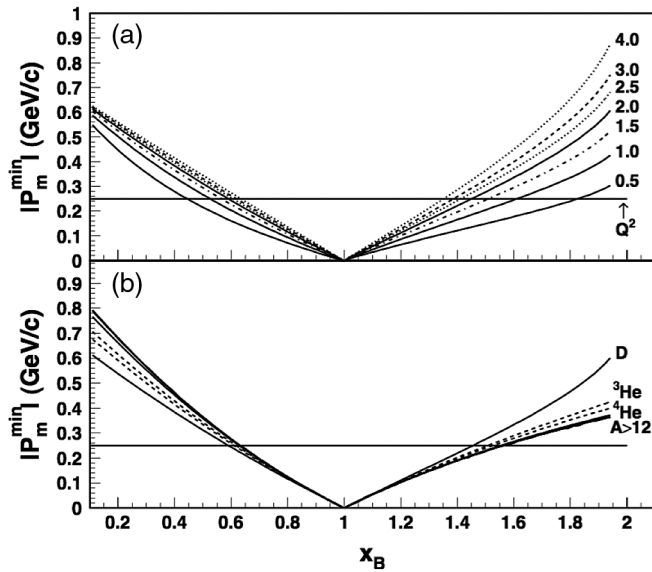


FIG. 13. The minimum momentum of the struck nucleon in inclusive (e, e') scattering as a function of x_B . (a) The minimum momentum for deuterium for a variety of momentum transfers. (b) The minimum momentum for a variety of nuclei at $Q^2 = 2$ GeV². The residual $A-1$ system is assumed to be in its ground state. From Egiyan *et al.*, 2003.

$$n(p) = \frac{-1}{2\pi p} \frac{dF(p)}{dp}. \quad (11)$$

Figure 14 shows the deuteron momentum distribution derived in this manner.

The original y -scaling model discussed here assumes that the residual $A-1$ nucleus is in a low-lying state. This procedure neglects the possibly large excitation energy of the residual nucleus, which is an important feature of the spectral function. As a result, for scattering by a nucleon in a SRC, the same internal momenta corresponds to a very different value of y for different nuclei.

Another approach is to compare the momentum distributions in different nuclei with reduced uncertainties by taking ratios of cross sections. We write the momentum density in terms of the light-cone variable α_m for the interacting nucleon belonging to the correlated pair,

$$\alpha_m = 2 - \frac{\nu - q + 2M}{2M} \left(1 + \sqrt{1 - 4M^2/W^2} \right). \quad (12)$$

Using this variable, the cross-section ratios do not depend on Q^2 in the kinematic range of the SLAC experiments (Day *et al.*, 1987). The onset of the plateaus discussed next occurs for the same values of α_m but for slightly different values of x_B .

Then the ratios of cross sections can be expressed in terms of the light-cone spectral function at large Q^2 and $1.5 < x_B < 2$ as (Frankfurt *et al.*, 1993)

$$\frac{\sigma_{A_1}(x_B, Q^2)}{\sigma_{A_2}(x_B, Q^2)} = \frac{\int \rho_{A_1}(\alpha_m, p_t) d^2 p_t}{\int \rho_{A_2}(\alpha_m, p_t) d^2 p_t} \approx \frac{n_A(p)}{n_D(p)}. \quad (13)$$

Thus this ratio of cross sections should be a function of α_m only, which, since it is a function of (Q^2, x_B) , is directly

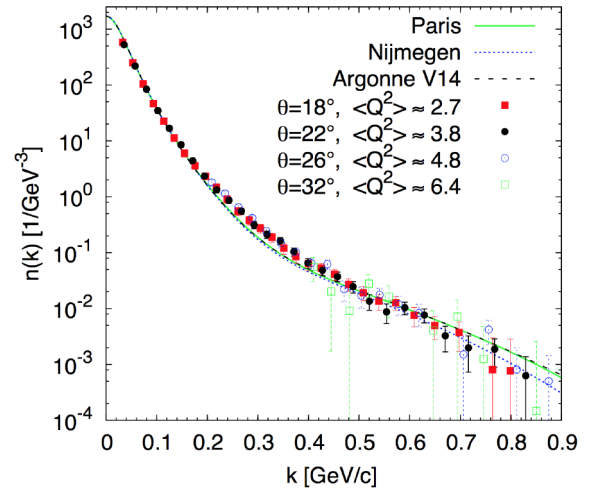


FIG. 14. Momentum distribution of the deuteron. Points show the results extracted from the experimental scaling function $F(y)$ at four different momentum transfers. Curves show the calculated momentum distributions using three different NN potentials Paris (Lacombe *et al.*, 1981), Nijmegen (Stoks *et al.*, 1994), and Argonne V14 (Wiringa, Stoks, and Schiavilla, 1995). The figure uses k for momentum instead of p . From Fomin *et al.*, 2012.

related to y , the minimum momentum of the struck nucleon. The approximate equality shown in Eq. (13) holds for $1.3 \leq \alpha_m \leq 1.7$ and $p > p_F$. The second approximate equality appearing in Eq. (13) is obtained using the relation $|\mathbf{p}| \approx M|1 - \alpha_m|/\sqrt{\alpha_m(2 - \alpha_m)}$. Measured ratios should be less sensitive to the influence of final state interactions, as discussed next. Nevertheless, the accuracy of replacing cross-section ratios by ratios of densities, as shown in Eq. (13), needs to be studied further. Furthermore, as yet there is no separate calculation of the numerator term of Eq. (13), i.e., the basic nuclear cross section for the (e, e') reaction at large values of x_B .

Physics at large values of x_B .—The next step is to use the inclusive (e, e') cross section to look for the effects of SRC pairs in nuclei by choosing kinematics where mean-field nucleons cannot contribute to the reaction. This is done by using $x_B > 1$. Just as conservation of four-momentum ensures that $x_B = 1$ is the kinematic limit for scattering from a single nucleon, $x_B = 2$ is the kinematic limit for scattering from a cluster of two nucleons and $x_B = 3$ is the kinematic limit for scattering from a three-nucleon cluster.

As a result, we can expand the (e, e') cross section into pieces due to electrons scattering from nucleons in two-, three-, and more-nucleon SRCs (Frankfurt and Strikman, 1981, 1988; Frankfurt *et al.*, 1993)

$$\sigma(x_B, Q^2) = \sum_{j=2}^A a_j(A) \sigma_j(x_B, Q^2), \quad (14)$$

where $\sigma_j(x_B, Q^2) = 0$ for $x_B > j$ and the $\{a_j(A)\}$ are proportional to the probability of finding a nucleon in a j -nucleon cluster. This is analogous to treating the nuclear structure in terms of independent nucleons, independent nucleon pairs, etc. Equation (14) is based on the lack of interference between amplitudes arising from scattering by clusters of different nucleon number that occurs because the important final states are different. Its importance lies in the fact that in a given kinematic region the ratio of cross sections can be used to determine information about short-range correlations.

If we consider only the a_2 term, then we can write

$$a_2(A) = \frac{2 \sigma_A(x_B, Q^2)}{A \sigma_d(x_B, Q^2)}. \quad (15)$$

This approximation should be valid for $1.5 < x_B \leq 2$. The effect of neglecting clusters of three or more nucleons has never been studied.

If the momentum distribution for $|y| > p_{\text{Fermi}}$ is dominated by nucleons in SRC pairs, then we expect that the momentum distributions for nucleus A and for deuterium should be almost identical. This similarity should show up as a plateau in the per nucleon cross-section ratio of the two nuclei. Figure 15 shows a sketch of this process.

The cross-section ratio of nucleus A to deuterium or to ${}^3\text{He}$ has been measured at SLAC (Frankfurt *et al.*, 1993) and at Jefferson Lab (Egiyan *et al.*, 2003, 2006; Fomin *et al.*, 2012). They have all observed a plateau in the cross-section ratio at $Q^2 > 1.4 \text{ GeV}^2$ and in the range $1.5 \leq x_B \leq 1.9$; see Fig. 16. This corresponds to $y \geq p_{\text{thresh}} = 275 \pm 25 \text{ MeV}/c$, which is

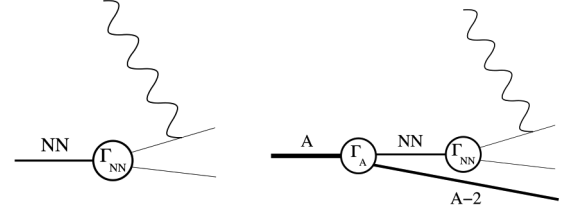


FIG. 15. Electron quasielastic scattering from a nucleon in deuterium (left) and from a nucleon in a SRC pair in a heavier nucleus (right). The labels Γ_{NN} and Γ_A refer to the deuteron and nuclear vertex functions, respectively.

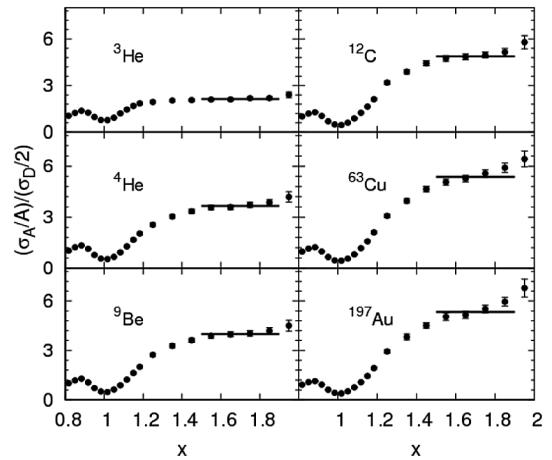
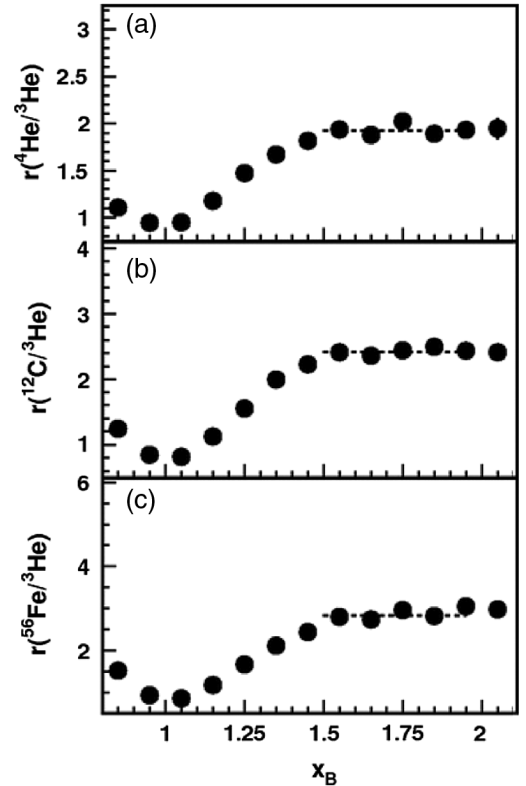


FIG. 16. Inclusive per nucleon cross-section ratios of (top) nuclei to ${}^3\text{He}$ at $1.4 < Q^2 < 2.6 \text{ GeV}^2$ and (bottom) nuclei to deuterium at $Q^2 = 2.7 \text{ GeV}^2$. Adapted from (top) Egiyan *et al.*, 2006, and (bottom) Fomin *et al.*, 2012.

slightly larger than the Fermi momentum in medium and heavy nuclei. The value of Q^2 is large enough to ensure that contributions from uncorrelated nucleons (with momentum governed by the size of the nucleus) are negligible.

However, in order to relate these observed plateaus to the ratio of momentum distributions in the different nuclei, we need to take into account the FSI of the nucleon with its correlated partner and with the residual system. For $Q^2 > 1 \text{ GeV}^2$ and $0.35 < \nu < 1 \text{ GeV}$, the space-time physics (Frankfurt *et al.*, 1993; Frankfurt, Sargsian, and Strikman, 2008) of the inclusive process tells us that final state interaction effects occur predominantly within the two-nucleon correlation. Such effects are independent of the nuclear target and should be small for large values of ν . The relevant values of ν are large enough so that final state interactions within the pair are not very important (Frankfurt and Strikman, 1981, 1988). Therefore, the effects of FSI will be approximately the same for high-momentum nucleons in deuterium and in heavier nuclei and will predominantly cancel in the cross-section ratios.

Some measurements (Egiyan *et al.*, 2003, 2006) applied isoscalar corrections to the ratios of Eq. (15) (i.e., they corrected for the unequal electron-proton and electron-neutron cross sections). Since the discovery of pn dominance in SRC pairs (see Sec. II.B), these corrections are no longer applied (Fomin *et al.*, 2012).

The flatness of the cross-section ratio plateau at $Q^2 > 1.4 \text{ GeV}^2$ and from $1.5 \leq x_B \leq 1.9$, and its approximate independence of Q^2 in this region where SRC effects dominate indicate the similarity of the momentum distributions in the two nuclei for $p > p_{\text{thresh}}$ and the validity of the expansion in Eq. (14). The onset of the plateau at $x_B = 1.5$ for $Q^2 > 1.4 \text{ GeV}^2$ indicates that the momentum distributions become similar at a threshold momentum of $p_i = p_{\text{thresh}} = 275 \pm 25 \text{ MeV}/c$ (Egiyan *et al.*, 2003). The height of the plateau $a_2(A)$ indicates the relative probability that a nucleon in nucleus A has high momentum ($p > p_{\text{thresh}}$) relative to a nucleon in deuterium.

In a naive model, this relative probability for a nucleon to have high momentum equals the relative probability that it belongs to an NN -SRC pair. However, even if all nucleons with $p > p_{\text{thresh}}$ belong to an NN -SRC pair as evident from the exclusive measurement (see Sec. II.B), we still need to consider the effects of pair motion. The high-momentum NN pair in the deuteron has center-of-mass momentum $p_{\text{c.m.}} = 0$. The nonzero center-of-mass momentum distribution of the pair in heavier nuclei will smear the high-momentum tail of the nucleon momentum distribution, increasing the cross-section ratio in the plateau region (Ciofi degli Atti *et al.*, 1991; Fomin *et al.*, 2012; Vanhalst, Ryckebusch, and Cosyn, 2012). This was found to be about a 20% effect in Fe. Thus, while the ratio of the proportion of high-momentum nucleons in Cu to deuterium is $a_2(A) = 5.4 \pm 0.1$, the ratio of the number of SRC NN pairs in Cu to deuterium (using the Fe correction factor) is about 20% less, $R_{2N} = 4.3 \pm 0.3$ (Fomin *et al.*, 2012).

Multiplying the 4% probability for a nucleon in deuterium to have momentum $p > p_{\text{thresh}}$ by the measured ratios in the plateau region [$a_2(A)$], as indicated by Eq. (13), gives us the

probabilities for a nucleon to have high momentum in ${}^4\text{He}$, C, Fe/Cu, and Au to be 14%, 19%, 21%, and 21%, respectively (Fomin *et al.*, 2012; Hen, Piaseutzky, and Weinstein, 2012).

Thus, the existence of a plateau in the measured per nucleon cross-section ratios of various nuclei to deuterium or ${}^3\text{He}$ at $Q^2 > 1.4 \text{ GeV}^2$ and $1.5 \leq x_B \leq 1.9$ shows that the momentum distributions of all nuclei at high momentum are similar and are thus dominated by $2N$ -SRC, that the threshold for “high momentum” is $p_{\text{thresh}} = 275 \pm 25 \text{ MeV}/c$, and that the probabilities for nucleons in nuclei to have high momentum range from 4% in deuterium to 21% in heavy nuclei.

While the inclusive scattering cross-section ratios of carbon and iron to ${}^3\text{He}$ measured by Egiyan are flat for $1.5 < x_B < 2$, the ratios of carbon, copper, and gold to deuterium measured by Fomin appear to slope upward slightly. This is not due to the choice of nucleus in the denominator, since the ratio of ${}^3\text{He}$ to deuterium measured by Fomin is flat. This is also probably not due to c.m. motion effects as these are similar for ${}^4\text{He}$ and ${}^{12}\text{C}$ (Tang *et al.*, 2003; Shneur *et al.*, 2007; Korover *et al.*, 2014), which do show flat ratios and are expected to be the same for heavy nuclei (Ciofi degli Atti and Simula, 1996; Colle *et al.*, 2014). This might be due to differences in kinematics. The Egiyan data cover $1.4 < Q^2 < 2.6 \text{ GeV}^2$ (concentrated at the lower values), while the Fomin data were taken at $Q^2 = 2.7 \text{ GeV}^2$. At $Q^2 = 1.5 \text{ GeV}^2$ and $1.5 \leq x_B \leq 2$, the minimum momentum of the struck nucleon ranges from 250 to 500 MeV/c , covering the expected region of tensor force dominance. However, at $Q^2 = 2.7 \text{ GeV}^2$, the minimum momentum of the struck nucleon ranges from 320 to 700 MeV/c , where central correlations could become important. It would be useful to measure the Q^2 dependence of the cross-section ratios in future SRC measurements.

D. Universal properties of short-range correlations in nuclei

The combined results from the exclusive and inclusive measurements described in Secs. II.B and II.C lead to a universal picture of SRC pairs in nuclei. In the conventional momentum-space picture, the momentum distribution for all nuclei and nuclear matter can be divided into two regimes, above and below the Fermi momentum (see Fig. 17). The region below the Fermi momentum accounts for about 80% of the nucleons in medium and heavy nuclei (i.e., $A \geq 12$) and can be described using mean-field approximations. The region with momenta greater than the Fermi momentum accounts for about 20%–25% of the nucleons (see the pie chart in Fig. 8) and is dominated by nucleons belonging to NN -SRC, predominantly pn -SRC.

The SRC dominance of the high-momentum tail implies that the shape of the momentum distributions of all nuclei at high momenta is determined by the short-range part of the fundamental NN interaction. The average number of SRC pairs is determined by global properties of the nucleus.

The specific predominance of pn -SRC over pp - and nn -SRC is largely associated with the large contribution of the tensor part of the NN interaction at short distances (Sargsian *et al.*, 2005; Schiavilla *et al.*, 2007; Alvioli, Ciofi degli Atti, and Morita, 2008), implying that the high-momentum distribution in heavier nuclei is approximately proportional to the

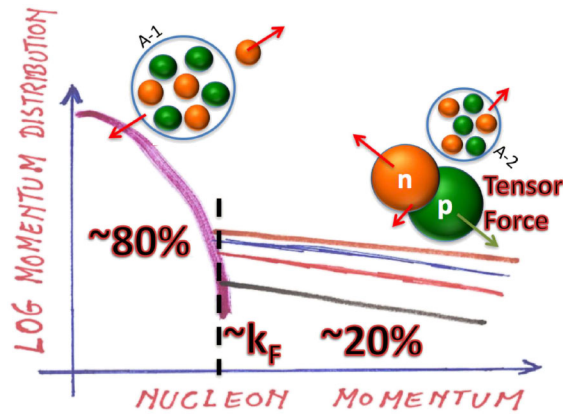


FIG. 17. A qualitative sketch of the dominant features of the nucleon momentum distribution in nuclei. At $k < k_F$, the nucleon momentum is balanced by that of the other $A - 1$ nucleons and can be described by mean-field models. At $k > k_F$, the nucleon belongs to a pn -SRC pair and its momentum is balanced by that of one other nucleon.

deuteron momentum distribution. Experimental and theoretical studies of the latter show that, for $300 \leq k \leq 600$ MeV/ c , $n(k) \propto 1/k^4$ (Hen, Weinstein *et al.*, 2015). This specific functional form follows directly from the dominance of the tensor force acting in second order; see Appendix A.1 for details.

The predominance of np -SRC pairs implies that, even in asymmetric nuclei, the ratio of protons to neutrons in SRC pairs will equal 1. This, in turn, implies that in neutron-rich nuclei, a larger fraction of the protons will be in an SRC pair (Hen *et al.*, 2014; Sargsian, 2014a), i.e., that a minority nucleon (e.g., a proton) has a higher probability of belonging to a high-momentum SRC pair than a majority nucleon (e.g., a neutron). This effect should grow with the nuclear asymmetry and could possibly invert the kinetic energy sharing such that the minority nucleons move faster on average than the majority. This asymmetry could have wide ranging implications for the Neutrinos at the Tevatron (NuTeV) anomaly (Zeller *et al.*, 2002) (see Secs. III.D.1 and VI.A.5), the nuclear symmetry energy and neutron star structure and cooling rates (Hen, Li *et al.*, 2015; Hen, Steiner *et al.*, 2016), neutrino-nucleus interactions (Acciarri *et al.*, 2014; Weinstein, Hen, and Piasetzky, 2016), and more. The study of the nuclear asymmetry dependence of the number of SRC pairs and their isospin structure is an important topic that could be studied in future high-energy radioactive beam facilities.

III. DEEP INELASTIC SCATTERING AND THE EMC EFFECT

Basic models of nuclear physics describe the nucleus as a collection of unmodified nucleons moving nonrelativistically under the influence of two-nucleon and three-nucleon forces, which can be treated approximately as a mean field. In such a picture, the partonic structure functions of bound and free nucleons should be identical. Therefore, it was generally expected that, except for nucleon motion effects, DIS experiments which are sensitive to the partonic structure of the nucleon would give the same result for all nuclei.

Instead, the measurements (Aubert *et al.*, 1983; Arneodo, 1994; Geesaman, Saito, and Thomas, 1995; Piller and Weise, 2000; Norton, 2003; Frankfurt, Guzey, and Strikman, 2012; Hen *et al.*, 2013; Malace *et al.*, 2014) show a reduction of the structure function of nucleons bound in nuclei relative to nucleons bound in deuterium in the valence quark region. We term this reduction the EMC effect. Since its discovery, over 30 years ago, a large experimental and theoretical effort has been put into understanding the origin of the effect. While theorists have had no difficulty in creating models that qualitatively reproduce nuclear DIS data by itself, there is no generally accepted model. This is because the models are either not consistent with or do not attempt to explain other nuclear phenomena.

The nuclear deep inelastic scattering data also show a reduction in the small x_B region of the structure function, known as the shadowing region. The physics of shadowing has been well reviewed (Frankfurt, Guzey, and Strikman, 2012) recently and is not a subject of the present review.

Section I.B showed that the nucleon-nucleon interaction leads to the existence of SRC pairs in nuclei and Sec. II showed the evidence for and our knowledge of the properties of these pairs.

This section will describe deep inelastic scattering and its relationship to nucleon parton distributions. The EMC effect and the limitations of conventional nuclear physics to explain it will then be discussed. Section IV presents the phenomenological relationship between the number of SRC pairs in a nucleus and the strength of the EMC effect and uses that relationship to gain new insight into the origin of the EMC effect.

A. DIS and nucleon structure functions

We begin with a brief description of deep inelastic scattering on a nucleon. See one of the many texts for details, e.g., Close (1979), Halzen and Martin (1984), Roberts (1994), Thomas and Weise (2001), or Collins (2013). The latest information is contained in the Particle Data Group tables (Olive *et al.*, 2014). The inclusive deep inelastic scattering process (e, e') involves a lepton scattering from a target, with only the final state lepton being detected. If spin variables are not observed, the process depends on only two variables, which are traditionally chosen to be the electron energy loss ν and negative of the four-momentum transfer from the lepton to the target $Q^2 = \mathbf{q}^2 - \nu^2$; see Fig. 18. At large enough values of

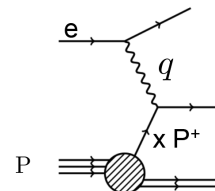


FIG. 18. Deep inelastic scattering at large values of Q^2 . A lepton (labeled e) scatters from a nucleon by emitting a spacelike virtual photon with four-momentum q , which is absorbed on a single quark with momentum fraction $x_B P^+$. Only the outgoing lepton is subsequently detected.

ν and Q^2 , conservation of momentum and energy leads to the result that the dynamical information can be encoded (at a given scale) in the structure functions $q(x_B)$, which is interpreted as the fraction of the target momentum carried by the struck quark.

Let us see how this arises. Four-momentum conservation, the idea that the quark is briefly free after absorbing the high-momentum photon, and ignoring the emissions of gluons gives

$$(k+q)^2 = m_q^2, \quad (16)$$

where k is the four-momentum of a quark in the target, and m_q is the quark mass. Let the spatial momentum of the photon lie in the negative z direction and using the light-front momentum variables, e.g., $P^\pm \equiv P^0 \pm P^3$, where P^μ is the target four-momentum, we have $q^- = \nu + \sqrt{\nu^2 + Q^2} = \nu + |\mathbf{q}|$, $q^+ = \nu - |\mathbf{q}|$, $q^- \gg q^+$, so that Eq. (16) can be rewritten as

$$k^+ = \frac{Q^2 - k^2 - q^+k^- + m_q^2}{\nu + \sqrt{\nu^2 + Q^2}}. \quad (17)$$

If the quark is on its mass shell (as is the case with light-front wave functions) then $k^2 = m_q^2$. Furthermore, if the quantity $q^+k^- \ll Q^2$, the numerator becomes simply Q^2 . Then one defines a dimensionless, Lorentz invariant variable by dividing the resulting equation by P^+ , so that

$$\frac{k^+}{P^+} \approx \frac{Q^2}{P^+(\nu + \sqrt{\nu^2 + Q^2})} \equiv \xi, \quad (18)$$

where ξ is the Nachtmann variable. We see that the fraction of target momentum (plus component) is simply ξ . This explains why deep inelastic scattering shows the scaling phenomenon. The relevant dynamical variable k^+/P^+ depends only on one specific combination of ν and Q^2 . Note that this description is frame independent. One need not go to the infinite momentum frame to understand scaling or the parton model.

If one further takes the Bjorken limit ($\nu^2 \gg Q^2$), then

$$\frac{k^+}{P^+} = \frac{Q^2}{2P^+q_\mu} \equiv x_B.$$

The dominant dependence on x_B is called Bjorken scaling, and its discovery, using hydrogen and deuterium targets (to obtain the neutron information), was the primary evidence for the existence of quarks within the nucleon.

Quarks are confined, so they are never on their mass shell. The off-mass shell effects, however, decrease with increasing values of Q^2 and are regarded as ‘‘higher twist.’’ Such effects could be important at Jefferson Lab energies. Effects of final state interactions (which depend on the kinematics of the probing beam) are not contained in the light-front wave function (Cosyn, Melnitchouk, and Sargsian, 2014).

Suppose the struck quark is confined in a nucleon of four-momentum p^μ that is bound within a nucleus of momentum P^μ . Then we have

$$\frac{k^+ p^+}{p^+ P^+} = \xi, \quad (19)$$

where a nucleus of momentum P^+ contains a nucleon of momentum of p^+ which contains a quark of momentum k^+ . This is the origin of the convolution model to be discussed in Sec. III.C.1. Therefore, in order to calculate deep inelastic scattering from nuclei we need to know the nuclear wave function, expressed in light-front variables.

More formally, one derives the expression for the momentum distribution (the probability that a quark has a given value of k^+/P^+), known as a quark distribution function, by starting with the square of the invariant scattering amplitude. The important part of this amplitude depends on the hadronic tensor $W^{\mu\nu}$, which is a matrix element of a commutator of electromagnetic current operators. After expanding in terms of the separation r of the spatial variable of the two current operators, the momentum distribution (for a specific flavor of quark) is given in the Bjorken scaling limit (in which the variable Q^2 is not explicit) by the Fourier transform (Thomas and Weise, 2001)

$$q(\xi) = \frac{1}{2\pi} \int dr^- e^{iq^+r^-} \langle P | \psi_+^\dagger(r^-) \psi_+(0) | P \rangle_c, \quad (20)$$

where $|P\rangle_c$ is the proton wave function, the subscript c denotes a connected matrix element, ψ is the quark field operator, the subscript $+$ denotes multiplication by the projection operator $(1 + \gamma^0 \gamma^3)/2$, and r^- is the minus component of the separation distance.

Parton distributions are needed for a wide variety of applications in high-energy physics. $q(x_B, Q^2)$ has been determined for various flavors and for a wide range of values of x and Q^2 . Vast amounts of data are now codified as parton distributions, giving the probability as a function of Q^2 that a given flavor of quark carries a momentum fraction x_B ; see Fig. 19.

This section is concerned with nucleon targets, but (as previously mentioned) we need to know how to evaluate a nuclear version of Eq. (20), which would involve nuclear wave

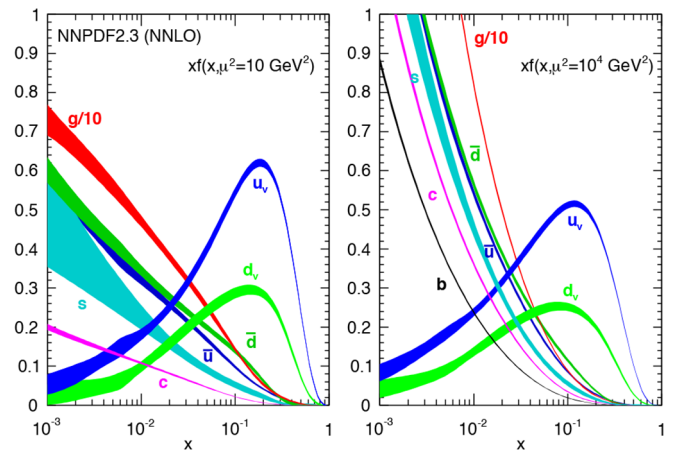


FIG. 19. The bands show x_B times the unpolarized parton distributions for the different parton flavors $\{u_v, d_v, u, d, s = \bar{s}, c = \bar{c}, b = \bar{b}, \text{ and } g\}$ obtained in NNLO NNPDF2.3 global analysis (Ball *et al.*, 2013), at $Q^2 = 10$ and 10^4 (GeV/c) 2 , with $\alpha_s(M_Z^2) = 0.118$. Here $x = x_B$. From the PDG, Olive *et al.*, 2014.

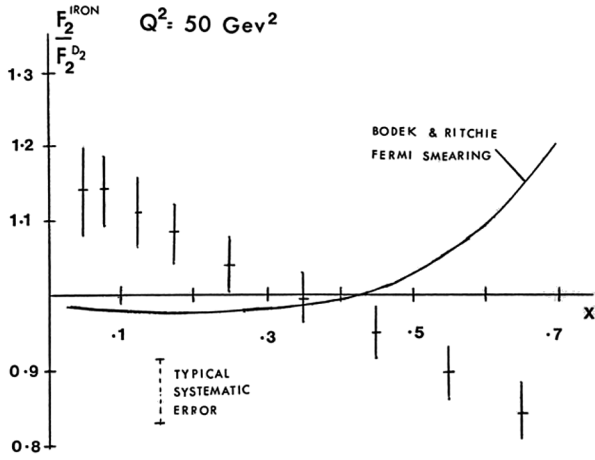


FIG. 20. Image of the EMC data as it appeared in the November 1982 issue of the CERN Courier. This image nearly derailed the refereed publication, as the editor argued that the data had already been published. From [Aubert *et al.*, 1983](#).

functions expressed in terms of light-front variables. This difficulty has been handled ([Frankfurt and Strikman, 1981, 1988](#); [Blunden, Burkardt, and Miller, 1999](#); [Miller and Machleidt, 1999b](#); [Miller, 2000](#); [Miller and Smith, 2002](#); [Smith and Miller, 2002](#)). One can implement light-front coordinates using a simple transformation. This works because the nucleus does not contain a significant $N\bar{N}$ content.

B. The EMC effect

As stated, the discovery of Bjorken scaling was made using hydrogen and deuterium targets. It occurred to many experimentalists that MeV-scale nuclear effects should be negligible at GeV-scale momentum and energy transfers and that therefore they could increase their experimental statistics by using nuclear targets. Surprisingly, the CERN European Muon Collaboration found that the per nucleon (e, e') cross-section ratio of iron to deuterium was not unity ([Aubert *et al.*, 1983](#)); see Fig. 20. This surprising result, now called the EMC effect, was confirmed by many groups, culminating with the high-precision electron and muon scattering data from SLAC, Fermilab, New Muon Collaboration (NMC) at CERN, and Jefferson Lab; see Fig. 21. See one of the many EMC reviews for details ([Arneodo, 1994](#); [Geesaman, Saito, and Thomas, 1995](#); [Piller and Weise, 2000](#); [Norton, 2003](#); [Hen *et al.*, 2013](#); [Malace *et al.*, 2014](#)).

The conclusion from the combined experimental evidence was that the effect had a universal shape, was independent of the squared four-momentum transfer Q^2 starting from remarkably small values of Q^2 (see Fig. 22), increased with nuclear mass number A , and increased with the average nuclear density. An early study ([Bickerstaff and Miller, 1986](#)) of the Q^2 dependence of nuclear effects showed that the nuclear binding and dynamical rescaling models predict very little variation with Q^2 over the range from 4 to 10^4 GeV 2 .

One way to characterize the strength of the EMC effect is to measure the average slope of the cross-section ratio for $0.35 \leq x_B \leq 0.7$. Plotting this slope versus the average nuclear density for light nuclei (see Fig. 23) shows that the EMC effect

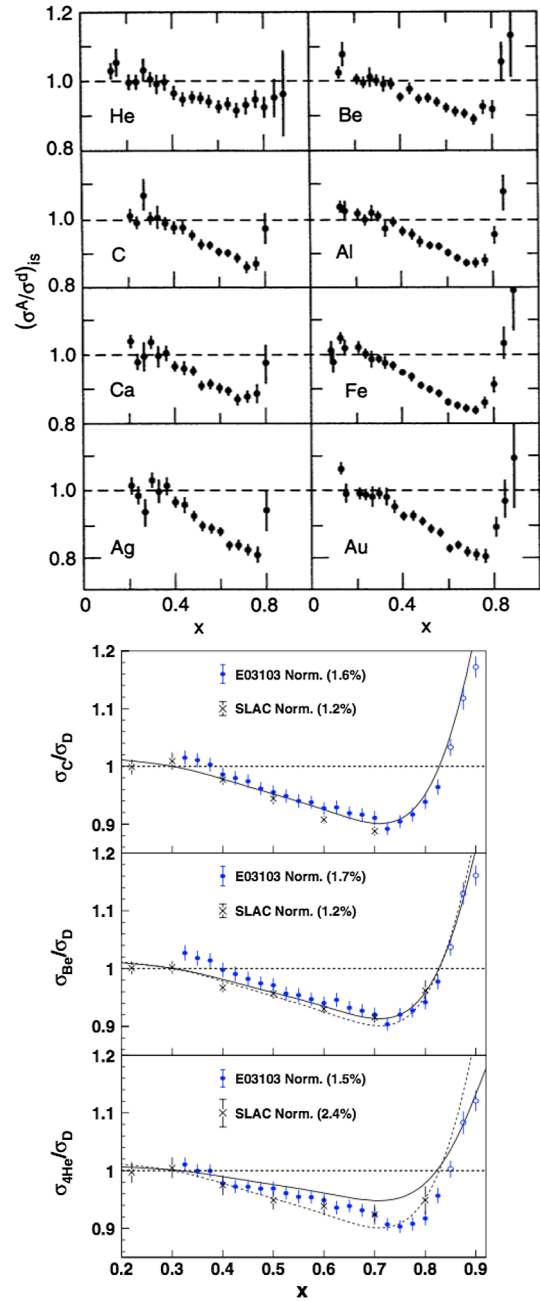


FIG. 21. The per nucleon cross-section ratio of various nuclei to deuterium as measured at (top) SLAC ([Gomez *et al.*, 1994](#)) and (bottom) Jefferson Lab ([Seely *et al.*, 2009](#)). The solid curves show the A -dependent fit to the SLAC data ([Gomez *et al.*, 1994](#)), while the dashed curve is the SLAC fit to ^{12}C . From (top) [Gomez *et al.*, 1994](#), and (bottom) [Seely *et al.*, 2009](#).

does not simply depend on average density. Since ^9Be can be described as a pair of tightly bound alpha particles plus one additional neutron, it was suggested that the local density is more important than the average density ([Seely *et al.*, 2009](#)). See an early discussion by [Frankfurt and Strikman \(1981\)](#).

The immediate parton model interpretation of the data at high x is that the valence quarks of a nucleon bound in a nucleus carry less momentum than those of free nucleons. This notion seems uncontested, but determining the underlying origin remained an elusive goal for a long time.

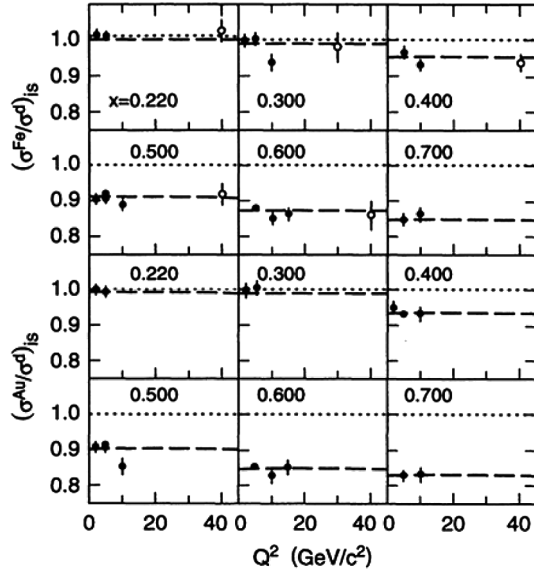


FIG. 22. The Q^2 dependence of the EMC ratio for iron at various values of x_B . From Gomez *et al.*, 1994.

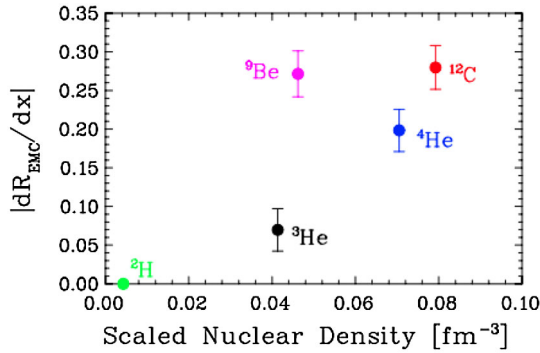


FIG. 23. The slope of the EMC effect for $0.35 \leq x_B \leq 0.7$ plotted vs the average nuclear density for various light nuclei as measured at Jefferson Lab. From Seely *et al.*, 2009.

The great number of models created to explain the EMC effect caused Miller (1988) to write that ‘‘EMC means everyone’s model is cool.’’

C. Why conventional nuclear physics cannot explain the EMC effect

1. Nucleons only

One must first try to explain the EMC effect using only the simple kinematic effects of binding energy and Fermi motion without modifying the bound nucleon structure. If the nucleon structure function is not modified and is the same on and off the energy shell (nucleon-only hypothesis), then evaluation of the diagram of Fig. 24 leads to the following simple convolution formula:

$$\frac{F_{2A}(x_A)}{A} = \int_{x_A}^A dy f_N(y) F_{2N}(x_A/y), \quad (21)$$

where P is the total four-momentum of the nucleus, and

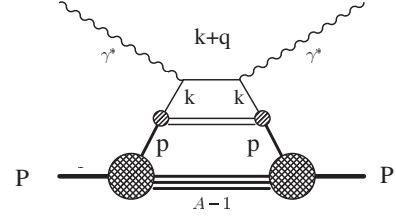


FIG. 24. Deep inelastic scattering diagram. A virtual photon γ^* of momentum q is absorbed on a quark of momentum k contained in a nucleon of momentum p in a nucleus of momentum P . The imaginary part of this diagram corresponds to the hadronic tensor $W^{\mu\nu}$. Adapted from Miller and Smith, 2002.

$$x_A \equiv \frac{Q^2 A}{2P \cdot q} = \frac{x_B A M}{M_A} \quad (22)$$

with M and M_A as the free nucleon and nuclear masses, respectively. x_A can be thought of as a version of x_B corrected for the average nucleon binding energy. The variable $y = A p^+ / P^+$ is the fraction of the nuclear momentum (per nucleon) carried by a single nucleon, and $f_N(y)$ is the corresponding probability distribution. The origin of the convolution formula can be understood using the simple terms of Sec. III.A. Suppose the struck quark is confined in a nucleon (of four-momentum p) that is bound within a nucleus of momentum P . Then from Eq. (19) we have

$$\xi \approx k^+ / P^+ = (k^+ / p^+) (p^+ / P^+) = x_A / y. \quad (23)$$

This accounts for a nucleon in the nucleus of momentum p^+ that contains a quark of momentum k^+ . A proper evaluation of deep inelastic scattering from nuclei therefore involves knowledge of the nuclear wave function, expressed in light-front variables.

There were many attempts to explain the EMC effect without invoking medium modifications. We cite a few of the references with others to be found in the reviews: Jung and Miller (1988, 1990), Ciofi Degli Atti and Liuti (1989), Akulinichev and Shlomo (1990), Dieperink and Miller (1991), Marco, Oset, and Fernandez de Cordoba (1996), Benhar, Pandharipande, and Sick (1997, 1999), and Benhar and Sick (2012).

The appeal of the nucleon-only idea can be understood using a simple caricature of the probability that the nucleon carries a momentum fraction y . The width of the function $f_N(y)$ is determined by the Fermi momentum divided by the nucleon mass, which is small. In the absence of interactions, $f_N(y)$ is peaked at $y = 1$. If the average separation energy $S \equiv \epsilon M$ (which for nuclear matter can be as large as 70 MeV) (Dieperink and Miller, 1991; Benhar, Pandharipande, and Sick, 1997, 1999; Benhar and Sick, 2012), then $f_N(y)$ is peaked at about $y = 1 - \epsilon$. Taking for simplicity a zero width approximation

$$f_N(y) = \delta[y - (1 - \epsilon)], \quad (24)$$

then the convolution formula [Eq. (21)] tells us that

$$\frac{F_{2A}(x_A)}{A} \approx F_{2N}\left(\frac{x_A}{1-\epsilon}\right). \quad (25)$$

As shown in Fig. 19 the structure function falls rapidly with increasing x_B , so that a slight increase in the argument leads to a significant decrease in the structure function. In particular,

$$\frac{F_{2A}(x_A)}{AF_{2N}(x_A)} \approx 1 + \epsilon \frac{F'_{2N}(x_A)}{F_{2N}(x_A)} \approx 1 - \gamma\epsilon, \quad (26)$$

where we assumed $F_{2N}(x_B) \sim (1-x_B)^\gamma$ at large x_B with $3 \leq \gamma \leq 4$.

Frankfurt and Strikman (1987) using a more detailed calculation found that a value of $\epsilon = 0.04$ was sufficient to reproduce the early EMC data. However, we show that the ideas of shifting the value of x_A based on binding energy or separation energy considerations violates rigorous (Collins, 2013) baryon and momentum sum rules and therefore cannot be a viable explanation of the EMC effect. Consider a nuclear model in which nucleons are the only degrees of freedom. There is a conserved baryon current and an energy-momentum tensor expressed in terms of these constituents. This means that when expressed in terms of the convolution approach of the previous section we must have the momentum sum rule

$$\int dy y f_N(y) = 1, \quad (27)$$

where the factor of y represents the momentum. The use of Eq. (24) in Eq. (27) leads immediately to a substantial violation of the momentum sum rule

$$\int dy y f_N(y) = 1 - \epsilon. \quad (28)$$

Frankfurt and Strikman (1987) also included an important relativistic correction known as the “flux factor,” which significantly reduces the effects of nuclear binding.

Going beyond the zero width approximation only makes this problem worse (Miller and Machleidt, 1999a). The inclusion of the effects of short-range correlations broadens the function $f_N(y)$ leading to a value of the ratio that exceeds unity for small values of x , an effect found earlier by Dieperink and Miller (1991). A violation of the sum rule by a few percent is actually a big violation, because the EMC effect itself is only a 10%–15% effect. Thus nucleon-only models are logically inconsistent and therefore wrong, even if they can be arranged to describe the data.

One might argue that sum rules cannot be applied directly to the data because of the need to incorporate initial and final state interactions. Nevertheless, in using the convolution formalism in the nucleon-only approximation one must use a light-front wave function of the nucleus consistent with the conservation of baryon number and momentum as discussed. There is no way to avoid the constraints imposed by the sum rules.

Indeed, the application of sum rules and simple reasoning shows that Eq. (21) leads to the result that the nucleon-only hypothesis cannot explain the EMC effect. Under the Hugenholtz–van Hove theorem (Hugenholtz and van Hove, 1958; Miller and Smith, 2002; Smith and Miller, 2002)

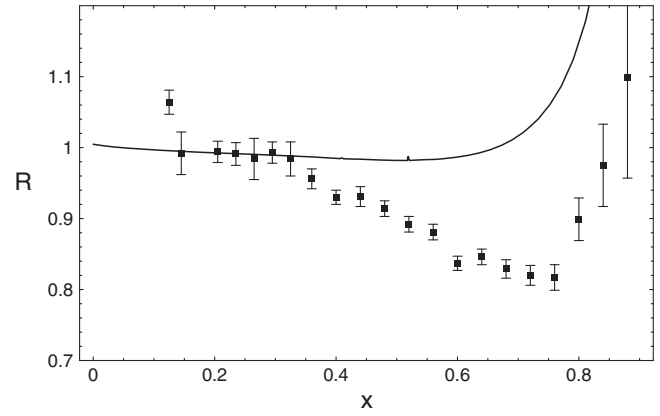


FIG. 25. The measured EMC effect in gold (Gomez *et al.*, 1994) compared to a nucleons-only calculation of the EMC effect in lead. From Smith and Miller, 2002.

nuclear stability (pressure balance) implies (in the rest frame) that $P^+ = P^- = M_A$. But to an excellent approximation $P^+ = A(M_N - 8 \text{ MeV})$. Thus an average nucleon has $p^+ = M_N - 8 \text{ MeV}$. As caricatured in Eq. (24), the function $f_N(y)$ is narrowly peaked because the Fermi momentum is much smaller than the nucleon mass. This means that the value of y in the integral of Eq. (21) is constrained to be very near unity. Thus F_{2A}/A is well approximated by F_{2N} and one gets no substantial EMC effect this way (Miller and Smith, 2002; Smith and Miller, 2002). This is shown as the solid curve in Fig. 25.

2. Nucleons plus pions

Nucleons-only models fail, but it was natural to consider the idea that the missing momentum ϵ of Eq. (28) is carried by non-nucleonic degrees of freedom, e.g., pions (Ericson and Thomas, 1983; Llewellyn Smith, 1983). In this case,

$$P^+ = P_N^+ + P_\pi^+ = M_A. \quad (29)$$

Many (Frankfurt and Strikman, 1988; Arneodo, 1994; Geesaman, Saito, and Thomas, 1995; Piller and Weise, 2000) found that using $P_\pi^+/M_A = 0.04$ is sufficient to account for the EMC effect. However, if nuclear pions carry 4% of the nuclear momentum (in the rest frame the plus component of momentum is the nuclear mass), then there should be more nuclear sea quarks (i.e., both quarks and antiquarks). This enhancement should be observable in a nuclear Drell-Yan experiment (Bickerstaff, Birse, and Miller, 1984, 1986; Ericson and Thomas, 1984). The idea (see Fig. 26) is that a quark from an incident proton (defined by a large value of x_1) annihilates an antiquark from the target nucleus (defined by a smaller value of x_2). A significant enhancement of pions would enhance the antiquarks and enhance the nuclear Drell-Yan reaction. But no such enhancement was observed (Alde *et al.*, 1990) as shown in Fig. 27. This caused Bertsch, Frankfurt, and Strikman (1993) to announce “a crisis in nuclear theory” because conventional theory does not work. This statement is the verification of the title of this section.

The reader might ask at this stage if the two-pion exchange effects discussed in the Appendix and Secs. I and II lead to a

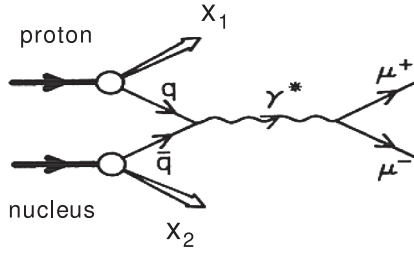


FIG. 26. The Drell-Yan process. A quark with momentum fraction x_1 from the incident proton annihilates with an antiquark from the nuclear target with momentum fraction x_2 to form a timelike virtual photon which decays to a $\mu^+\mu^-$ pair. Adapted from Bickerstaff, Birse, and Miller, 1986.

significant pion content and an enhanced sea in the nucleus. Explicit calculations show that the pionic content associated with the tensor potential is very small (Miller, 2014).

Subsequent work has confirmed that an intrinsic modification of the nucleon structure function is needed to explain the EMC effect (Kulagin and Petti, 2006, 2010, 2014; Frankfurt and Strikman, 2012; Hen *et al.*, 2013). This result had been expected for some time, as stated explicitly “The change of the structure functions in nuclei (EMC effect) gives direct evidence for the modification of quark properties in the nuclear medium” (Walecka, 2005). The following sections discuss specific proposals for such modifications.

D. Beyond conventional nuclear physics: Nucleon modification

The failure of the nucleon-only or nucleon + pion models to explain the EMC and Drell-Yan data indicates that the structure of a nucleon bound in a nucleus significantly differs from that of a free nucleon. The medium modifies the nucleon.

This is not surprising, as there are evident simple examples. A free neutron undergoes β decay, so it can be thought of as having a $|pe^- \nu\rangle$ component. When bound in a stable nucleus, the neutron is stable. This “medium modification” suppresses the $|pe^- \nu\rangle$ component. Additionally, in the $(e, e'p)$ reaction shown in Fig. 28, four-momentum conservation shows that the

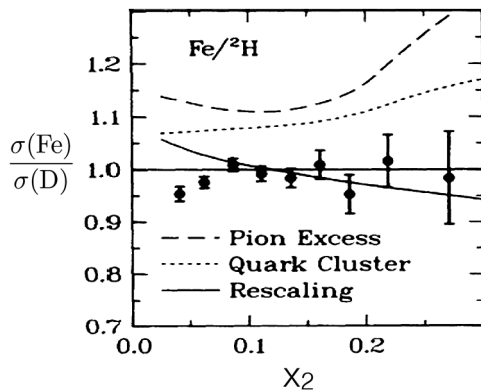


FIG. 27. Drell-Yan experimental results. Ratio of Drell-Yan cross sections as a function of the momentum fraction x_2 of a quark in the nucleus. The version of the rescaling model does not reproduce the nuclear deep inelastic scattering data (Bickerstaff, Birse, and Miller, 1985, 1986). Adapted from Alde *et al.*, 1990.

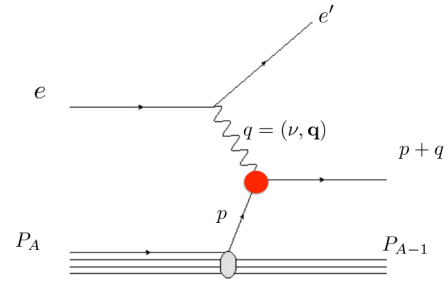


FIG. 28. The $A(e, e'p)$ reaction in the plane wave impulse approximation. A nucleus of four-momentum P emits a nucleon of four-momentum p that absorbs a virtual photon of four-momentum q to make a nucleon of four-momentum $p + q$, with $(p + q)^2 = M^2$, where M is the nucleon mass. The blob represents the in-medium electromagnetic form factors.

square of the initial four-momentum of the struck nucleon p cannot satisfy $p^2 = M^2$. Thus the form factor of a nucleon bound in the nucleus cannot be the same as that for a free nucleon; it is instead the amplitude for a transition between a virtual nucleon of mass $\sqrt{p^2}$ and a physical nucleon of mass M .

Now we must ask: what is the origin of the medium modification? This question is coupled to the broader questions listed in Sec. I and more deeply to the very nature of confinement.

The parton model interpretation of the large- x_B part of the EMC effect is that the medium reduces the nuclear structure functions for large x_B , so that there are fewer high-momentum quarks in a nucleus than in free space. This momentum reduction leads, via the uncertainty principle, to the notion that quarks in nuclei are confined in a larger volume than that of a free nucleon.

There are two general ways to realize this simple idea: mean-field effects cause bound nucleons to be larger than free ones, or nucleon-nucleon interactions at close range cause the nucleon structure to be modified, by including either NN^* configurations or six-quark configurations that are orthogonal to the two-nucleon wave functions. All of the papers seeking to explain the EMC effect using medium modification use one of the two ideas (that are sketched in Fig. 29).

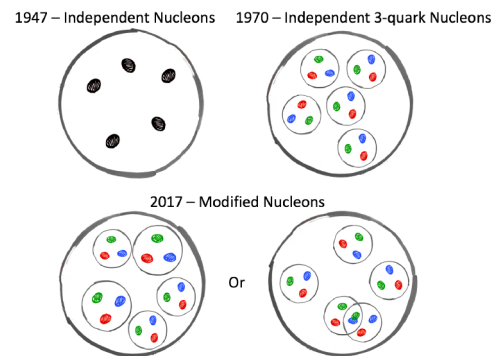


FIG. 29. Evolution of nuclear physics from structureless nucleons in the 1940s to independent three-quark nucleons in the 1970s to the modified nucleons of today, either modified single nucleons (left) or modified two-nucleon configurations (right).

Since only about 20% of nucleons belong to SRC pairs (Fig. 17), 5 times more nucleons would be modified by mean-field effects than by nucleon-nucleon interactions at close range. Therefore, if nucleons are modified only at short range, then the modifications needed to explain the EMC effect would have to be 5 times larger than if all nucleons were modified by mean-field effects.

A phenomenological assessment of this idea in which the mean-field and SRC-related origins of the EMC effect were treated phenomenologically was made by Hen *et al.* (2013). The separation of the spectral function Eq. (7) into terms arising from low-lying excited states P_0 and higher-energy continuum states related to short-range correlations P_1 was used. In the mean-field model, a nucleus-independent modification of F_2 was included in the contribution to the nucleon distribution function $f_N(y)$ [Eq. (21)] arising from P_0 . In the alternate model a much larger nucleus-independent modification of F_2 was included in the contribution to $f_N(y)$ arising from P_1 . Both approaches gave reasonably good descriptions of the nuclear DIS data.

We next describe specific models associated with the two different mechanisms.

1. Mean field

In mean-field models of nucleon modification, the interaction between nucleons occurs by the exchange of mesons between quarks confined in different nucleons. Four general models of the quarks confined in the nucleon have been used for this. The earliest model [quark-meson coupling (QMC)] used the Massachusetts Institute of Technology (MIT) bag model to represent the three confined quarks in the proton (Guichon, 1988; Guichon *et al.*, 1996; Stone *et al.*, 2016). Later work used the QMC model with more general confinement mechanisms (Blunden and Miller, 1996), the covariant Nambu–Jona-Lasinio (NJL) model (Cloet, Bentz, and Thomas, 2006, 2009, 2016) and the chiral quark soliton model (Diakonov *et al.*, 1996; Smith and Miller, 2003, 2004, 2005). In these models the attraction needed to produce a bound state is generated by the exchange of scalar quantum numbers [either by a scalar meson (Guichon, 1988; Guichon *et al.*, 1996; Stone *et al.*, 2016) or by pairs of pions (Smith and Miller, 2003, 2004, 2005)] and the repulsion needed to obtain nuclear saturation is caused by exchange of vector mesons. Within these mean-field models the exchanged mesons are treated as classical static fields, and as such these mesons do not interact with the photon probe.

We next explain two classes of models. The chiral quark soliton model (CQSM) is based on the instanton-dominated nature of the vacuum (Negele, 1999). The coupling of quarks to vacuum instantons spontaneously generates a constituent quark mass of about 400 MeV. These quarks interact with pions through an effective CQSM Lagrangian. This model reproduces nucleon properties well, including structure functions which vanish at $x_B = 0$ and 1 (Diakonov *et al.*, 1996).

Nuclei are formed by collections of such nucleons exchanging scalar and vector mesons (Smith and Miller, 2003, 2004, 2005). Excellent saturation properties were obtained. The dominant effect of the medium is a slight broadening of the effective potential that binds the quarks in the nucleon. The

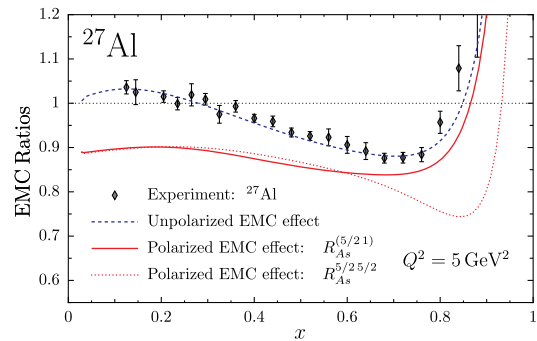


FIG. 30. The measured EMC effect for ^{27}Al (Gomez *et al.*, 1994) compared to QMC calculations of both the regular and the polarized EMC effects. From Cloet, Bentz, and Thomas, 2006.

use of the medium-modified wave function to compute structure functions allows one to account for the EMC effect, while still agreeing with the Drell-Yan data. This indicates that the sea is not very modified.

The next model places an NJL-model nucleon in the medium (NJLMM) which is a relativistic extension of the earlier QMC including the effects of spontaneous symmetry breaking. Here the external scalar field enhances the lower component of the quark's Dirac wave function by about 15%. This model describes the EMC effect well (see Fig. 30). It also predicts an enhancement of the EMC effect for spin structure functions (Cloet, Bentz, and Thomas, 2005b) in nuclei which could be measured at Jefferson Lab (see Sec. VI.A.4).

The NJLMM predicts the effects of having different numbers of neutrons N and protons Z . Cloet, Bentz, and Thomas (2009) explained that a neutron or proton excess in nuclei leads to an isovector-vector mean field which, through its coupling to the quarks in a bound nucleon, causes the quark distributions to be evaluated at a shifted value of the Bjorken scaling variable (Mineo *et al.*, 2004; Detmold, Miller, and Smith, 2006). In relativistic mean-field models, the effect of a vector field is to shift the energy and therefore the value of the plus component of momentum of the single-particle state. The isovector-vector mean field is represented by the ρ^0 , and in this work its strength is chosen to reproduce the nuclear symmetry energy. In a nucleus such as ^{56}Fe or ^{208}Pb where $N > Z$, the ρ^0 field causes the u quark to feel a small additional vector attraction and the d quark to feel additional repulsion. This effect leads to a significant correction to the NuTeV measurement of $\sin^2 \Theta_W$ (Zeller *et al.*, 2002). The sign of this correction is largely model independent, and it accounts for approximately two-thirds of the NuTeV anomaly. Thus the NuTeV measurement provides further evidence for the medium modification of the bound nucleon wave function.

Both sets of mean-field models predict modification of nucleon electromagnetic form factors. The QMC model predicts modifications to both G_E and G_M (Lu *et al.*, 1999), while the chiral quark soliton model modifies only G_E (Smith and Miller, 2004). Both models predict the same ratio G_E/G_M . Note that electron-nucleus quasielastic data were used (Sick, 1985) to put a limit of between 3% and 6% on the possible increase of the nucleon radius in nuclear matter. None of the mean-field models discussed here violate this limit.

The QCD eigenstates of a free nucleon form a complete set. Thus the medium-modified nucleon can be regarded as a superposition of the nucleon and all of its excited states.

Despite the general success of mean-field models it must be noted that none predicts significant extra high-momentum strength in the nuclear momentum distribution. Therefore, it is very difficult to see how they could reproduce the plateaus observed in the cross-section ratios at $x_B \geq 1.5$ seen in Sec. II.C.

2. Suppression of pointlike configurations

We can also make a more general model of the nucleon as a superposition of various configurations or Fock states, each with a different quark-gluon structure. Figure 31 shows a two-component nucleon where one component is “bloblike” (BLC) with the normal nucleon size and the other is “pointlike” (PLC). The BLC can be thought of as an object that is similar to a nucleon. The PLC is meant to represent a three-quark system of small size that is responsible for the high- x behavior of the distribution function. The smaller the number of quarks, the more likely one can carry a large-momentum fraction. Furthermore, because the PLC is smaller than the BLC, the uncertainty principle tells one that quarks confined in the PLC have higher momentum. The small-sized configuration (with its small number of $q\bar{q}$ pairs) is very different than a low-lying nucleon excitation.

When placed in a nucleus, the bloblike configuration feels the regular nuclear attraction and its energy decreases. The pointlike configuration feels far less nuclear attraction because the effects of gluons emitted by small-sized configurations are canceled in low-momentum transfer processes. This effect is termed color screening and has been verified in several different reactions (Frankfurt, Miller, and Strikman, 1994; Dutta, Hafidi, and Strikman, 2013). The nuclear attraction increases the energy difference between the BLCs and the PLCs, therefore reducing the PLC probability (Frankfurt and Strikman, 1985). The PLC is suppressed. Reducing the probability of PLCs in the nucleus reduces the quark momenta in agreement with the EMC effect.

This idea was studied (Frank, Jennings, and Miller, 1996) using a relativistic constituent quark model for the nucleon (Schlumpf, 1992, 1993). A nucleon is placed in the nucleus and therefore subject to a mean field that vanishes for configurations in which the three quarks are close together. The quark momentum distribution decreases for $x_B > 0.3$; see

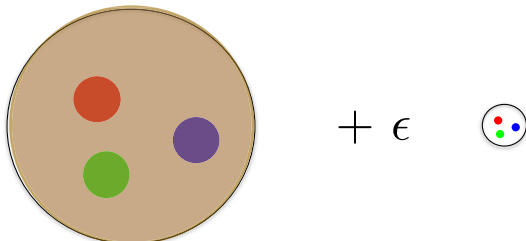


FIG. 31. Two-component nucleon model: normal-sized component plus pointlike configuration component.

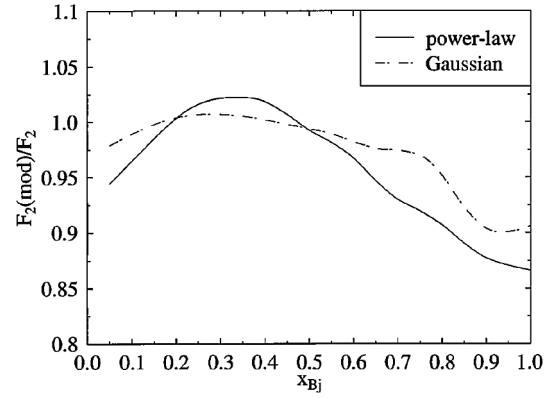


FIG. 32. The ratio of F_2 in the nucleus to the free F_2 (the EMC ratio) in the pointlike configuration suppression model. From Frank, Jennings, and Miller, 1996.

Fig. 32. The effects of nucleon motion are not included, so there is no rise for large values of x_B , and the dip at low values of x_B would be removed by such effects. This model gives only a 2.5% enhancement at $x_B = 0.5$ because the enhancing effects of large virtuality discussed below were not included. The PLC model, being a modification at large values of x_B , does not contradict the nuclear Drell-Yan data; see Sec. III.

The notion that different constituents of the nucleon have different sizes and therefore different interaction strengths is directly related to medium modifications of all kinds. The main features of this idea can be understood using a simple schematic two-component model of the nucleon with a dominant normal-sized bloblike constituent (denoted by B) and a very small pointlike constituent (denoted by P). The Hamiltonian is given by the matrix

$$H_0 = \begin{bmatrix} E_B & V \\ V & E_P \end{bmatrix}, \quad (30)$$

where $E_P \gg E_B$. Because of the hard-interaction potential V that connects the two components, the eigenstates of H_0 are $|N\rangle$ and $|N^*\rangle$ rather than $|B\rangle$ and $|P\rangle$. In lowest-order perturbation theory, the eigenstates are given by

$$|N\rangle = |B\rangle + \epsilon|P\rangle, \quad (31)$$

$$|N^*\rangle = -\epsilon|B\rangle + |P\rangle, \quad (32)$$

with $\epsilon = V/(E_B - E_P)$. We assume $|V| \ll E_P - E_B$, so that the nucleon is mainly $|B\rangle$ and its excited state is mainly $|P\rangle$, and also take $V > 0$. We use the notation $|N^*\rangle$ to denote the state that is mainly a PLC, but the PLC as discussed does not resemble a low-lying baryon resonance.

Now suppose the nucleon is bound to a nucleus. The nucleon feels an attractive nuclear potential H_1 :

$$H_1 = \begin{bmatrix} U & 0 \\ 0 & 0 \end{bmatrix} \quad (33)$$

to represent the idea that only the large-sized component of the nucleon feels the influence of the nuclear attraction.

The treatment of the nuclear interaction U as a number is clearly a simplification. The interaction varies with the relevant kinematics, and our model explicitly includes this dependence. Our model is similar to the model of [Frankfurt and Strikman \(1985\)](#), with the important difference that the medium effects will enter as an amplitude instead of as a probability. In [Frank, Jennings, and Miller \(1996\)](#) the PLC is subject to a nonzero, but small, attractive potential that fluctuates with the nucleon configurations. The complete Hamiltonian $H = H_0 + H_1$ is now given by

$$H = \begin{bmatrix} E_B - |U| & V \\ V & E_P \end{bmatrix}, \quad (34)$$

in which the attractive nature of the nuclear binding potential is emphasized. Then interactions with the nucleus increase the energy difference between the BLC and the PLC, which decreases the PLC probability.

The medium-modified nucleon and its excited state $|N\rangle_M$ and $|N^*\rangle_M$ are now (using first-order perturbation theory)

$$|N\rangle_M = |B\rangle + \epsilon_M |P\rangle, \quad (35)$$

$$|N^*\rangle_M = -\epsilon_M |B\rangle + |P\rangle, \quad (36)$$

where

$$\epsilon_M = \frac{V}{E_B - |U| - E_P} = \epsilon \frac{E_B - E_P}{E_B - |U| - E_P} \quad (37)$$

so that the PLC probability in the medium is suppressed. Both ϵ_M and ϵ are less than zero, so that $\epsilon_M - \epsilon > 0$.

The medium-modified nucleon $|N\rangle_M$ may be expressed in terms of the unmodified eigenstates $|N\rangle, |N^*\rangle$ as

$$|N\rangle_M \approx |N\rangle + (\epsilon_M - \epsilon)|N^*\rangle. \quad (38)$$

Within this model the medium-modified nucleon contains a component that is an excited state of a free nucleon. The amount of modification $\epsilon_M - \epsilon$, which gives a deviation of the EMC ratio from unity, is controlled by the potential U . An initial pioneering qualitative description of the EMC effect was obtained ([Frankfurt and Strikman, 1985](#)) (at $x_B = 0.5$, where effects of Fermi motion are small) using $U = -40$ MeV and $E_P - E_B \sim 500$ MeV. The present treatment instead calculates the effects of the medium on the amplitude instead of the probability, so that the effects are generally larger. We explore this further in [Sec. IV.B](#).

The PLC-suppression model also predicts changes to the elastic electric and magnetic form factors $G_{E,M}$. The electromagnetic form factor in free space is obtained as

$$F = \frac{1}{1 + \epsilon^2} (\langle B|J|B\rangle + 2\epsilon\langle B|J|P\rangle + \epsilon^2\langle P|J|P\rangle), \quad (39)$$

where momentum and spin labels have been suppressed.

It is instructive to examine what to expect at both high- and low-momentum transfer. At low-momentum transfer the first term dominates so that the spatial extent of the nucleon and its

modification in the medium are important. [Frankfurt and Strikman \(1985\)](#) estimated the value of $\langle r^2 \rangle$. Assuming that only the bloblike configuration $|B\rangle$ contributes to this long-ranged observable, one finds

$$\langle r^2 \rangle = \frac{\langle B|r^2|B\rangle}{1 + \epsilon^2}. \quad (40)$$

In the medium the potential U acts, so the value of ϵ is changed to ϵ_M . Since $|\epsilon_M| < |\epsilon|$, immersion of the nucleon in the medium suppresses the pointlike components and increases $\langle r^2 \rangle$. The effect is of order $\epsilon(\epsilon_M - \epsilon)$, which was estimated to be between 2% and 5%.

At high-momentum transfer, the term $2\epsilon\langle B|J|P\rangle$ becomes dominant. Then the change in the form factor is of order $\epsilon - \epsilon_M$, which is a larger effect.

Application of the PLC-suppression idea presented in the present two-state model is schematic: it does not distinguish between the electric G_E and magnetic G_M form factors.

A more detailed evaluation was included by [Frank, Jennings, and Miller \(1996\)](#). Medium modifications of the proton form factors were predicted as shown in [Fig. 33](#). The important modifications shown by the red arrows occur at larger values of momentum transfer than currently accessible experimentally. [Figure 33](#) shows fairly significant effects greater than about 10% (consistent with our present analysis) for the individual form factors. Experimentally it is easier to measure the medium modifications of the ratio G_E/G_M . The figure shows that since both G_E and G_M are decreased, the change in the ratio G_E/G_M is expected to be smaller.

In addition to the medium modifications, [Frank, Jennings, and Miller \(1996\)](#) also predicted the more spectacular decrease ([Jones *et al.*, 2000](#); [Gayou *et al.*, 2002](#); [Punjabi *et al.*, 2005](#)) in the free-proton ratio G_E/G_M with increasing values of Q^2 .

3. Six-quark bags and the EMC effect

One of the earliest attempts to understand the EMC effect ([Carlson and Havens, 1983](#); [Jaffe, 1983](#); [Bickerstaff, Birse, and Miller, 1984](#)) was to hypothesize that part of the time one nucleon is part of a six-quark configuration ([Pirner and Vary, 1981](#)) [who predicted the existence of plateaus in (e, e') cross-section ratios] that is orthogonal to any two-nucleon wave

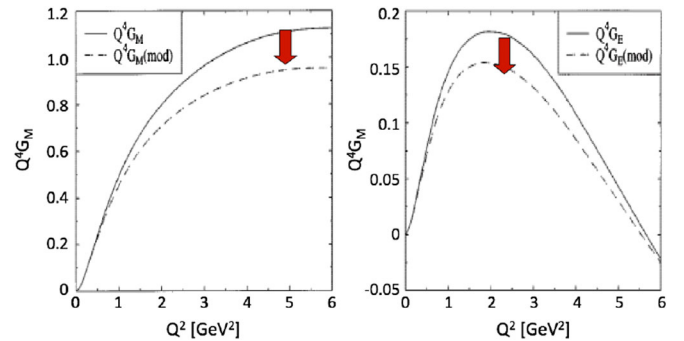


FIG. 33. Medium modification of form factors. Figure adapted with slight modifications. Adapted from [Frank, Jennings, and Miller, 1996](#).

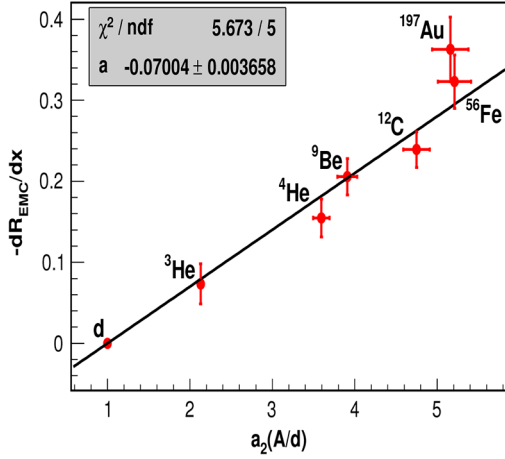


FIG. 34. The slope of the EMC effect (R_{EMC} , ratio of nuclear to deuteron cross section) for $0.35 \leq x_A \leq 0.7$ plotted vs $a_2(A)$, the SRC scale factor (the relative probability that a nucleon belongs to an SRC NN pair) for a variety of nuclei. The fit parameter $a = -0.070 \pm 0.004$ is the intercept of the line constrained to pass through the deuteron (and is therefore also the negative of the slope of that line). From Hen *et al.*, 2013.

function. Because a six-quark configuration is larger than a nucleon, the quarks are partially deconfined. Larger confinement volumes are associated with lower momenta and therefore with a suppression of the structure function. The idea was usually implemented through the MIT bag model or by guessing the related structure functions. Several reviews discuss this idea (Gerald A. Miller, 1984; Berger and Coester, 1987; Frankfurt and Strikman, 1988; Sloan, Voss, and Smadja, 1988; Mulders, 1990; Arneodo, 1994; Geesaman, Saito, and Thomas, 1995; Norton, 2003). It was relatively easy to use this idea to compute a wide variety of nuclear phenomena (Miller and Kisslinger, 1983; Guichon and Miller, 1984; G. A. Miller, 1984; Gerald A. Miller, 1984; Koch and Miller, 1985; Miller, 2014), but the calculation of each new observable was accompanied by the need to incorporate an additional free parameter. The use of six-quark

models that describe nuclear DIS led to predictions of large effects in the nuclear Drell-Yan process discussed in Sec. III.C, but little modification was seen (Fig. 27), severely limiting the applicability of six-quark bag models. In addition, in some applications the necessary six-quark bag probability needed to reproduce the EMC effect is so large as to conflict with knowledge of nuclei (Farrar *et al.*, 1988).

For a recent study of the possible influence of hidden-color and short-range correlation effects at EIC energies, see Miller, Sievert, and Venugopalan (2016).

IV. THE EMC-SRC CORRELATION

A. Experimental overview

While there is no obvious connection between DIS scattering from quarks in the nucleus at $0.3 \leq x_B \leq 0.7$ and QE scattering from nucleons in the nucleus at $1.5 \leq x_B < 2$, analysis of world data showed a remarkable correlation (see Fig. 34) between the magnitude of the EMC effect in nucleus A and the probability that a nucleon in that nucleus is part of a $2N$ -SRC pair (Weinstein *et al.*, 2011; Hen, Piasetzky, and Weinstein, 2012).

The strength of the EMC effect for nucleus A is characterized as the slope of the ratio of the per nucleon deep inelastic electron scattering cross sections of nucleus A relative to deuterium dR_{EMC}/dx in the region $0.35 \geq x_B \leq 0.7$ (Seely *et al.*, 2009). This slope is proportional to the value of the cross-section ratio at $x_B \approx 0.5$, but is unaffected by overall normalization uncertainties that merely raise or lower all of the data points together. Table I shows data from the x_A corrected EMC data base of Hen *et al.* (2013) which used the EMC data of Gomez *et al.* (1994) and Seely *et al.* (2009).

The SRC scale factors were determined from the isospin-corrected per-nucleon ratio of the inclusive (e, e') cross sections on nucleus A and ^3He or deuterium. Columns 2–4 of Table I show the SRC scale factors measured by Frankfurt *et al.* (1993), Egiyan *et al.* (2006), and Fomin *et al.* (2012). The large uncertainties in the SRC ratios of Frankfurt *et al.* (1993) are due to extrapolating data from different experiments measured

TABLE I. A compilation of world data on SRC scaling factors $a_2(A)$ and EMC slopes dR_{EMC}/dx . Columns 2–4 show the SRC scaling factors extracted from various measurements. Column 5 shows the SRC scale factor prediction of Weinstein *et al.* (2011) based on the EMC-SRC correlation. Column 6 shows the world average of the EMC effect slope as compiled by Weinstein *et al.* (2011), using the data of Gomez *et al.* (1994) and Seely *et al.* (2009). See the text for details.

Nucleus	Frankfurt <i>et al.</i> (1993) $a_2(A)$	Egiyan <i>et al.</i> (2006) $a_2(A)$	Fomin <i>et al.</i> (2012) Excluding the c.m. motion correction	Weinstein <i>et al.</i> (2011) EMC-SRC prediction $a_2(A)$	Weinstein <i>et al.</i> (2011) EMC slope (dR_{EMC}/dx)
Column No.	2	3	4	5	6
^3He	1.7 ± 0.3	1.97 ± 0.10	2.13 ± 0.04		-0.070 ± 0.029
^4He	3.3 ± 0.5	3.80 ± 0.34	3.60 ± 0.10		-0.197 ± 0.026
^9Be			3.91 ± 0.12	4.08 ± 0.60	-0.243 ± 0.023
^{12}C	5.0 ± 0.5	4.75 ± 0.41	4.75 ± 0.16		-0.292 ± 0.023
^{56}Fe (^{63}Cu)	5.2 ± 0.9	5.58 ± 0.45	5.21 ± 0.20		-0.388 ± 0.032
^{197}Au	4.8 ± 0.7		5.16 ± 0.22	6.19 ± 0.65	-0.409 ± 0.039
EMC-SRC slope		0.079 ± 0.006	0.084 ± 0.004		
$\frac{\sigma(u+p)}{\sigma_d} \Big _{x_B=0.7}$		1.032 ± 0.004	1.034 ± 0.004		
χ^2/ndf		0.7688/3	4.895/5		

at different kinematics. The SRC ratios measured by Egiyan *et al.* (2006) were used in the original EMC-SRC analysis of Weinstein *et al.* (2011). The later results of Fomin *et al.* (2012) include ^{63}Cu rather than ^{56}Fe ; the SRC scaling factor of ^{63}Cu is assumed to be the same as that of ^{56}Fe . The values of ^9Be and ^{197}Au in the fifth column are those predicted by Weinstein *et al.* (2011) based on the measured EMC effect and the linear EMC-SRC correlation. These predictions are in remarkable agreement with the later results of Fomin *et al.* (2012). Following Hen, Piasetzky, and Weinstein (2012), the (Fomin *et al.*, 2012) results are shown without the center-of-mass motion correction (i.e., including inelastic, radiative, and Coulomb corrections only). Applying the SRC-pair center-of-mass motion correction decreases the ratios by 10% to 20%.

The EMC effect correlates imperfectly with other A -dependent quantities [see Seely *et al.* (2009) and Arrington, Daniel *et al.* (2012) and references therein]. In general, nuclei with $A \geq 4$ fall on one straight line but deuterium and ^3He do not. This is true when the EMC effect is plotted versus A , $A^{-1/3}$, or the average nuclear separation energy. When plotting the EMC effect versus average nuclear density, ^9Be is a clear outlier (see Fig. 23). This indicates that the excellent correlation with the SRC scale factor is not just a trivial by-product of their mutual A dependence.

The correlation between the EMC effect and the SRC scale factor is robust (Hen, Piasetzky, and Weinstein, 2012). It applies to both SRC data sets of Egiyan *et al.* (2006) and Fomin *et al.* (2012). The quality of the correlation also does not depend on the corrections applied to the SRC data. These corrections include isoscalar cross-section corrections, center-of-mass motion corrections, and isoscalar pair-counting corrections. The isoscalar correction to the SRC scale factors accounts for the different elementary electron-neutron and electron-proton cross sections. This has a negligible effect on the fit quality and the extracted fit parameter. Fomin *et al.* did not apply this correction, arguing that short-range correlations are dominated by np pairs. Fomin *et al.* also argued that the SRC scale factors measured the relative probability of finding a high-momentum nucleon in nucleus A relative to deuterium and that these scale factors needed to be corrected for the c.m. motion of the pair in order to determine the relative probability that a nucleon in nucleus A belongs to an SRC pair. As shown in both Hen, Piasetzky, and Weinstein (2012) and Arrington, Daniel *et al.* (2012), including the pair c.m. motion correction improves the EMC-SRC correlation only slightly.

This EMC-SRC correlation gives new insight into the origin of the EMC effect. As discussed in Sec. III, many different explanations of the EMC effect have been proposed since 1983. After accounting for the standard nuclear effects of binding energy and Fermi motion, explanations for the EMC effect fall into two general categories, those that require modifications of mean-field nucleons and those that require modifications of high-momentum (large virtuality) nucleons.

The linear correlation between the strength of the EMC effect and the SRC scale factors indicates that possible modifications of nucleon structure occurs in nucleons belonging to SRC pairs. This implies that the EMC effect, like short-range correlations, is a short-distance, high-virtuality, and high-density phenomenon.

B. Theory overview

1. High-momentum nucleons and PLC suppression

Next we try to use the EMC-SRC correlation to better understand the relationship between short-range correlations measured in the $A(e, e')$ reaction and deep inelastic scattering reactions. Both processes involve a probe that strikes a nucleon of four-momentum p in the nucleus (see Fig. 28). It is natural to expect that the medium modification depends on the virtuality $v(\mathbf{p}, E)$ of the struck nucleon (Ciofi degli Atti *et al.*, 2007):

$$v \equiv p^2 - M^2 = (P_A - P_{A-1})^2 - M^2. \quad (41)$$

In the $(e, e'p)$ reaction in PWIA (see Fig. 28), the nucleon initial momentum opposes the $A-1$ recoil momentum $\mathbf{p} = -\mathbf{P}_{A-1}$. Using the recoil mass $M_{A-1}^* = M_A - M + E$, where $E > 0$ represents the excitation energy of the spectator nucleus [known as the removal energy (Ciofi degli Atti and Simula, 1996)], we find

$$v(\mathbf{p}, E) = \left(M_A - \sqrt{(M_{A-1}^*)^2 + \mathbf{p}^2} \right)^2 - \mathbf{p}^2 - M^2, \quad (42)$$

which reduces to

$$v(\mathbf{p}, E) \approx -2M \left(\frac{A}{A-1} \frac{\mathbf{p}^2}{2M} + E \right) \quad (43)$$

in the nonrelativistic limit. The magnitude of the virtuality $v(\mathbf{p}, E)$ increases with both the $A-1$ excitation energy and the initial momentum of the struck nucleon.

Frankfurt and Strikman (1985) and Ciofi degli Atti *et al.* (2007) obtained a relation between the potential U of Sec. III.D.2 and the virtuality $v(\mathbf{p}, E)$ by using an extension of the Schrödinger equation to an operator form:

$$\frac{\mathbf{p}^2}{2M_r} + U = -E, \quad (44)$$

where $M_r = M(A-1)/A$, and U is the interaction that both binds the nucleon to the nucleus and modifies its structure. The simple idea behind Eq. (44) is that if the nucleon binding energy is fixed, then the NN interaction energy U must become more negative as the kinetic energy becomes more positive. In this work the modification of nuclear properties was found to be proportional to $v(\mathbf{p}, E)$ for moderate values of the virtuality. It should be noted that the short-range correlations give a dominant contribution to the average nucleon virtuality, which naturally leads to an approximate proportionality of the EMC effect to a_2 .

Comparing this equation with Eq. (43) one finds

$$U = \frac{v(\mathbf{p}, E)}{2M_r}, \quad (45)$$

so that the modification of the nucleon due to the PLC suppression is proportional to its virtuality. Potentially large

values of the virtuality greatly enhance the difference between ϵ_m and ϵ .

Now we need to understand how the structure function changes in the medium. In principle one needs to calculate the hadronic tensor $W^{\mu\nu}$ and $q(x)$ for the medium-modified nucleon of Eq. (38) by replacing the state $|P\rangle$ in Eq. (20) by the state $|N\rangle_M$. To leading order, the change in the structure function will be linear in $\epsilon_M - \epsilon$. The hadronic part is an off-diagonal matrix element between a free physical nucleon $|N\rangle$ and a free physical state $|N^*\rangle$. Thus the modification is the product of a coefficient that depends on the medium and a term that is independent of the medium.

These hadronic matrix elements have not yet been calculated. Instead we adopt a phenomenological approach, based on the suppression of pointlike configurations (Frankfurt and Strikman, 1985; Frank, Jennings, and Miller, 1996), where the medium-modified quark structure function is given by

$$q_M(x) = q(x) + (\epsilon_M - \epsilon)f(x)q(x), \quad (46)$$

with the suppression of pointlike components manifest by the condition $df/dx < 0$, so that the ratio of structure functions is given by $R(x) = q_M(x)/q(x)$, so that

$$\frac{dR}{dx} = (\epsilon_M - \epsilon)\frac{df}{dx}. \quad (47)$$

Equation (47) is only meaningful for $x_B < 0.7$ where Fermi motion effects can be ignored. Given that $\epsilon_M - \epsilon > 0$ (as discussed), Eq. (47) shows that the slope of the EMC ratio is negative, consistent with observations.

Ciofi degli Atti *et al.* (2007) calculated the expected size of the modification of Eq. (45) using the spectral function $P(\mathbf{p}, E)$ of Ciofi degli Atti and Simula (1996) (as discussed in Sec. I.B.3). The average values of the virtuality are quite large, as can be seen from Table II. The average kinetic and removal energies in channel 1 (high excitation final states) are much larger than the corresponding quantities in channel 0 (low excitation final states) and the high-momentum components are linked to high removal energies (Ciofi degli Atti, Pace, and Salme, 1980). Ciofi degli Atti *et al.* (2007) showed that these values of the virtuality, for reasonable choices of E_B and E_P , can account for the EMC effect at $x_B \approx 0.5$.

This shows that high-momentum nucleons in nuclei can cause the EMC effect. Now we need to find a similar relation between these high-momentum nucleons and the plateaus observed at high x_B in inclusive (e, e') QE scattering. We first

TABLE II. The virtualities (in MeV) for channels 0 and 1 [see Eq. (7)] and their sum (Ciofi degli Atti *et al.*, 2007).

A	$\langle v_0(\mathbf{p}, E) \rangle / 2M$	$\langle v_1(\mathbf{p}, E) \rangle / 2M$	$\langle v(\mathbf{p}, E) \rangle / 2M$
^3He	-7.15	-27.44	-34.59
^4He	-26.82	-42.58	-69.40
^{12}C	-33.17	-49.11	-82.28
^{16}O	-31.40	-48.28	-79.68
^{40}Ca	-35.00	-49.54	-84.54
^{56}Fe	-31.66	-50.76	-82.44
^{208}Pb	-32.87	-59.33	-92.20

review the kinematics. We assume that the virtual photon is absorbed by one of the baryons contained in an interacting system of two baryons $M_2 \approx M_d$. The virtual photon hits a baryon of momentum p in a “deuteron” of momentum P , and the second, spectator baryon has momentum $p_s = P - p$. The struck nucleon has final momentum $p_f = p + q$. Let the plus component of p be given as aM_d . The light-front fraction a is related to the Frankfurt-Strikman variable α by $a = \alpha M/M_d$. Then

$$p_f^- = \frac{p_\perp^2 + M^2}{aM_d + q^+} > 0, \quad (48)$$

$$p_s^- = \frac{p_\perp^2 + M^2}{(1-a)M_d} > 0. \quad (49)$$

In our convention $q^+ < 0$ so that Eq. (48) tells us that $a > 0$ and Eq. (49) tells us that $a < 1$. Conservation of energy tells us that $p_f^+ + p_f^- + p_s^+ + p_s^- = 2(M_d + \nu)$, which leads to a quadratic equation for a :

$$(aM_d + q^+)(1-a)M_d = \frac{M_d + q^+}{M_d + q} (p_\perp^2 + M^2). \quad (50)$$

The condition that Eq. (50) for a has real roots leads to limits on the value of p_\perp .

Figure 35 shows the results of a specific example using $Q^2 = 2.7 \text{ GeV}^2$ and $p_\perp = 0$. Solving Eq. (50) gives the resulting values of α as a function of x_B . We see that α is considerably greater than 1 for $1.5 < x_B < 1.8$, corresponding to the plateau region of Fig. 16. Using the displayed values of α we can calculate $v(\mathbf{p}, E = p^0)$:

$$v(\mathbf{p}, p^0) = p^+ p^- - p_\perp^2 - M^2, \quad (51)$$

where

$$p^+ = aM_d, \quad p^- = \frac{M^2 + p_\perp^2}{aM_d + q^+} - q^-.$$

Then the use of Eq. (45) gives the values shown in Fig. 35: Thus, for $1.5 < x_B < 1.8$, we have

$$270 < |U| < 600 \text{ MeV}. \quad (52)$$

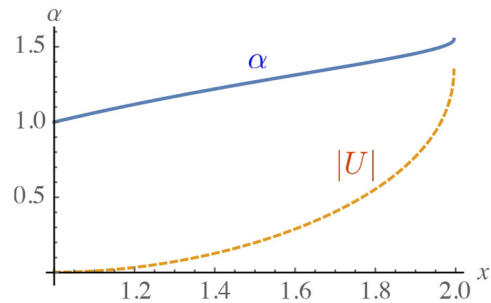


FIG. 35. α (solid line), $|U|$ (dashed line) for $Q^2 = 2.7 \text{ GeV}^2$ and $p_\perp = 0$. The quantity $|U|$ is presented in units of the nucleon mass M and is proportional to the virtuality $v(\mathbf{p}, E)$ via Eq. (45)

Such large values of $|U|$ can only arise from hard interactions of two nucleons, i.e., at short range.

Thus (e, e') at high x_B is associated with short-range correlations. Next we relate the virtuality to the observed plateaus in the cross-section ratios. Ciofi degli Atti and Simula (1996b) showed that, for large values of $|\mathbf{p}|$,

$$n_A(\mathbf{p}) \approx n_A^{(1)}(\mathbf{p}) \approx a_2(A)n_D(\mathbf{p}). \quad (53)$$

This relation is explained in the Appendix.

To summarize, there is a consistent picture in which short-range correlations are involved with significant modification of the nuclear quark distribution function by suppressing the pointlike configurations. The key feature is that larger values of the nuclear excitation energy E , associated with the short-range correlations, correspond to larger values of virtuality and therefore to more significant deformations of the nucleon. These very same short-range correlations are also responsible for the validity of Eq. (53) for large values of momentum (where the virtuality is large), which via the logic of Frankfurt and Strikman (1981, 1988) and Frankfurt *et al.* (1993) is responsible for the cross-section ratio plateaus. The spectral function $P(\mathbf{p}, E)$ contains the information necessary to compute both the virtuality needed to understand the DIS EMC effect and the momentum probability $n_A(\mathbf{p})$ needed to understand the plateaus.

2. Effective field theory

It is not necessary that the suppression of pointlike configurations for off-shell nucleons be the sole origin of the EMC effect. Indeed another dynamical idea could also account for the experimental findings. For example, the presence of non-nucleonic six-quark clusters (Sec. III.D) in nuclei could be important. A more general approach, using EFT, which is not specific as to the underlying mechanism of medium modification, has been presented (Beane and Savage, 2005; Chen and Detmold, 2005; Chen *et al.*, 2016). Chen *et al.* (2016) showed that the empirical linear relation between the magnitude of the EMC effect in deep inelastic scattering on nuclei and the short-range correlation scaling factor a_2 extracted from high-energy quasielastic scattering at $x_B \geq 1$ is a natural consequence of scale separation and derived the relationship using effective field theory.

Their EFT analysis proceeds by studying the dominant (leading-twist) parton distributions determined by target matrix elements of bilocal light-cone operators. Applying the operator product expansion, the Mellin moments of the parton distributions,

$$\langle x_B^n \rangle_A(Q) = \int_{-A}^A x_B^n q_A(x_B, Q) dx_B, \quad (54)$$

are determined by matrix elements of local operators. Each of the QCD operators is matched to hadronic operators (Chen and Detmold, 2005). The relative importance of the hadronic operators in a nuclear matrix element can be systematically estimated from EFT power counting. The nuclear matrix element is given by

$$\langle x_B^n \rangle_A(Q) = \langle x_B^n \rangle_N(Q) [A + \alpha_n(\Lambda, Q) \langle A | (N^\dagger N)^2 | A \rangle_\Lambda], \quad (55)$$

where α_n depends on Λ but not A and is completely determined by the two-nucleon system. This relation is valid for all n , so after an inverse Mellin transform, the isoscalar parton distribution functions (PDFs) satisfy

$$\frac{1}{A} F_2^A(x_B, Q) = F^N(x_B, Q) + g_2(A, \Lambda) \tilde{f}_2(x_B, Q, \Lambda), \quad (56)$$

where

$$g_2(A, \Lambda) = \frac{1}{A} \langle A | (N^\dagger N)^2 | A \rangle_\Lambda, \quad (57)$$

and $f_2(x_B, Q, \Lambda)$ is an unknown function independent of A . This feature is similar to that of our Eq. (47). Indeed, Eq. (56) was also obtained phenomenologically by Frankfurt and Strikman (1981, 1988) using the impulse approximation. Equation (56) appears also in Kulagin and Petti (2006, 2010, 2014) and Hen *et al.* (2013). Note that g_2 receives dominant contributions from the single-nucleon density.

The factorization scale of the PDF is $\mu_f = Q$, while Λ is the nuclear physics ‘‘ultraviolet’’ cutoff that separates the high-energy parton physics from lower-energy hadronic and nuclear effects. The two scales must be significantly separated for the EFT description to be valid.

The second term on the right-hand side of Eq. (56) is the nuclear modification of the structure function. The shape of distortion, i.e., the x_B dependence of f_2 , which is due to physics above the scale Λ , is A independent and hence universal among nuclei. The magnitude of distortion g_2 , which is due to physics below the scale Λ , depends only on A and Λ .

At smaller values of Q^2 , the previous analysis was generalized to apply to the (e, e') cross section at large x_B , so that

$$\sigma_A/A = \sigma_N + g_2(A, \Lambda)\sigma_2(\Lambda), \quad (58)$$

where E_0 (incident electron energy), x_B , and Q^2 dependence of σ_i is suppressed. With σ_N vanishing for $x_B > 1$, for both DIS and QE,

$$a_2(A, x_B > 1) = \frac{g_2(A, \Lambda)}{g_2(2, \Lambda)}. \quad (59)$$

In principle, a_2 could depend on E , x_B , and Q^2 . However, the EFT factorization shows that this dependence cancels at this order yielding a plateau in a_2 as observed experimentally at $1.5 < x_B < 2$. (The influence of Fermi motion extends the contribution of the single-nucleon PDF to x_B above 1, pushing the onset of the plateau to larger values of x_B .) The function a_2 was also computed using the Green’s function Monte Carlo method (Carlson *et al.*, 2015) and it agrees well with the data.

Equation (56) and the definition $R(A, x_B) \equiv F_2^A/AF_2^N$ lead to the result that

$$\frac{dR(A, x_B)}{dx_B} = C(x_B)[a_2(A) - 1], \quad (60)$$

has a linear relation with a_2 , with $C(x_B) = g_2(2)[f_2' F_2^N - f_2 F_2^{N'}]/[F_2^N + g_2(2)f_2]^2$ independent of A and Λ (here

$f' = df/dx_B$). This means that EFT naturally accounts for the linear relation between the EMC slope and the height of the plateau. However, the sign of the EMC effect is not explained.

3. The isovector EMC effect

This SRC-related PLC-suppression model also leads to an explanation of the NuTeV anomaly (Sargsian, 2014b). We discussed the dominance of the pn SRCs, relative to the pp and nn correlations, for nuclear internal momenta between 300 and 600 MeV/ c that is caused by the effects of the tensor force. The pp and nn components of the NN SRC are strongly suppressed since they are dominated by the central NN potential with relative $L = 0$. The resulting picture for nuclear matter consisting of protons and neutrons at densities in which internucleon distances are about 1.7 fm is rather unique: it represents a system with suppressed pp and nn but enhanced pn interactions. Using this idea Sargsian (2014a) predicted two new properties for the nuclear momentum distributions for momenta between the Fermi momentum and about 600 MeV/ c . There is an approximate equality of p - and n -momentum distributions weighted by their relative fractions in the nucleus $x_p = Z/A$ and $x_n = (A - Z)/Z$:

$$x_p n_p^A(p) \approx x_n n_n^A(p) \quad (61)$$

with $\int d^3 p n^A(p) = 1$. The probability of a proton being in a high-momentum NN SRC is inversely proportional to its relative fraction x_p and can be related to the momentum distribution in the deuteron $n_D(p)$:

$$n_p^A(p) = \frac{1}{2x_p} a_2(A, N) n_D(p) \quad (62)$$

and similarly for neutrons. The main prediction of Eq. (62) is that high-momentum protons and neutrons became increasingly unbalanced as the ratio $(N - Z)/(N + Z)$ increases. Using Eq. (62) one can calculate the fraction of the protons having momenta greater than the Fermi momentum as

$$P_p(A, N) \approx \frac{1}{2x_p} a_2(A, N) \int d^3 p n_D(p) \Theta(p - k_F), \quad (63)$$

and similarly for neutrons. For example, in iron, $P_p = 23\%$ and $P_n = 20\%$.

The energetic protons in neutron-rich nuclei will result also in the stronger nuclear modification of u quarks as compared to d quarks and the effect grows with A . The predicted effects can also be checked in parity violating deep inelastic scattering off heavy nuclei (Cloet, Bentz, and Thomas, 2012; Souder, 2016); see Sec. VI.A.5.

4. Summary

In summary, driven by the short-range correlations between two nucleons, the strong connection between the EMC effect and the plateaus observed in (e, e') scattering at high x_B is both a natural consequence of the impulse approximation of scattering theory and also of effective field theory. In the impulse approximation the relevant ratio is that of momentum-

space densities; in the EFT the relevant ratio is that of coordinate-space densities. The Appendix shows that ratios of these are the same as long as large values of momenta are used in the impulse approximation and small values of relative distance are used in the EFT. This means that the relation shown in Fig. 34 is derived using two very different techniques. The fact that using two different technical approaches, each driven by short-range physics, leads to the same conclusion gives significant credence to the interpretation that the same short-range physics accounts for both the EMC effect and the QE cross-section plateaus.

The underlying mechanism of the distortion of the nucleon structure is not yet established and could occur from PLC suppression or from other mechanisms. Nevertheless, it is very clear that the relation shown in Fig. 34 is no accident. There is a true underlying cause of the EMC effect and the observed plateaus in ratios of (e, e') scattering cross sections.

C. Are the nucleons in the correlated pair really nucleons?

According to the logic presented here, most of the correlated pair consists of nucleons, but the part that is responsible for the EMC effect consists of non-nucleonic configurations. This conclusion is valid for both classes of models of the EMC effect: the mean-field based or SRC based. The non-nucleonic configurations could be a medium-modified single nucleon, or NN^* or N^*N^* configurations, or even more complex six-quark configurations.

D. Determining the structure function of a free neutron

Determining the structure function of the neutron is challenging because a free neutron target does not exist. Experimentalists have therefore used deuteron or ^3He targets to extract the neutron structure. This implies that our knowledge of the neutron structure function is intimately connected with medium effects in light targets. As we shall see, medium effects in the deuteron must be accounted for accurately if one hopes to correctly understand the free neutron structure function.

1. The deuteron in-medium correction effect

The deuteron in-medium correction (IMC) effect refers to the difference between the DIS cross section for the deuteron and the sum of the DIS cross sections for a free proton and neutron (Frankfurt and Strikman, 1985; Melnitchouk, Schreiber, and Thomas, 1994b). The term IMC was introduced by Weinstein *et al.* (2011) who showed that one can use the EMC-SRC correlation as a phenomenological tool to constrain the deuteron IMC effect and thus extract the free neutron structure function. Following Weinstein *et al.* (2011), we can extrapolate the linear fit to the EMC-SRC correlation to the limit of $a_2(A) \rightarrow 0$. This is the limit of no correlations, which is equivalent to a free proton-neutron pair. The intersection of this limit with the y axis is therefore the IMC ratio of the free proton-neutron pair to the deuteron.

The $a_2(A) \rightarrow 0$ extrapolation to the y axis of the EMC-SRC correlation gives $dR_{\text{EMC}}/dx_{A(A)=0} = -0.070 \pm 0.004$. Since the EMC effect is linear for $0.3 \leq x_A \leq 0.7$ for all nuclei with $A > 2$, we assume that the EMC effect is also linear in this

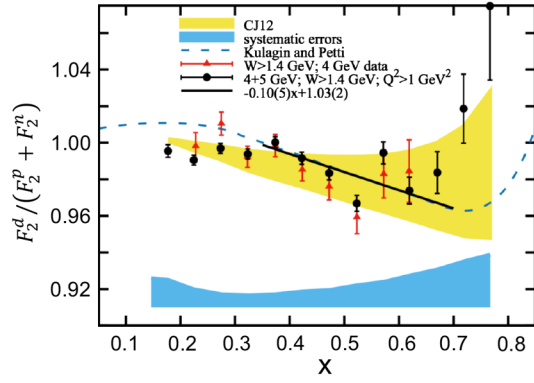


FIG. 36. The deuteron IMC ratio $R_{\text{EMC}}^d = F_2^d / (F_2^n + F_2^p)$ as extracted from the BONuS data. Total systematic uncertainties are shown as a band arbitrarily positioned at 0.91 (blue). The yellow band shows the CJ12 (Owens, Accardi, and Melnitchouk, 2013) limits expected from their nuclear models. The black points are the combined 4- and 5-GeV data, whereas the red points are the 4-GeV data alone. The dashed blue line shows the calculations of Kulagin and Petti (2006). The solid line (black) is the fit to the black points for $0.35 < x_B < 0.7$. From Griffioen *et al.*, 2015.

region for the deuteron. This implies that the EMC effect for the deuteron relative to a free proton plus neutron can be written as

$$\frac{\sigma_d}{\sigma_p + \sigma_n} = 1 - a(x_B - b) \quad \text{for } 0.3 \leq x_B \leq 0.7,$$

where σ_d and σ_p are the measured DIS cross sections for the deuteron and free proton, σ_n is the free neutron DIS cross section that we want to extract, $a = |dR_{\text{EMC}}^d/dx|_{a_2(A)=0} = 0.070 \pm 0.004$, and $b = 0.34 \pm 0.02$ is the average value of x_B where the EMC ratio is unity.¹ This implies that $\sigma_d / (\sigma_p + \sigma_n)$ decreases linearly from 1 to 0.97 as x_B increases from 0.3 to 0.7. We can then use this relationship to extract the free neutron cross section in this x_B range, as shown in the next section.

The uncertainty quoted for the IMC slope is due to the EMC and SRC data and to the fit. It does not include any uncertainty due to corrections applied to the EMC and SRC data. As stated, if we include the proposed correction for $a_2(A)$ due to the c.m. motion of the correlated pair, then the fit parameter increases by 25% and so does the free proton plus neutron EMC effect. These effects are discussed in detail by Hen, Piastetzky, and Weinstein (2012).

Following the prediction of the IMC effect, the BONuS Collaboration (Tkachenko *et al.*, 2014) published their experimental extraction of the IMC effect, measured at $Q^2 > 1 \text{ GeV}^2$ and $W > 1.4 \text{ GeV}$; see Fig. 36 (Griffioen *et al.*, 2015). A linear fit for $0.35 < x < 0.7$ yields $dR_{\text{EMC}}^d/dx = -0.1 \pm 0.05$ where the uncertainties come from the fit. This result is consistent with the IMC prediction of -0.07 . For

¹The x_A correction does not significantly change the slope a of the EMC-SRC correlation, and it increases the b parameter by less than the uncertainty reported in Weinstein *et al.* (2011).

$x < 0.5$ the EMC ratios R_{EMC}^d agree within uncertainties with those obtained using more stringent cuts in W . The ratio for $x_B > 0.5$ continues the trend of the lower- x_B data, with a hint of the expected rise above $x_B = 0.7$ as seen in R_{EMC}^A for heavier nuclei, but these high- x_B values are more uncertain because there are fewer data points for resonance averaging.

2. The free neutron structure function

If the structure function F_2 is proportional to the DIS cross section (i.e., if the ratio of the longitudinal to transverse cross sections is the same for n , p , and d) [see the discussion in Geesaman, Saito, and Thomas (1995)], then the free neutron structure function $F_2^n(x_B, Q^2)$ can also be deduced from the measured deuteron and proton structure functions and from the deuteron IMC effect:

$$F_2^n(x_B, Q^2) = \frac{2F_2^d(x_B, Q^2) - [1 - a(x_B - b)]F_2^p(x_B, Q^2)}{1 - a(x_B - b)}, \quad (64)$$

which leads to

$$\frac{F_2^n(x_B, Q^2)}{F_2^p(x_B, Q^2)} = \frac{2F_2^d(x_B, Q^2)/F_2^p(x_B, Q^2) - [1 - a(x_B - b)]}{1 - a(x_B - b)}. \quad (65)$$

This is valid only for $0.35 \leq x_B \leq 0.7$.

Figure 37 shows the ratio of F_2^n/F_2^p extracted by Weinstein *et al.* (2011) using the IMC-based correction and the $Q^2 = 12 \text{ GeV}^2$ ratio F_2^d/F_2^p from Arrington *et al.* (2009). Note that the ratio F_2^d/F_2^p is Q^2 independent from $6 \leq Q^2 \leq 20 \text{ GeV}^2$

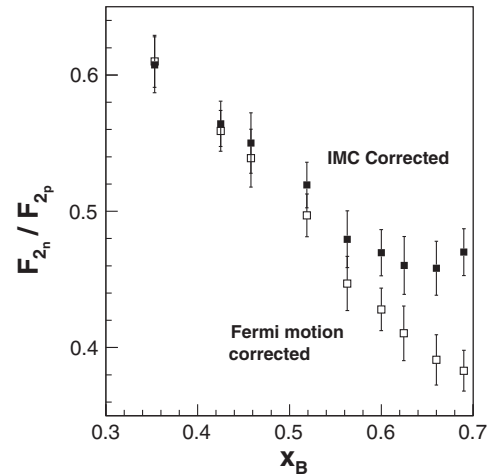


FIG. 37. The ratio of neutron to proton structure functions $F_2^n(x_B, Q^2)/F_2^p(x_B, Q^2)$ as extracted from the measured deuteron and proton structure functions F_2^d and F_2^p . The solid symbols show F_2^n/F_2^p extracted by Weinstein *et al.* (2011) from the deuteron IMC ratio and the world data for F_2^d/F_2^p at $Q^2 = 12 \text{ GeV}^2$ (Arrington *et al.*, 2009). The open symbols show F_2^n/F_2^p extracted from the same data correcting only for nucleon motion in deuterium using a relativistic deuteron momentum density (Arrington *et al.*, 2009). From Weinstein *et al.*, 2011.

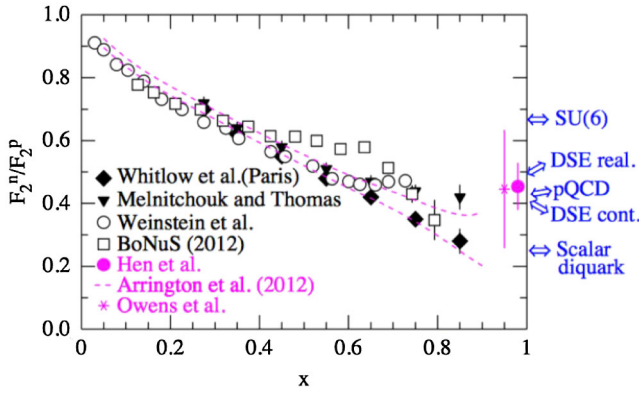


FIG. 38. F_2^n/F_2^p as a function of x_B . Results from the IMC and other phenomenological extractions are compared to selected theoretical predictions. See Holt (2013) and Roberts, Holt, and Schmidt (2013) for details. From Holt, 2013.

for $0.4 \leq x_B \leq 0.7$ (Arrington *et al.*, 2009). The dominant uncertainty in this extraction is the uncertainty in the measured F_2^n/F_2^d . The IMC-based correction increases the extracted free neutron structure function (relative to that extracted using the deuteron momentum density) by an amount that increases with x_B (Arrington *et al.*, 2009). This is qualitatively similar to the recent extraction of Cosyn and Sargsian (2016). Thus, the IMC-based F_2^n strongly favors model-based extractions of F_2^n that include nucleon modification in the deuteron (Melnitchouk and Thomas, 1996).

The IMC-based extraction of F_2^n/F_2^p , extrapolated in the region of $x_B < 0.3$, is compared in Fig. 38 to several other experimental and phenomenological extractions of this ratio. Also shown are several QCD predictions; see Holt (2013) and Roberts, Holt, and Schmidt (2013) for details.

3. The d/u ratio at large x_B

The ratio of the neutron structure function F_2^n to the proton structure function F_2^p is particularly interesting as it can be related, within the parton model, to the ratio of the d -quark and u -quark distributions. The latter provides a unique opportunity for studying the flavor and spin dynamics of quarks in the nucleon, with the d/u quark distribution ratio, in particular, being very sensitive to different mechanisms of spin-flavor symmetry breaking (Melnitchouk and Thomas, 1996; Holt and Roberts, 2010).

Historically, proton DIS data placed strong constraints on the u -quark distribution, while neutron structure functions were used to constrain the d -quark distribution and form the d/u ratio. Specifically, the d/u ratio in the valence quark dominance domain (i.e., at large x_B) was extracted from the F_2^n/F_2^p structure function ratio using

$$F_2^n/F_2^p = [1 + 4(d_v/u_v)]/[4 + (d_v/u_v)],$$

where the absence of free neutron targets meant that the neutron structure function was not measured directly, but instead extracted from deuterium DIS data. However, uncertainties in the nuclear corrections in the deuteron, such as those associated with nucleon off-shell effects and the

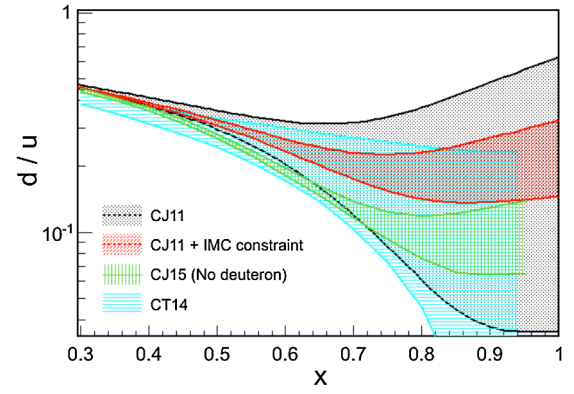


FIG. 39. d/u ratio at $Q^2 = 12 \text{ GeV}^2$ with the full theoretical uncertainty from Accardi *et al.* (2011) (black) and with the IMC constraint at the 90% C.L. (red) from Hen, Accardi *et al.* (2011). Also shown for comparison are recent extractions that do not include nuclear corrections from the CJ15 (Accardi *et al.*, 2016) and CT14 (Dulat *et al.*, 2016) PDF extractions.

large-momentum components of the deuteron wave function, give rise to significant uncertainties in the resulting d/u ratio for $x_B \gtrsim 0.5$ (Accardi *et al.*, 2011).

To rectify the situation, Hen, Accardi *et al.* (2011) used the phenomenological IMC corrected extraction of F_2^n/F_2^p as an added constraint on the extraction of the d/u ratio in the global analysis of the CTEQ-JLab Collaboration (Accardi *et al.*, 2011).

New data on charged lepton and W boson asymmetry measured at the Fermilab Tevatron (Abazov *et al.*, 2013, 2014, 2015) are sensitive to the large- x_B d/u ratio with no nuclear uncertainties (Accardi *et al.*, 2016).

Figure 39 shows the d/u ratio at large x_B extracted from a global QCD analysis using DIS data without [CJ11 (Accardi *et al.*, 2011)] and with [CJ11 + IMC (Hen, Accardi *et al.*, 2011)] the IMC constraint and using the new asymmetry data with no nuclear corrections applied [CJ15 (Accardi *et al.*, 2016) and CT14 (Dulat *et al.*, 2016)]. As can be seen, while the various extractions somewhat differ at large x_B , the IMC constraints and the new asymmetry data both constrain the CJ11 analysis similarly.

To summarize, the use of the IMC-extracted neutron structure function directly constrains the d -quark PDF for $x \lesssim 0.7$ and indirectly for $x \rightarrow 1$. We find the d/u ratio in the limit $x \rightarrow 1$ to be 0.23 ± 0.09 at the 90% confidence level, in overall agreement with new extractions using charged lepton and W boson asymmetry data and in agreement with the models of Farrar and Jackson (1975) and Cloet, Bentz, and Thomas (2005a) which predict intermediate values of d/u between the SU(6) symmetry and scalar diquark dominance limits.

V. EXISTING SEARCHES FOR MEDIUM-MODIFIED ELECTROMAGNETIC FORM FACTORS

We showed that the experimental and theoretical evidence indicates that the structure of the nucleon is modified by its immersion in a nucleus. The only models that account for the EMC effect, the plateaus of the high- x_B (e, e') reaction, and

the lack of a medium effect in the nuclear Drell-Yan data are those involving short-range correlations. Nevertheless, the task of understanding the EMC and SRC effects is not complete. The available models need to be improved (discussed in Sec. VI.B). We need models that are sufficiently complete that they can explain both the EMC effect and the nuclear Drell-Yan data, and also predict and account for new independent phenomena.

If the nuclear medium modifies the bound nucleon structure functions (and thus their wave functions), then it almost certainly will modify their electromagnetic form factors. All of the medium modification models include modifications of bound electromagnetic form factors; see Sec. III. These effects could be manifest in quasielastic nucleon knockout ($e, e'N$) cross sections and in the inclusive longitudinal $A(e, e')$ response. The influence of nucleon modification on the nuclear elastic form factor cannot be detected because the distribution of nucleons in the nucleus is imprecisely known.

This section discusses the experimental evidence for modification of bound nucleon form factors.

A. Polarization transfer in the $(\vec{e}, e'\vec{p})$ reaction

Polarization transfer in the $H(\vec{e}, e'\vec{p})$ reaction was used to measure the ratio of the free proton electromagnetic form factors G_E/G_M with much smaller systematic uncertainties than previous methods (Perdrisat, Punjabi, and Vanderhaeghen, 2007). This technique was then applied to measure the ratio of bound proton electromagnetic form factors using the quasielastic $A(\vec{e}, e'\vec{p})$ reaction (Dieterich *et al.*, 2001; Strauch *et al.*, 2003; Paolone *et al.*, 2010; Malace *et al.*, 2011; Strauch, 2012). The ratio of the longitudinal and transverse polarization transfers is proportional to the ratio of G_E/G_M for the free proton $P'_x/P'_z \propto G_E/G_M$ (Perdrisat, Punjabi, and Vanderhaeghen, 2007). For a bound proton, one must also correct for the effects of meson exchange currents, isobar configurations, and especially final state interactions. After using a model to correct for these effects, the polarization double ratio

$$R \equiv \left(\frac{P'_x}{P'_z} \right)_A / \left(\frac{P'_x}{P'_z} \right)_{\text{H}} \quad (66)$$

should be sensitive to medium modification of the form factor ratio. The induced polarization P_y [measured in the $(e, e'\vec{p})$ reaction] should be more sensitive to final state interactions and much less sensitive to medium-modification effects.

Figure 40 shows the ${}^4\text{He}(\vec{e}, e'\vec{p}){}^3\text{H}$ double ratio R and the induced polarization P_y measured at small values of missing momentum ($p_{\text{miss}} < 150 \text{ MeV}/c$) over a range of Q^2 . Relativistic distorted-wave-impulse approximation calculations by the Madrid group (Caballero *et al.*, 1998; Udias *et al.*, 1999; Udias and Vignote, 2000) can explain only the data if they include medium-modified form factors. They calculated the induced polarization and the polarization-transfer ratio using the unmodified but off-shell cc1 and cc2 (De Forest, 1983) current operators and the optical potentials of Horowitz (1985) and Murdock and Horowitz (1987) to

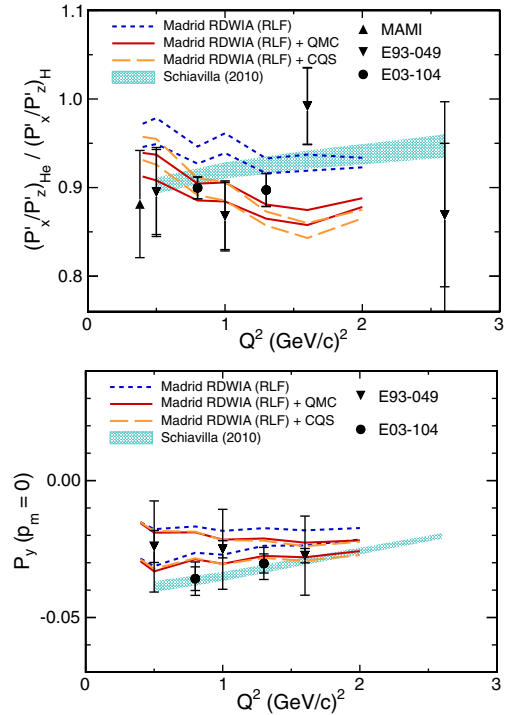


FIG. 40. The measured ${}^4\text{He}(\vec{e}, e'\vec{p}){}^3\text{H}$ polarization-transfer double ratio R (upper panel) and induced polarization P_y (lower panel) as a function of Q^2 . Open symbols: Dieterich *et al.* (2001) and Strauch *et al.* (2003); solid circles: Paolone *et al.* (2010) and Malace *et al.* (2011). The data are compared to DWIA calculations from Schiavilla *et al.* (2005) (updated in 2010) using unmodified form factors and from the Madrid group (Caballero *et al.*, 1998; Udias *et al.*, 1999; Udias and Vignote, 2000) using the cc1 (lower set of curves) and cc2 (upper set of curves) off-shell current operators in combination with unmodified (black dashed lines), QMC modified (red solid lines), and CQS modified (red dashed line) in medium form factors. See text for details. From Strauch, 2012.

account for final state interactions. No charge exchange effects (photon knocks out neutron, which undergoes a charge exchange reaction) were included. This unmodified calculation agreed with the induced polarization data when using the cc1 current operator. However, good agreement with the measured value of R was achieved only by including either the QMC (Lu *et al.*, 1999) or CQS (Smith and Miller, 2004) medium-modified form factors.

Schiavilla *et al.* (2005) calculated P_y and R using DWIA. They computed the final state interactions using an optical potential that includes both spin-independent and spin-dependent charge exchange terms. However, they updated their calculation in 2010 with new parameters. While their calculation describes both P_y and R without medium-modified form factors, its significance is decreased because they did not follow the standard procedure (Austern, 1970) of independently constraining the parameters of the optical potential they used to describe the final state interactions. Thus our view is that the results of the nuclear polarization experiments strongly indicate that medium effects do influence electromagnetic form factors. We eagerly await new experiments with improved precision and at larger values of p_{miss} which would confirm or rule out this interpretation.

Experiments performed at the Mainz Microtron (MAMI) using the A1 beam line (Yaron *et al.*, 2016) measured the polarization-transfer ratio R for deuterium and ^{12}C at lower Q^2 ($Q^2 = 0.175$ and 0.4 GeV^2) but higher virtuality than at Jefferson Lab. For deuterium, the ratio R decreases significantly with virtuality and is consistent with that previously measured on ^4He . This indicates that the effect in nuclei is due to the virtuality of the knocked-out proton and not due to the average nuclear density. The deuteron calculations (Arenhovel, Leidemann, and Tomusiak, 2005) predicted this decrease and associate most of it with FSI (Yaron *et al.*, 2016). The $\approx 10\%$ differences between the data and calculations may indicate the need for in-medium modifications. The carbon data are still under analysis. Other double polarization experiments were not sensitive to the effects of nucleon modification (Passchier *et al.*, 2002; Mihovilovic *et al.*, 2014; Mayer *et al.*, 2017).

Jefferson Lab experiment E12-11-002 will measure polarization-transfer observables as a function of virtuality for both ^4He and ^2H and will measure the proton recoil polarization at $Q^2 = 1.8 \text{ GeV}^2$ to help us better understand the effects of medium modifications and FSI.

B. Polarization transfer in the $(\vec{e}, e'\vec{n})$ reaction

A complementary experiment would be the measurement of polarization transfer to the neutron in quasielastic scattering in the $(\vec{e}, e'\vec{n})$ reaction. Cloet *et al.* (2009) studied possible in-medium changes of the bound neutron electromagnetic form-factor ratio with respect to the free ratio, the superratio $(G_E^*/G_M^*)/(G_E/G_M)$. At small values of Q^2 this superratio depends on the in-medium modifications of the neutron magnetic moment and the effective electric and magnetic radii. The superratio of the neutron is dominated by the expected increase of the electric charge radius in the nuclear medium and is found to be greater than 1. In contrast, the proton superratio is predicted to be smaller than 1. A comparison of high-precision measurements of the reactions $^2\text{H}(\vec{e}, e'\vec{n})p$ and $^4\text{He}(\vec{e}, e'\vec{n})^3\text{H}$ would test these predictions.

However, a major drawback to nuclear polarization-transfer measurements, no matter whether the proton or neutron is detected, is that medium modifications that affect both G_E and G_M will cancel in the ratio; see Fig. 33, for example.

C. The (e, e') reaction and the Coulomb sum rule (CSR)

This sum rule (McVoy and Van Hove, 1962; De Forest and Walecka, 1966) states that the integral of the $A(e, e')$ longitudinal response function at fixed momentum transfer over all energy transfers should equal the total charge of the nucleus Z . The first CSR experiment (Altemus *et al.*, 1980) observed that the sum rule was “quenched,” i.e., they measured less than Z . This indicated that the cross section for scattering from a bound nucleon was significantly less than the free cross section. Thus, Cloet, Bentz, and Thomas (2016) said that the first hints of QCD effects in nuclei came from quasielastic electron scattering on nuclear targets (Altemus *et al.*, 1980; Noble, 1981; Mezziani *et al.*, 1984). However, later work cast doubt on this result.

The (e, e') inclusive cross section can be written as

$$\frac{d^2\sigma}{d\Omega d\nu} = \sigma_{\text{Mott}} \left[\frac{Q^4}{|\mathbf{q}|^4} R_L(\nu, |\mathbf{q}|) + \left(\frac{Q^2}{2|\mathbf{q}|^2} + \tan^2 \frac{\theta}{2} \right) R_T(\nu, |\mathbf{q}|) \right], \quad (67)$$

where σ_{Mott} is the Mott cross section, R_L and R_T are the longitudinal and transverse response functions, and θ is the electron scattering angle. In the nonrelativistic limit of the impulse approximation (De Forest and Walecka, 1966; Bertozzi *et al.*, 1972) one has

$$R_L(\omega, \mathbf{q}) = \left\langle A \left| \sum_{i=1}^Z e^{i\mathbf{q}\cdot\mathbf{r}_i} \delta(\omega - H) \sum_{j=1}^Z e^{-i\mathbf{q}\cdot\mathbf{r}_j} \right| A \right\rangle G_E^2(q^2),$$

where H is the nuclear Hamiltonian, the ground-state energy is taken as 0, and for simplicity we assume that neutrons do not contribute. The nonrelativistic formulation is valid only when $\mathbf{q}^2 \approx Q^2$. Since R_L is proportional to the square of G_E , its sensitivity to medium effects is greater than that of the polarization-transfer measurements.

The Coulomb sum is the integral over all values of ν (including the inaccessible timelike regime where $\nu > |\mathbf{q}|$):

$$\frac{R_L(q)}{G_E^2(q^2)} = \frac{\int d\nu R_L(\nu, \mathbf{q})}{G_E^2(q^2)} = \left\langle A \left| \sum_{i,j=1}^Z e^{i\mathbf{q}\cdot(\mathbf{r}_i - \mathbf{r}_j)} \right| A \right\rangle. \quad (68)$$

Splitting Eq. (68) into terms with $i = j$ and $i \neq j$ we get

$$\frac{R_L(q)}{G_E^2(q^2)} = Z + Z(Z-1) \int d^3r d^3r' e^{i\mathbf{q}\cdot(\mathbf{r} - \mathbf{r}')} \rho_2(\mathbf{r}, \mathbf{r}'), \quad (69)$$

where ρ_2 is the two proton density function; see Eq. (A8). At large enough momentum transfer the second term vanishes as $1/|\mathbf{q}|^4$, so that one finds the CSR:

$$\lim_{Q^2 \rightarrow \infty} \frac{R_L(q)}{G_E^2(q^2)} = Z. \quad (70)$$

Since electron scattering cannot measure the cross section in the timelike region, the Coulomb sum is properly defined (Cloet, Bentz, and Thomas, 2016) as an integral over ν from energies just above the elastic peak to $|\mathbf{q}|$:

$$S_L(|\mathbf{q}|) = \int_{\nu^+}^{|\mathbf{q}|} d\nu \frac{R_L(\nu, |\mathbf{q}|)}{ZG_{Ep}^2(Q^2) + NG_{En}^2(Q^2)}. \quad (71)$$

The quantity S_L can be correctly compared with the results obtained from electron scattering.

The initial motivation to measure the Coulomb sum rule (De Forest and Walecka, 1966) was to learn about ρ_2 . However, the recent focus has been to learn about nucleon medium modification at large values of the momentum transfer where the effect of ρ_2 is negligible.

Cloet, Bentz, and Thomas (2016) discussed the interesting history of the theory. Calculations (Saito, Tsushima, and Thomas, 1999; Horikawa and Bentz, 2005) in which the

internal structural properties of bound nucleons are self-consistently modified by the nuclear medium unsurprisingly predict significant quenching of the CSR. However, calculations that assume an unmodified nucleon electromagnetic current (Do Dang *et al.*, 1987; Mihaila and Heisenberg, 2000; Carlson *et al.*, 2002; Kim, Yu, and Cheoun, 2006), including the state-of-the-art Green's function Monte Carlo result for ^{12}C from Lovato *et al.* (2013, 2016), found modest or no quenching of the CSR. More recently Cloet, Bentz, and Thomas (2016) used an NJL model in the medium to find a dramatic reduction of the Coulomb sum rule for $|\mathbf{q}| \gtrsim 0.5$ GeV, driven by changes to the bound proton Dirac form factor.

The experimental status of the CSR has been unclear. The initial measurements found quenching of the CSR for ^{12}C , ^{40}Ca , and ^{56}Fe (Altemus *et al.*, 1980; Mezziani *et al.*, 1984). However, a reanalysis of these data (Jourdan, 1995, 1996), utilizing an alternative prescription for the Coulomb corrections, concluded that there is no quenching. The analysis of the Coulomb corrections in those works was later challenged (Aste, Arx, and Trautmann, 2005; Aste, 2008; Wallace and Tjon, 2008). These papers supported the conclusion that quenching of the CSR occurs as reported by Morgenstern and Mezziani (2001). New results at high-momentum transfer and on a variety of nuclear targets from Jefferson Lab Experiment E05-110 (Choi, Chen, and Mezziani, 2005) are eagerly anticipated. Verification or disproof of the CSR quenching should reveal critical aspects of nucleon modification in nuclei.

VI. FUTURE DIRECTIONS IN NUCLEAR DEEP INELASTIC SCATTERING AND DETECTING SHORT-RANGE CORRELATIONS

A. Experiment

There are several different experimental approaches to understanding the EMC-SRC correlation and the origin of the EMC effect. The most promising approach is to directly test the EMC-SRC correlation by measuring the change in the bound nucleon structure function with nucleon momentum using tagged structure function measurements.

The second approach is to test other predictions of models of the EMC effect by measuring other quantities related to nucleon modification, including the bound ratio of electric to magnetic elastic form factors using polarization transfer $A(\vec{e}, e' \vec{p})$ and the Coulomb sum rule.

Finally, we can learn more about SRC and about the EMC effect individually in several ways. The first way is to extend EMC and SRC inclusive measurements to more nuclei over a wider range of momentum transfer. We can also extend semiexclusive and exclusive SRC measurements in a similar manner to obtain more detailed information, especially about the potential isospin dependence of the EMC effect, SRCs, and their correlations. We can select the nucleons we study by measuring the polarized EMC effect and we can measure the isospin dependence of the EMC effect in asymmetric nuclei by measuring parity violating deep inelastic scattering.

1. Tagged structure function measurements

The EMC effect is measured in inclusive (e, e') DIS from a nucleon in a nucleus. In order to learn more about the DIS reaction, we can “tag” the reaction by detecting a recoiling nuclear fragment in coincidence with the scattered electron. By wisely choosing the nuclear fragment and kinematics, we can restrict the initial state of the struck nucleon (the nucleon that absorbed the virtual photon) and thereby learn more about the microscopic origin of the EMC effect.

The simplest example for such a process is DIS on the deuteron. If we can detect a *recoil* nucleon with momentum \mathbf{p} that did not interact in the DIS reaction and did not have a final state interaction (i.e., a spectator), then we know that the struck nucleon had initial momentum $-\mathbf{p}$. We can then measure the DIS cross section for scattering from a nucleon in the nucleus as a function of its initial momentum. This will allow us to extract F_2 and hence the quark distributions. In particular, F_2 can be measured as a function of virtuality. This experiment thus provides an opportunity to test the importance of the effects of virtuality.

This was initially studied with 5.7 GeV electrons incident on deuterium, measuring the scattered electron and the recoil proton with the CLAS spectrometer (Klimenko *et al.*, 2006). While this measurement did not have the kinematic reach to unambiguously measure a change in the nucleon structure function, they did show that protons emitted at large angles $\theta_{pq} > 120^\circ$ (where θ_{pq} is the angle between the proton and the virtual photon) were predominantly spectators. Later theoretical works support this observation (Palli *et al.*, 2009; Cosyn and Sargsian, 2011).

In practice, experiments will measure the ratio of cross sections at fixed recoil momentum and different values of x'_B , where

$$x'_B = \frac{Q^2}{2p_\mu q^\mu} = \frac{Q^2}{2[(M_d - E_S)\nu + \mathbf{p}_S \cdot \mathbf{q}]}$$

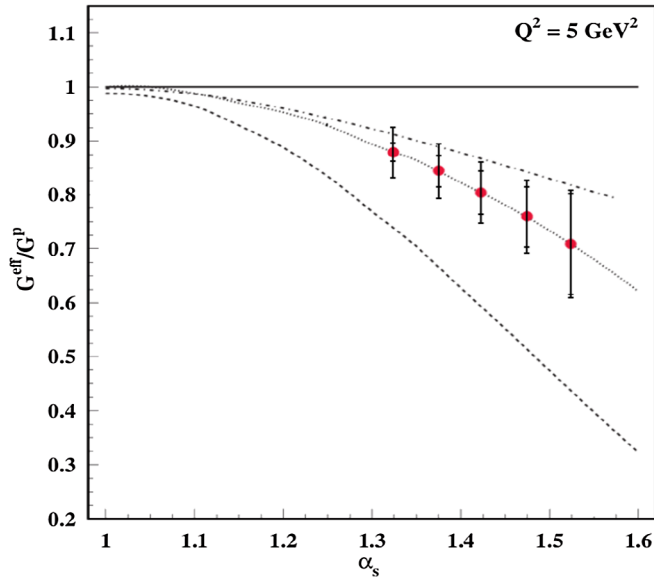
is the value of x_B in the frame of the struck nucleon, M_d is the deuteron mass, and E_S and \mathbf{p}_S are the energy and momentum of the spectator nucleon. These data will be used to extract (Hen, Weinstein *et al.*, 2011; Hen, Weinstein, Piasetzky, and Hakobyan, 2014)

$$\frac{F_2^{\text{bound}}(x_B^{\text{hi}}, q_1^2, \mathbf{p}_S)}{F_2^{\text{free}}(x_B^{\text{hi}}, Q_1^2)} = \frac{\sigma_{\text{DIS}}(x_B^{\text{hi}}, Q_1^2, \mathbf{p}_S)}{\sigma_{\text{DIS}}(x_B^{\text{low}}, Q_2^2, \mathbf{p}_S)} \frac{\sigma_{\text{DIS}}^{\text{free}}(x_B^{\text{low}}, Q_2^2)}{\sigma_{\text{DIS}}^{\text{free}}(x_B^{\text{hi}}, Q_1^2)} R_{\text{FSI}}, \quad (72)$$

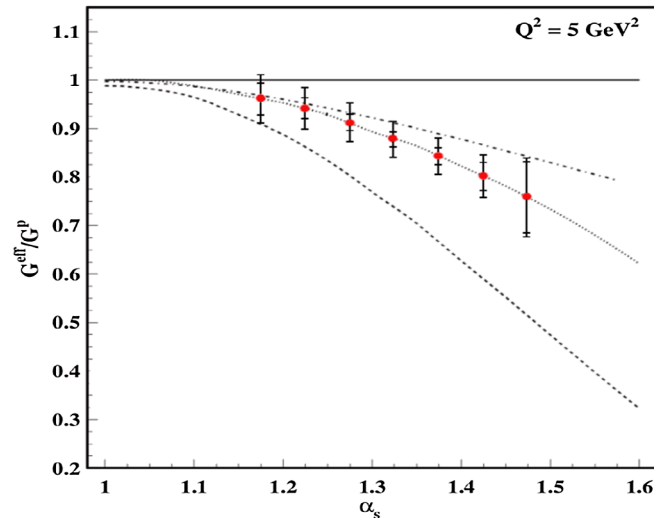
where $\sigma_{\text{DIS}}^{\text{free}}$ is the free-nucleon DIS cross section, R_{FSI} is a correction factor for the effects of final state interactions, $x_B^{\text{low}} \approx 0.3$ where the EMC effect is very small (i.e., where the EMC ratio is very close to 1), and $x_B^{\text{hi}} > 0.45$.

By measuring the ratio of the bound to free-nucleon structure functions as a function of spectator momentum (i.e., of nucleon initial momentum), these experiments will answer the crucial question of which nucleons are modified and to what extent. Little momentum dependence would imply that the mean-field nucleons are modified and large-momentum dependence would imply that SRC nucleons are modified.

There are two approved Jefferson Lab experiments to measure this reaction. Experiment E12-11-107 (Hen, Weinstein *et al.*, 2011) measured neutron modification by detecting the scattered electrons in the Hall C magnetic spectrometers and the spectator protons in a set of gas electron multiplier detectors and scintillators covering scattering angles from about 80° to 170° . The expected results are shown in Fig. 41(b). Experiment E12-11-003A (Hen, Weinstein, Piasetzky, and Hakobyan, 2014) will measure proton modification by detecting the scattered electrons in the CLAS12 forward detector and the spectator neutrons in a large scintillator



(a) Bound proton structure via $d(e, e' n_{recoil})X$ scattering



(b) Bound neutron structure via $d(e, e' p_{recoil})X$ scattering

FIG. 41. The expected results from future Jefferson Lab tagged DIS measurements. The dashed lines are obtained from the color screening models (Frankfurt and Strikman, 1985), the dotted lines are from the color delocalization models (Close, Roberts, and Ross, 1983), and the dot-dashed lines are from the off-shell models (Melnitchouk, Schreiber, and Thomas, 1994a). From Hen, Weinstein *et al.*, 2011 and Hen, Weinstein, Piasetzky, and Hakobyan, 2014.

array covering scattering angles from 160° to 170° . The expected results are shown in Fig. 41(b).

A second category of experiments consists of measuring the tagged EMC ratio. We can tag different reaction mechanisms by detecting either a spectator nucleon or a recoil $A - 1$ nucleus. The main idea is that the electron scatters from a quark in one nucleon. If that nucleon belongs to an SRC NN pair, then its partner nucleon will leave the nucleus. If that nucleon does not belong to an NN SRC pair, then the $A - 1$ nucleus is much more likely to recoil intact. In either case, proper interpretation of the results of such measurements requires full understanding of many-body FSI effects that, to the best of our knowledge, so far were only studied for the deuteron. Instead of the inclusive cross-section ratio, the tagged EMC ratio is

$$R = \frac{\sigma_A(e, e' p_S)/A}{\sigma_d(e, e' p_S)/2}$$

integrated over spectator momenta and angles. Typically, backward angles $\theta_{pq} > 120^\circ$ are chosen to minimize FSI.

If the spectator is a proton and has momentum greater than $300 \text{ MeV}/c$, then it is expected to belong to an np SRC pair. If nucleon modification is due to nucleons belonging to SRC pairs, then nucleon modification should be the same in deuterium and in the heavier nucleus and therefore the tagged EMC ratio should be independent of x_B and should be equal to $a_2(A)$, the relative probability of finding a nucleon in an SRC pair in nucleus A relative to d .

Large uncertainty in interpreting these tagged EMC measurements stems from the possibility that the fragments of the struck nucleon will break up another SRC pair as they exit the nucleus, significantly increasing the number of backward nucleons. This effect should be smaller for light nuclei. A larger complication arises from the nuclear spectral function that associated high-momentum nucleons with large excitation energies that will be distributed to the different fragments and need to be taken into account.

If the measured spectator is an $A - 1$ nucleus, then the struck nucleon almost certainly did not belong to an SRC pair. Assuming one can overcome these complications, comparing the tagged EMC ratio for ^4He with spectator (proton + deuteron) or with spectator ^3He can give further insight as to whether nucleon modification depends on the struck nucleon momentum or on the struck nucleon SRC pairing.

2. Inclusive EMC and SRC measurements

The inclusive EMC and SRC measurements described in Secs. II and III were performed on a limited number of nuclei and, in the case of SRC measurements and the JLab EMC measurements, in a limited kinematic range. Therefore, it is natural to extend both EMC and SRC measurements to additional nuclei over a wider kinematic range.

Figure 42 shows nuclei that can or will be measured at Jefferson Lab as a function of their proton (Z) and neutron (N) numbers. A wise selection of nuclei allows for a systematical experimental study of SRC and the EMC effect for fixed nuclear asymmetry as a function of mass number and for fixed mass number as a function of asymmetry. The planned

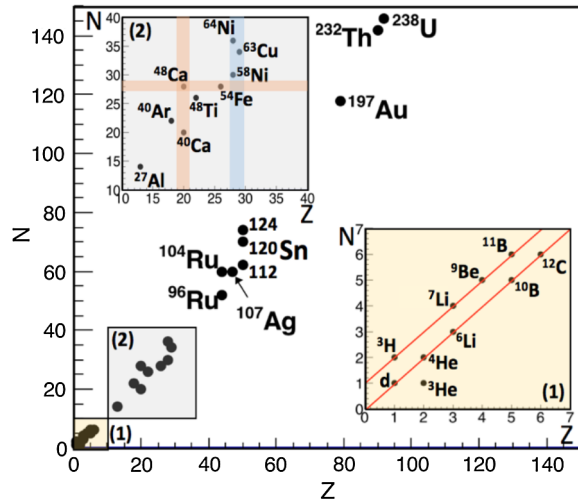


FIG. 42. Phase space of nuclei considered for future EMC and SRC measurements at Jefferson Lab as a function of their proton (Z) and neutron (N) numbers. The two insets focus on the light and medium mass nuclei regimes. For light nuclei one can systematically study a series of symmetric nuclei and the detailed effect of the addition of one neutron (proton). For medium mass nuclei the horizontal and vertical bands mark nuclei with a similar number of protons (neutrons) and a varying number of neutrons (protons) allowing one to study the effect of nuclear asymmetry.

Jefferson Lab measurements (Arrington and Day, 2006; Arrington, Gaskell, and Daniel, 2010; Petratos *et al.*, 2010; Solvignon-Slifer and Arrington, 2011) will systematically measure both the size of the EMC effect and the height of the SRC plateau over many nuclei from ${}^3\text{He}$ and ${}^3\text{H}$ to ${}^{208}\text{Pb}$, covering a wide range of mass numbers and nuclear asymmetries (N/Z). Measurements with unstable nuclei at other laboratories could significantly extend the available range of nuclear asymmetry.

Light and heavy nuclei can exhibit significantly different nuclear effects. Medium and heavy nuclei ($A \geq 10$) exhibit properties of nuclear saturation and can be relatively well described using effective theories for strongly interacting many-body Fermi systems. However, light nuclei span a wide range of nuclear densities and asymmetries, with some nuclei exhibiting a rich clusterlike substructure.

In the case of the EMC effect, special care should be given to “standard” nuclear structure effects that do affect the DIS cross-section ratio and can therefore potentially mimic an isospin dependent. Therefore, any measurement of the ratio of the EMC effect in isospin asymmetric nuclei (e.g., ${}^3\text{He}/{}^3\text{H}$, ${}^{48}\text{Ca}/{}^{40}\text{Ca}$, etc.) should be compared to a calculation of standard nuclear effects that take into account differences in the proton and neutron momentum distributions and pairing probabilities. These can be studied indirectly by inclusive QE (e, e') reactions or directly using semi-inclusive and exclusive ($e, e'N$) and ($e, e'pN$) reactions. In the case of light nuclei *ab initio* few-body calculations can also provide relevant information.

An additional advantage of light-nuclei studies is the ability to compare the experimental results with detailed *ab initio* nuclear structure calculations. Assuming reaction mechanisms such as FSI, MEC, and others are under control, such comparisons of experiment and theory can offer significant

insight into the underlying microscopic physics. For heavy nuclei, such *ab initio* calculations of short-range nuclear structure are still limited, but rapid progress is being made (Wiringa *et al.*, 2014; Carlson *et al.*, 2015; Hagen *et al.*, 2015).

In addition to extending the range of nuclei measured, it is also important to extend the measured Q^2 range. This is especially important for SRC studies where the minimum initial momentum depends strongly on Q^2 (see Fig. 13). The SRC cross-section ratios of Egiyan *et al.* (2003) were measured at $1.4 \leq Q^2 \leq 2.6 \text{ GeV}^2$ with most of the data at $Q^2 < 2 \text{ GeV}^2$ [see Fig. 16(a)]. They observed flat plateaus in the cross-section ratio for $1.5 \leq x_B \leq 1.9$, which corresponds to $250 \leq p_{\text{min}} \leq 500 \text{ MeV}/c$ which is where we expect tensor correlations to dominate. By contrast, the SRC cross-section ratios of Fomin *et al.* (2012) which were measured at $Q^2 = 2.7 \text{ GeV}^2$ exhibit “plateaus” that are not quite as flat, especially for heavier nuclei [see Fig. 16(a)]. At $Q^2 = 2.7 \text{ GeV}^2$, $1.5 \leq x_B \leq 1.9$ corresponds to $325 \leq p_{\text{min}} \leq 700 \text{ MeV}/c$, which extends beyond the tensor correlation region into the central correlation region. Measuring the Q^2 dependence of the SRC plateaus will help us quantitatively relate the experimental results to detailed *ab initio* nuclear structure calculations—a needed comparison that has not been done to date.

The Q^2 dependence of the EMC effect has been studied over a wide kinematical regime. However, there are still several intriguing questions about higher twist effects that should be studied systematically. The Jefferson Lab 6 GeV EMC effect measurements included data with invariant mass $W > 1.4 \text{ GeV}$, a region that is dominated by resonance production rather than DIS. The fact that the measured EMC ratios agreed with the SLAC data, measured at higher W , showed that resonance contributions largely cancel in the A/d ratio. By covering a broader kinematic range, the future 12 GeV measurements will help quantify this issue. A review of the possibility of studying the large x_B at the LHC has been presented by Freese, Sargsian, and Strikman (2015).

3. Semi-inclusive and exclusive SRC measurements

In the context of the EMC effect, the interpretation of planned future experiments in isospin asymmetric nuclei (e.g., ${}^3\text{He}/{}^3\text{H}$, ${}^{48}\text{Ca}/{}^{40}\text{Ca}$) requires understanding the differences in the proton and neutron momentum distributions and SRC pairing probabilities, as these enter into the baseline calculation of standard nuclear effects and EMC model calculations that are to be compared with the experimental data.

The required information about high-momentum nucleons and SRC in nuclei can be obtained by scattering an electron or other probe from a nucleus and detecting one or more of the ejected nucleons. $A(e, e'p)$ experiments can measure the amounts of high-momentum nucleons in different nuclei and how that changes with nuclear isospin asymmetry.

The fact that the $A(e, e'p)$ reaction is mainly sensitive to the protons in nuclei whereas the (e, e') reaction is sensitive to all nucleons in nuclei make their measurements complementary and crucial to allow for a detailed study of the dependence of SRC effects on the nuclear asymmetry. While more challenging to perform, $A(e, e'n)$ measurements can complement the other reactions and yield additional information on the role of protons and neutrons in asymmetric nuclei.

One Jefferson Lab experiment (Hen, Weinstein, Gilad, and Boeglin, 2014) measured ${}^3\text{H}$ and ${}^3\text{He}(e, e'p)$ as a function of p_{miss} in kinematics where FSI are small in order to determine the ratio of the ${}^3\text{He}$ and ${}^3\text{H}$ momentum distributions. In the naive SRC picture, this ratio should be 2 at low p_{miss} because there are twice as many protons in ${}^3\text{He}$ as in ${}^3\text{H}$ and it should decrease to 1 at high p_{miss} because there are two pn pairs each in ${}^3\text{He}$ and ${}^3\text{H}$.

Similar experiments in medium mass nuclei could measure how the number of high-momentum protons changes as you add eight neutrons from ${}^{40}\text{Ca}$ to ${}^{48}\text{Ca}$ and by adding six more protons from ${}^{48}\text{Ca}$ to ${}^{54}\text{Fe}$ (Hen, Weinstein *et al.*, 2016). Ongoing Jefferson Lab CLAS data-mining analysis of $A(e, e'n)$ and $A(e, e'p)$ scattering off ${}^{12}\text{C}$, ${}^{27}\text{Al}$, ${}^{56}\text{Fe}$, and ${}^{208}\text{Pb}$ is expected to provide new insight into isospin asymmetry effects on SRCs.

We can gain more information about SRC pairing in nuclei by knocking out a high-initial momentum nucleon and detecting its correlated partner, with either electron or proton probes $A(e, e'pN)$ or $A(p, 2pN)$. By extending the range of missing momentum we can study the transition from tensor dominance (at $300 \leq p_{\text{miss}} \leq 500$ MeV/ c) to the scalar repulsive core (at higher p_{miss}). By focusing on lower p_{miss} , we can map the transition from the mean field to the SRC-dominated domain (the nuclear ‘‘Migdal jump’’). By extending the A dependence of SRC-pair abundancies and properties we can learn about SRC-pair quantum numbers and provide data for a quantitative theory of SRCs.

4. Polarized EMC measurements

Motivated by open questions about the EMC effect and the ‘‘proton spin crisis,’’ Jefferson Lab will perform the first measurement of the spin-dependent EMC effect utilizing CLAS12 in Hall B with 11 GeV polarized electrons and polarized targets (Kuhn and Brooks, 2014). They will determine the ratio of the double-spin asymmetries in ${}^7\text{Li}$ (using ${}^7\text{LiD}$) in which a highly polarized proton is embedded in the nuclear medium, and on the proton (using ${}^6\text{LiH}$). The double spin asymmetry is measured as

$$A_{\parallel} = \frac{d\sigma_{\downarrow\uparrow} - d\sigma_{\uparrow\uparrow}}{d\sigma_{\downarrow\uparrow} + d\sigma_{\uparrow\uparrow}}$$

and is approximately equal to the ratio of polarized to unpolarized structure functions: $g_1^{{}^7\text{Li}}/F_1^{{}^7\text{Li}}$. Many systematic uncertainties will cancel in the asymmetries and in the ratios of asymmetries. Together with the unpolarized structure function (also to be measured at Jefferson Lab), they will also extract $g_1^{{}^7\text{Li}}$ and, using a sophisticated modern wave function model, extract the in-medium proton spin structure function $g_1^{p\parallel{}^7\text{Li}}$ for a proton bound in ${}^7\text{Li}$. They will cover a kinematic range of $1 < Q^2 < 15$ GeV 2 and $0.06 < x_B < 0.8$.

Mean-field models of nucleon modification predict stronger effects than in the unpolarized structure functions. On the other hand, since nucleons in tensor correlations tend to have opposite spin to the overall nuclear spin, the EMC effect could be minimal or even in the opposite direction. These data will provide new constraints on models for the EMC effect, some

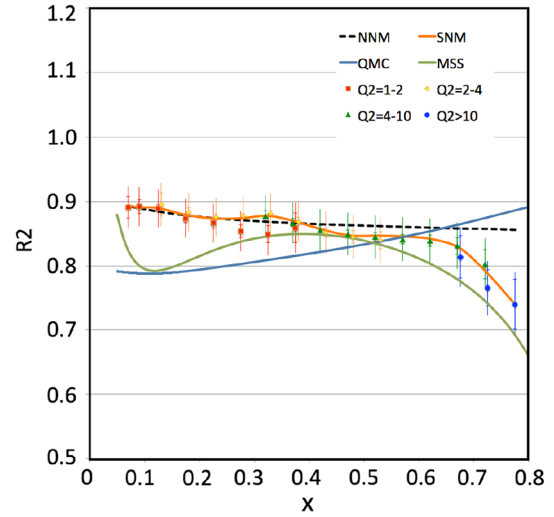


FIG. 43. The expected results of the polarized EMC effect measurement at Jefferson Lab. The ratio of the parallel double-spin asymmetry A_{\parallel} for ${}^7\text{Li}(\vec{e}, e')$ to $\vec{p}(\vec{e}, e')$, normalized by multiplying it with the ‘‘naive’’ unpolarized structure function ratio for ${}^7\text{Li}$ over hydrogen, plotted vs x_B . The models are NNM (naive nuclear model with no Fermi motion, dashed line), SNM (standard nuclear model with Fermi motion and kinematical binding energy effects, upper solid line at low x), QMC (quark-meson coupling model, bottom solid line at low x), and MSS (modified sea scheme) [x rescaling (Fanchiotti *et al.*, 2014), mid solid line at low x]. Adapted from Kuhn and Brooks, 2014.

of which predict that medium modifications of quark distributions depend strongly on the quark helicities (see Fig. 43).

5. Parity violating deep inelastic scattering

There is some evidence that u - and d -quark distributions are modified differently in asymmetric nuclei. Theoretically, since protons move faster than neutrons in neutron-rich nuclei, if nucleon modification depends on nucleon virtuality (as in the PLC model), then we expect protons, with two u and one d quarks, to be more modified than neutrons.

Experimentally, the NuTeV experiment compared neutrino and antineutrino DIS off an iron target and extracted a value of the Weinberg mixing angle that differs from the standard model by about 3σ (Zeller *et al.*, 2002). While this led to much excitement and attempts to relate it to physics beyond the standard model, recently it was shown that an isospin-dependent EMC effect that affects protons more than neutrons could resolve the anomaly (Cloet, Bentz, and Thomas, 2009b).

A measurement of parity violation in $A(e, e')$ DIS would directly measure the $d - u$ difference as a function of x_B (Riordan, Beminiwatha, and Arrington, 2016). The difference in the left-right asymmetry for helicity $+1$ and -1 electrons is proportional to the product of the photon and Z amplitudes divided by the square of the photon amplitude. This asymmetry will be 10^2 to 10^3 parts per million for DIS scattering from a heavy nucleus:

$$A_{PV} \approx -\frac{G_F Q^2}{4\sqrt{2}\pi\alpha} \left[a_1(x) + \frac{1 - (1-y)^2}{1 + (1-y)^2} a_3(x) \right],$$

where $y = 1 - E/E'$, and a_1 and a_2 depend on the quark distributions. In the symmetric nucleus limit

$$a_1 \approx \frac{9}{5} - 4\sin^2\theta_W - \frac{12}{25} \frac{u_A^+ - d_A^+}{u_A^+ + d_A^+} + \dots,$$

where u_A refers to all the up quarks in the nucleus and the superscript $+$ refers to the sum of the quark and antiquark distributions. Thus the parity violating asymmetry is sensitive to the difference between the u - and d -quark distributions in the nucleus.

B. Theory

The review of the theory presented here shows that there is a strong connection between the cause of the EMC effect and the short-range correlations that cause the high- x_B plateau in (e, e') scattering on nuclei. Nevertheless, there are gaps in almost every part of the theory, from the initial state wave function, to the modification of nucleon structure, to the need to include the effects of final state interactions. We therefore present an outline of the necessary improvements.

The EMC effect is a modification of nucleon structure functions. Obtaining an understanding of this effect therefore requires a working understanding of the valence sector of the free-nucleon wave function, so that the effects of the medium on the relevant components can be correctly included. Lattice calculations (Ji, 2013; Lin *et al.*, 2015) and the Dyson-Schwinger approach (Cloet and Roberts, 2014) are making progress on computing free-nucleon parton distributions. It is also necessary to build nucleon models that are easily related to the output of these Euclidean-space theories (Burkardt, Frank, and Mitchell, 1997; Hobbs, Alberg, and Miller, 2016). A 21st century calculation of medium modifications cannot be made without inputs from such models.

The calculation of deep inelastic scattering from nuclei needs to be improved in several different ways. For example, the calculations using the PLC-suppression model have been made mainly for $x_B = 0.5$ (Ciofi degli Atti *et al.*, 2007), where effects of Fermi motion nearly vanish. To understand the EMC ratios it is necessary to be able to make accurate calculations for a range of values of $0.3 \leq x_B \leq 0.7$. So far this has been done (Freese, Sargsian, and Strikman, 2015) by assuming that no medium modification occurs for $x_B < 0.45$ and linearly interpolating in the region $0.45 < x_B < 0.65$. Calculations need to handle finite-sized nuclei without resorting to infinite nuclear matter calculations using a local density approximation. Such a program requires computation of nuclear spectral functions for finite-sized nuclei. This involves intensive numerical work, so it is important to present such spectral functions in an easily accessible manner.

We have seen that only models with medium modification arising from short-ranged effects can handle both the EMC effect and high- x_B (e, e') scattering. However, models in which the medium modification is driven by mean-field effects give an excellent description of the EMC effect; see, e.g., Cloet, Bentz, and Thomas (2005b, 2006, 2009). It would not be realistic to think that the ultimate accurate description would make use of only one of the two possible ideas. Therefore, it is important to build models of medium

modifications of nucleon wave functions that includes both mean-field effects and the effects of correlations. The necessary model of nuclei needs to be consistent with nuclear saturation properties, include non-nucleonic degrees of freedom and have those relativistic effects needed to compute nuclear deep inelastic scattering cross sections.

Many treatments of final state interactions for exclusive reactions [e.g., $(e, e'p)$ and $(e, e'pN)$] use complex optical potentials, which automatically violate current conservation. To fully understand spectroscopic factors and nucleon-nucleon correlations it is necessary to ensure that the reaction theory models conserve current. We also need to better understand electromagnetic current operators in models of the nucleon-nucleon interactions that employ low-momentum cutoffs.

There is a need to understand higher twist effects in nuclei, so we can understand why the EMC ratios measured at JLab are nearly the same as those measured at much higher energies at SLAC and CERN.

In addition to improving our understanding of the theoretical underpinnings of the causes of the EMC-SRC correlation, it is necessary to explore the implications of the EMC-SRC correlations and of pn dominance in SRC. The possible inversion of the kinetic energy sharing in asymmetric nuclei could significantly affect several subfields of physics. In astrophysics the nuclear symmetry energy is of fundamental importance. It describes the change in energy of a nuclear system when a proton is replaced by a neutron. np SRCs dramatically reduce the kinetic part of the symmetry energy (Hen, Li *et al.*, 2015) and work is ongoing to understand other effects. Additional implications of SRCs on nuclear systems include the nuclear response to neutrino scattering (Fields *et al.*, 2013; Fiorentini *et al.*, 2013), cooling rates of neutron stars, contact interactions in Fermi systems (Frankfurt, Sargsian, and Strikman, 2008; Hen, Weinstein *et al.*, 2015), and more. While the discussion of these effects extends beyond the scope of this review, they are extensively discussed in the literature.

VII. THE WAY WE THINK IT IS AND THE WAYS TO CHECK

This article has focused on explaining two seemingly unrelated phenomena: lepton-nucleus deep inelastic scattering and quasielastic electron-nucleus scattering at large values of x_B , and their surprising relation. DIS from a nucleus is very different than DIS from a collection of free nucleons; this is the EMC effect which is parametrized in terms of the slope of the EMC ratio R of bound to “free” cross sections. This slope cannot be explained unless the internal quark structure of a bound nucleon differs from that of a free nucleon.

Quasielastic scattering, in which a nucleon is knocked out of the nucleus intact, reveals plateaus in the cross-section ratios of nuclei to deuterium at large values of x_B that correspond to scattering from short-range correlated two-nucleon pairs. Different experiments show that the slope of the EMC effect is linearly proportional to the height of the plateaus. Further studies showed that the two-nucleon pairs consist of a neutron and a proton.

A review of the available experimental and theoretical evidence shows that the relation between the EMC slope dR/dx_B and the SRC plateau height is no accident. There is an underlying cause of both effects: the influence of strongly correlated neutron-proton pairs. These correlated pairs are temporary high-density fluctuations in the nucleus in which the internal structure of the nucleons is briefly modified. This conclusion needs to be quantified by future experiments and improved theoretical analyses that are discussed here.

The connection between the EMC effect and nucleon-nucleon correlations is very profound. Although the binding energy of a nucleon is less than 1% of its mass, the fact that the nucleon is made of quarks and gluons is manifest in two distinct sets of phenomena, via experiments that have been repeated several times. The direct influence of the quark presence in nuclei is now established.

This presence is a subtle effect as it must be, given the generally small deviation of R from unity, and does not arise via the usual low-energy, low-momentum transfer nuclear physics observables: binding energy, spectra, radii, electroweak transition rates, etc. Nonetheless, the quark presence cannot be denied. We expect that a deeper understanding of the EMC and SRC connection will ultimately lead to an improved understanding of the nature of confinement of light quarks.

The Jefferson-Lab 12 GeV program includes a series of approved experiments targeted at improving our understanding of the EMC effect, SRCs, and their connection. The forthcoming results of these experiments are expected to shed new light on the origin of the EMC effect and provide stringent constraints on current or future theoretical calculations.

ACKNOWLEDGMENTS

We thank our many colleagues for their efforts in accomplishing the research discussed in this review and also for the many insights that they have provided through discussions. This work of was supported by the U.S. Department of Energy Office of Science, Office of Nuclear Physics under Awards No. DE-FG02-97ER-41014, No. DE-FG02-94ER40818, and No. DE-FG02-96ER-40960 and by the Israel Science Foundation (Israel) under Grants No. 136/12 and No. 1334/16.

APPENDIX: EXPANDED EXPLANATIONS

1. Understanding the np relative wave function

The aim of this Appendix is to provide a qualitative explanation that the momentum space wave function of the deuteron, a very weakly bound system, has a significant high-momentum k tail. Indeed one sees an approximate k^{-4} behavior of the deuteron density for large values of k . This tail persists in nuclei because of short-range correlations between nucleons.

A $1/k^4$ density comes from $1/k^2$ in the wave function which can be obtained if the nucleon-nucleon interaction is a delta function in coordinate space, as occurs in leading order EFT or in the effective range expansion behavior. Such approximations are valid only at very small values of momentum $1/r_e \gg k \gg 1/a$, where there is an approximate scale invariance, where a is the scattering length of about 5 fm

and r_e is the effective range of about 2 fm. The $1/k^2$ behavior of the wave function emerges at large values of k due to the second-order effects of the one pion exchange (OPE) contribution to the tensor potential V_T . The Schrödinger equation for the spin-one two-nucleon system, which involves S and D state components, can be expressed as an equation involving the S state only by using $(-B - H_0)|\Psi_D\rangle = V_T|\Psi_S\rangle$, where B is the binding energy of the system and H_0 is the Hamiltonian excluding the tensor potential. Thus one obtains an effective S -state potential $V_{00} = V_T(-B - H_0)^{-1}V_T$ [Eq. (4)], where V_T connects the S and D states. The intermediate Hamiltonian H_0 is dominated by the effects of the centrifugal barrier and can be approximated by the kinetic energy operator (Brown and Jackson, 1976). This second-order term is large because it contains an isospin factor $(\tau_1 \times \tau_2)^2 = 9$, and because $S_{12}^2 = 8 - 2S_{12}$. Evaluation of the S -state potential, neglecting the small effects of the central potential in the intermediate D state, yields

$$V_{00}(k, k') \approx -M \frac{32f^4}{\mu^4 \pi^2} \int \frac{p^2 dp}{MB + p^2} I_{02}(k, p) I_{20}(p, k'), \quad (\text{A1})$$

where M is the nucleon mass, $f^2 \approx 0.08$ is the square of the πN coupling constant, μ is the pion mass, and $I_{LL'}$ are partial wave projections of the one pion exchange potential (OPEP) tensor interaction in momentum space. These are evaluated in (Haftel and Tabakin, 1970)

$$I_{02}(p, k) = I_{20}(p, k) = \frac{k^2 Q_2(z) + p^2 Q_0(z)}{2pk} - Q_1(z), \quad (\text{A2})$$

with $z \equiv (p^2 + k^2 + \mu^2)/(2pk)$, and Q_i are Legendre functions of the second kind in the conventions of Haftel and Tabakin (1970). The result, Eq. (A1), corrects errors in Hen, Weinstein *et al.* (2015). The errors do not affect the qualitative statements made in the cited paper, as we now demonstrate.

We use Eq. (A1) to estimate quantities of interest. We note the asymptotic property $\lim_{p \rightarrow \infty} I_{02}(p, k) = 1 - (k^2 + \mu^2)/p^2 + \dots$. Thus the integrand of Eq. (A1) is dominated by large values of p and diverges unless there is a cutoff. This means that $V_{00}(k, k')$ is approximately a constant, independent of k and k' . This is the signature of a short-ranged interaction. We expose this feature in more detail by assuming that for the important regions of the integral appearing in Eq. (A1) by treating the variables k and k' as small compared to the cutoff momentum. Then $I_{02}(0, p) \approx p^2/(p^2 + \mu^2)$, and

$$V_{00}(k, k') \approx -M \frac{32f^4}{\mu^4 \pi^2} \int_0^M \frac{p^2 dp}{MB + p^2} \left(\frac{p^2}{p^2 + \mu^2} \right)^2 (1 + \dots), \quad (\text{A3})$$

where we have cut off the linearly divergent integral for momenta $p > M$ and \dots represents terms of $\mathcal{O}((p^2 + \mu^2)/M^2)$. All realistic models of the NN interaction employ some sort of a cutoff, and a mass scale of the nucleon mass is typical of one-boson exchange potentials (Machleidt, Holinde, and Elster, 1987; Machleidt, 1989). Thus $V_{00}(k, k')$ is approximately independent of its momentum arguments, the hallmark of

short-ranged interactions. The use of Eq. (A3) provides an approximate upper limit.

The resulting asymptotic $1/k^4$ dependence of the square of the wave function can be seen by using the Lippmann-Schwinger equation in the form

$$\begin{aligned} \langle k|\psi_S\rangle &\approx \langle k|(-B-H_0)^{-1} \int d^3k' V_{00}(k, k') \langle k'|\psi_S\rangle \\ &\approx \frac{-V_{00}(0,0)}{B+k^2/M} \int d^3k' \psi_S(k') \\ &= \frac{-V_{00}(0,0)}{B+k^2/M} (2\pi)^{3/2} \psi_S(r=0), \end{aligned} \quad (\text{A4})$$

where the subscript S refers to the S state and the integral over all momenta k' leads to a proportionality to the coordinate-space wave function at the origin. In terms of the usual S -state radial wave function $u(r)$ we have

$$\psi_S(r=0) = \lim_{r \rightarrow 0} \frac{u(r)}{r} \frac{1}{\sqrt{4\pi}}. \quad (\text{A5})$$

Using known wave functions, we find $\lim_{r \rightarrow 0} u(r)/r = (0.0267, 0.0584, 0.0792) \text{ fm}^{-3/2}$ for the Nijmegen, Reid93 (Stoks *et al.*, 1994), and Argonne V18 (Wiringa, Stoks, and Schiavilla, 1995) potentials, respectively. The result Eq. (A3) shows the $1/k^2$ dependence of the wave function, with overall strength determined by the detailed potential models. The density is the square of the wave function $\sim 1/k^4$ with an overall strength varying by a factor of 9, depending on the potential used. Thus we find a high-momentum $1/k^4$ behavior far beyond the validity of the effective range approximation. Potentials without this high-momentum density have either a very weak tensor force or a cutoff at low momenta.

We can check the validity of these findings by computing the D state probability P_D :

$$\begin{aligned} P_D &= \langle \psi_S | V_T \frac{1}{(B+H_0)^2} V_T | \psi_S \rangle \\ &\approx \frac{32f^4}{\mu^4 \pi^2} (2\pi)^3 \psi^2(r=0) \int_0^M \frac{p^2 dp}{(B+p^2/M)^2} \left(\frac{p^2}{p^2 + \mu^2} \right)^2. \end{aligned} \quad (\text{A6})$$

We evaluate P_D using $u(r=0)$ for each of the Nijmegen, Reid93 (Stoks *et al.*, 1994), and Argonne V18 (Wiringa, Stoks, and Schiavilla, 1995) potentials. Numerical evaluation of Eq. (A6) yields $P_D = (2, 10, 18)\%$ for the three potentials, respectively. The actual value for all of these potentials is about $P_D = 6\%$. These results show that qualitative treatment here is adequate only for estimates that maintain the qualitative idea that the iterated effects of OPEP produce the $1/k^4$ behavior of the deuteron density. The results of this section depend on the chosen scale (M here). Choosing a sufficiently softer scale would modify the high-momentum dependence of the wave function. A detailed comparison of the momentum dependence of known deuteron wave functions has been presented by Hen, Weinstein *et al.* (2015).

Similar results that the relevant interaction matrix element is approximately independent of its momentum arguments have been obtained previously. Mosel's group (Lehr *et al.*, 2000, 2002; Konrad, Lenske, and Mosel, 2005) assumed this independence and used it to help to clarify the basic, fundamental origins of the nucleon spectral functions and the high-momentum tails. Using a constant interaction matrix element, along with the Fermi-gas model, and solving the relevant Dyson equation gave high-momentum tails with a density $\sim 1/k^4$, and spectral functions essentially identical to those of more detailed computations.

2. Basic terminology

We define some basic terms. The probability to find a nucleon at a coordinate \mathbf{x} (where this notation includes spatial position, nucleon spin, and isospin) is given by

$$\rho(\mathbf{x}) = \frac{1}{A} \langle \Psi | \sum_{i=1}^A \delta(\mathbf{x} - \mathbf{x}_i) | \Psi \rangle, \quad (\text{A7})$$

where $|\Psi\rangle$ is the relevant nuclear wave function. The quantity $\rho(\mathbf{x})$ is known as the density. The normalization is $\int d\mathbf{x} \rho(\mathbf{x}) = 1$, where the integral includes a sum over nucleon spin and isospin.

The two-body density in coordinate space is given by

$$\rho^{(2)}(\mathbf{x}, \mathbf{y}) = \frac{1}{A(A-1)} \langle \Psi | \sum_{i \neq j} \delta(\mathbf{x} - \mathbf{x}_i) \delta(\mathbf{y} - \mathbf{y}_j) | \Psi \rangle. \quad (\text{A8})$$

The integral of the two-body density over \mathbf{x} yields the density $\rho(\mathbf{y})$. The correlation function $C(\mathbf{x}, \mathbf{y})$ is the deviation of the two-body density from the mean-field approximation:

$$C(\mathbf{x}, \mathbf{y}) = \rho^{(2)}(\mathbf{x}, \mathbf{y}) - \rho(\mathbf{x})\rho(\mathbf{y}). \quad (\text{A9})$$

The quantity $C(\mathbf{x}, \mathbf{y})$ vanishes if the wave function $|\Psi\rangle$ can be represented as a product of single-nucleon wave functions. Furthermore, the stated normalization conditions lead to the result

$$\int d\mathbf{x} C(\mathbf{x}, \mathbf{y}) = 0, \quad \int d\mathbf{y} C(\mathbf{x}, \mathbf{y}) = 0. \quad (\text{A10})$$

It is useful to also define the probability $\rho_{2,1}(r)$ that if a nucleon is at a given position, another one is separated by a distance r :

$$\begin{aligned} \rho_{2,1}(r) &\equiv \frac{1}{4\pi r^2 A} \langle \Psi | \sum_{i \neq j} \delta(r - |\mathbf{r}_i - \mathbf{r}_j|) | \Psi \rangle \\ &= \int d^3R \rho_2(\mathbf{R} + \mathbf{r}/2, \mathbf{R} - \mathbf{r}/2), \end{aligned} \quad (\text{A11})$$

where \mathbf{R} is the center-of-mass position of the two-nucleon system.

The same kind of analysis can be done in momentum space. Evaluation of $\rho(\mathbf{x})$ requires the square of the coordinate-space representation of $|\Psi\rangle$, while that of $n(\mathbf{k})$ requires the

momentum-space representation of the same wave function. The probability for a nucleon to have a momentum \mathbf{k} is given by

$$n(\mathbf{k}) = \frac{1}{A} \langle \Psi | \sum_{i=1}^A \delta(\mathbf{k} - \mathbf{k}_i) | \Psi \rangle. \quad (\text{A12})$$

It is convenient to define a two-body density $n_2(\mathbf{K}, \boldsymbol{\kappa})$ in momentum space, which gives the probability of two nucleons having a total momentum of \mathbf{K} and a relative momentum $\boldsymbol{\kappa}$:

$$n_2(\mathbf{K}, \boldsymbol{\kappa}) = \frac{1}{A(A-1)} \left\langle \Psi \left| \sum_{i \neq j} \delta(\mathbf{K}/2 + \boldsymbol{\kappa} - \mathbf{k}_i) \times \delta(\mathbf{K}/2 - \boldsymbol{\kappa} - \mathbf{k}_j) \right| \Psi \right\rangle. \quad (\text{A13})$$

Experimentalists defined a correlation as existing if the system has $\kappa \gg K$, with $\kappa > k_F$ and $K < k_F$.

It is also useful to consider the integrated quantity

$$n_{2,1}(\boldsymbol{\kappa}) \equiv \int d^3K n_2(\mathbf{K}, \boldsymbol{\kappa}) = \frac{2}{A(A-1)} \left\langle \Psi \left| \sum_{i \neq j} \delta(\mathbf{k}_i - \mathbf{k}_j - 2\boldsymbol{\kappa}) \right| \Psi \right\rangle, \quad (\text{A14})$$

which is the momentum-space version of Eq. (A11).

A specific model for the two-nucleon density is used in the analysis of the data relevant to this review. For small relative distances r one writes the two-nucleon wave function $\Psi(\mathbf{R}, \mathbf{r})$ in the following form:

$$\Psi(\mathbf{R}, \mathbf{r}) = F_A(R) \psi_D(r), \quad r \ll R_A, \quad (\text{A15})$$

where R_A is the radius of the nucleus, and the often used assumption is that at short distances all relative wave functions are the same as that of the deuteron D . In this model

$$\rho_{2,1}^A(r) = \int d^3R F_A^2(R) \psi_D^2(r) \equiv a_2(A) \psi_D^2(r), \quad r \ll R_A. \quad (\text{A16})$$

In momentum space

$$\tilde{\Psi}(\mathbf{K}, \mathbf{k}) = \tilde{F}_A(K) \tilde{\psi}_D(k), \quad k \gg 1/R_A, \quad (\text{A17})$$

where the tilde denotes Fourier transform and the momentum variables are canonically conjugate to \mathbf{R} and \mathbf{r} . The one-body density $n_A(\mathbf{k}_1)$ is given by

$$n_A(\mathbf{k}_1) = \int d^3k_2 |\tilde{\Psi}(\mathbf{K}, \mathbf{k})|^2 = \int d^3P \tilde{F}_A^2(P) |\tilde{\psi}_D(\mathbf{k}_1 - \mathbf{P}/2)|^2 \quad (\text{A18})$$

$$\approx \int d^3P \tilde{F}_A^2(P) |\tilde{\psi}_D(\mathbf{k}_1)|^2 = a_2(A) |\tilde{\psi}_D(\mathbf{k}_1)|^2, \quad (\text{A19})$$

where $k_1 \gg 1/R_A$ is assumed and the relation in terms of $a_2(A)$ is an example of Parseval's theorem.

The next step is to relate the quantities $n_A(k_1)$ and $\rho_{2,1}(r)$. The use of Eqs. (A16) and (A19) leads immediately to the result

$$a_2(A) = \frac{\rho_{2,1}^A(r)}{r_{2,1}^D(r)} = \frac{n_A(k)}{n_D(k)} \quad (r \ll R_A, k > 1/R_A). \quad (\text{A20})$$

The early workers (Frankfurt *et al.*, 1993) used the ratio of momentum-space densities, and recent workers (Chen *et al.*, 2016) used the coordinate space version, but both are the same in the leading-order approximation of each approach.

3. Why center-of-mass and relative coordinates factorize

We provide a qualitative explanation of the factorization inherent in Eq. (A15). Start with the nonrelativistic nuclear Hamiltonian with only two-nucleon forces, and consider infinite nuclear matter. The basic assumption is the independent pair approximation. The idea is that the average separation between nucleons $d = 1.7$ fm, so that when one of the nucleons of the pair makes a close encounter with a third particle the collision occurs under conditions such that the original pair had no interactions at all (Gomes, Walecka, and Weisskopf, 1958). This idea was formally codified by Bethe and co-workers (Bethe, 1971), such that the results of the independent pair approximation appear as the first term in the hole-line expansion.

We explain how this works. Consider two nucleons in nuclear matter, which interact independently of the other nucleons (except for the influence of the Pauli principle). The two-nucleon Hamiltonian h is given by

$$h = h_0 + h_1, \quad (\text{A21})$$

$$h_0 = \frac{\mathbf{P}^2}{4M}, \quad h_1 = \frac{\mathbf{p}^2}{M} + Qv, \quad (\text{A22})$$

where \mathbf{P} is the center-of-mass momentum operator, \mathbf{p} is the relative momentum operator, v is the two-nucleon potential, and Q is an operator that projects both nucleon momenta to be greater than the Fermi momentum k_F . Since the two-nucleon Hamiltonian is a sum of two terms $h = h_0 + h_1$ that commute the solution to the Schrödinger equation $h|\psi\rangle = E|\psi\rangle$ is a product:

$$\psi(\mathbf{R}, \mathbf{r}) = F_A(\mathbf{R}) \chi(\mathbf{r}), \quad (\text{A23})$$

where

$$h_0 F(\mathbf{R}) = E_{\text{c.m.}} F_A(\mathbf{R}), \quad h_1 \chi(\mathbf{r}) = \epsilon \chi(\mathbf{r}), \quad E = E_{\text{c.m.}} + \epsilon \quad (\text{A24})$$

with

$$\psi(\mathbf{R}, \mathbf{r}) = e^{i\mathbf{K}\cdot\mathbf{R}} \chi(\mathbf{r}), \quad (\text{A25})$$

where we suppress notations regarding spin and isospin to simplify the discussion. In general the function $\chi(\mathbf{r})$ contains

all values of angular momentum and has both short-ranged and long-ranged aspects. The essence of Eq. (A15) is that for small values of $|\mathbf{r}|$ all relative wave functions look like the deuteron wave function:

$$\lim_{r \ll d} \chi(\mathbf{r}) = \gamma \psi_D(r), \quad (\text{A26})$$

where γ represents the probability amplitude that the wave function χ corresponds to the deuteron quantum numbers.

It is necessary to introduce a single-particle, mean-field operator U to extend this idea to finite-sized nuclei. In that case, Eq. (A25) is often replaced (Haxton, Gibson, and Henley, 1980) by

$$\psi(\mathbf{R}, \mathbf{r}) = \sum_{\alpha\beta} C_{\alpha\beta} \phi_{\alpha}(\mathbf{r}_1) \phi_{\beta}(\mathbf{r}_2) \chi(\mathbf{r}), \quad (\text{A27})$$

where $\phi_{\alpha,\beta}$ are solutions of the single-particle equation, and $C_{\alpha\beta}$ are coefficients computed using the shell model. The single particles vary over the size of the nucleus, while the variations of $\chi(\mathbf{r}) - 1$ occur over the range of the nucleon-nucleon interaction. If the size of the nucleus is much larger than this range, Eq. (A23) remains true. In these applications the Miller-Spencer correlation function (Miller and Spencer, 1976) has often been used to represent $\chi(\mathbf{r})$.

REFERENCES

- Abazov, Victor Mukhamedovich, *et al.* (D0 Collaboration), 2013, “Measurement of the muon charge asymmetry in $p\bar{p} \rightarrow W + X \rightarrow \mu\nu + X$ events at $\sqrt{s} = 1.96$ TeV,” *Phys. Rev. D* **88**, 091102.
- Abazov, Victor Mukhamedovich, *et al.* (D0 Collaboration), 2014, “Measurement of the W Boson Production Charge Asymmetry in $p\bar{p} \rightarrow W + X \rightarrow e\nu + X$ Events at $\sqrt{s} = 1.96$ TeV,” *Phys. Rev. Lett.* **112**, 151803; **114**, 049901(E) (2015).
- Abazov, Victor Mukhamedovich, *et al.* (D0 Collaboration), 2015, “Measurement of the electron charge asymmetry in $p\bar{p} \rightarrow W + X \rightarrow e\nu + X$ decays in $p\bar{p}$ collisions at $\sqrt{s} = 1.96$ TeV,” *Phys. Rev. D* **91**, 032007; **91**, 079901(E) (2015).
- Accardi, A., L. T. Brady, W. Melnitchouk, J. F. Owens, and N. Sato, 2016, “Constraints on large- x parton distributions from new weak boson production and deep-inelastic scattering data,” *Phys. Rev. D* **93**, 114017.
- Accardi, A., W. Melnitchouk, J. F. Owens, M. E. Christy, C. E. Keppel, L. Zhu, and J. G. Morfin, 2011, “Uncertainties in determining parton distributions at large x ,” *Phys. Rev. D* **84**, 014008.
- Acciarri, R., *et al.* (ArgoNeuT Collaboration), 2014, “Detection of back-to-back proton pairs in charged-current neutrino interactions with the ArgoNeuT detector in the NuMI low energy beam line,” *Phys. Rev. D* **90**, 012008.
- Akulonichev, S. V., and S. Shlomo, 1990, “Nuclear Binding Effect in Deep Inelastic Lepton Scattering,” *Phys. Lett. B* **234**, 170–174.
- Alde, D. M., *et al.*, 1990, “Nuclear dependence of dimuon production at 800-GeV. FNAL-772 experiment,” *Phys. Rev. Lett.* **64**, 2479–2482.
- Altemus, R., A. Cafolla, D. Day, J. S. McCarthy, R. R. Whitney, and J. E. Wise, 1980, “Longitudinal and Transverse Inelastic Electron Scattering from FE-56,” *Phys. Rev. Lett.* **44**, 965–968.
- Alvioli, M., C. Ciofi degli Atti, L. P. Kaptari, C. B. Mezzetti, and H. Morita, 2013, “Nucleon momentum distributions, their spin-isospin dependence, and short-range correlations,” *Phys. Rev. C* **87**, 034603.
- Alvioli, M., C. Ciofi degli Atti, and H. Morita, 2008, “Proton-neutron and proton-proton correlations in medium-weight nuclei and the role of the tensor force,” *Phys. Rev. Lett.* **100**, 162503.
- Alvioli, Massimiliano, Claudio Ciofi degli Atti, and Hiko Morita, 2016, “Universality of nucleon-nucleon short-range correlations: the factorization property of the nuclear wave function, the relative and center-of-mass momentum distributions, and the nuclear contacts,” *Phys. Rev. C* **94**, 044309.
- Anastasio, M. R., L. S. Celenza, W. S. Pong, and C. M. Shakin, 1983, “Relativistic Nuclear Structure Physics,” *Phys. Rep.* **100**, 327–401.
- Anderson, E. R., S. K. Bogner, R. J. Furnstahl, and R. J. Perry, 2010, “Operator Evolution via the Similarity Renormalization Group I: The Deuteron,” *Phys. Rev. C* **82**, 054001.
- Arenhovel, Hartmuth, Winfried Leidemann, and Edward L. Tomusiak, 2005, “General survey of polarization observables in deuteron electrodisintegration,” *Eur. Phys. J. A* **23**, 147–190.
- Arneodo, Michele, 1994, “Nuclear effects in structure functions,” *Phys. Rep.* **240**, 301–393.
- Arrington, J., F. Coester, R. J. Holt, and T.-S. H. Lee, 2009, “Neutron structure functions,” *J. Phys. G* **36**, 025005.
- Arrington, J., A. Daniel, D. B. Day, N. Fomin, D. Gaskell, and P. Solvignon, 2012, “Detailed study of the nuclear dependence of the emc effect and short-range correlations,” *Phys. Rev. C* **86**, 065204.
- Arrington, J., and D. Day, 2006, “Inclusive Scattering from Nuclei at $x > 1$ in the quasielastic and deeply inelastic regimes, Jefferson Lab Experiment E12-06-105.”
- Arrington, J., D. Gaskell, and A. Daniel, 2010, “Detailed studies of the nuclear dependence of F_2 in light nuclei, Jefferson Lab Experiment E12-10-008.”
- Arrington, J., D. W. Higinbotham, G. Rosner, and M. Sargsian, 2012, “Hard probes of short-range nucleon-nucleon correlations,” *Prog. Part. Nucl. Phys.* **67**, 898–938.
- Aste, Andreas, Cyrill von Arx, and Dirk Trautmann, 2005, “Coulomb distortion of relativistic electrons in the nuclear electrostatic field,” *Eur. Phys. J. A* **26**, 167–178.
- Aste, Andreas W., 2008, “Coulomb distortion effects in quasi-elastic (e,e’) scattering on heavy nuclei,” *Nucl. Phys. A* **806**, 191–215.
- Aubert, J. J., *et al.*, 1983, *Phys. Lett. B* **123**, 275.
- Austern, N., 1970, *Direct Nuclear Reaction Theories* (Wiley-Interscience, New York).
- Baghdasaryan, H., *et al.* (CLAS Collaboration), 2010, “Tensor correlations measured in ${}^3\text{He}(e, e'p)n$,” *Phys. Rev. Lett.* **105**, 222501.
- Ball, Richard D., *et al.*, 2013, “Parton distributions with LHC data,” *Nucl. Phys. B* **867**, 244–289.
- Beane, Silas R., and Martin J. Savage, 2005, “Dvcs-dissociation of the deuteron and the EMC effect,” *Nucl. Phys. A* **761**, 259–268.
- Bedaque, Paulo F., and Ubirajara van Kolck, 2002, “Effective field theory for few nucleon systems,” *Annu. Rev. Nucl. Part. Sci.* **52**, 339–396.
- Benhar, O., A. Fabrocini, and S. Fantoni, 1989, “The Nucleon Spectral Function in Nuclear Matter,” *Nucl. Phys. A* **505**, 267–299.
- Benhar, O., V. R. Pandharipande, and I. Sick, 1997, “Nuclear binding and deep inelastic scattering,” *Phys. Lett. B* **410**, 79–85.
- Benhar, O., V. R. Pandharipande, and I. Sick, 1999, “Density dependence of the EMC effect,” *Phys. Lett. B* **469**, 19–24.
- Benhar, Omar, and Ingo Sick, 2012, “Nuclear binding, correlations and the origin of EMC effect,” [arXiv:1207.4595](https://arxiv.org/abs/1207.4595).
- Berger, Edmund L., and F. Coester, 1987, “Nuclear Effects in Deep Inelastic Lepton Scattering,” *Annu. Rev. Nucl. Part. Sci.* **37**, 463–491.

- Bertozzi, W., J. Friar, J. Heisenberg, and J. W. Negele, 1972, "Contributions of neutrons to elastic electron scattering from nuclei," *Phys. Lett. B* **41**, 408–414.
- Bertsch, G. F., L. Frankfurt, and M. Strikman, 1993, "Where are the nuclear pions?" *Science* **259**, 773–774.
- Bethe, H. A., 1971, "Theory of nuclear matter," *Annu. Rev. Nucl. Part. Sci.* **21**, 93–244.
- Bickerstaff, R. P., M. C. Birse, and G. A. Miller, 1984, "Disentangling Explanations of Deep Inelastic Lepton Nucleus Scattering by Lepton Pair Production," *Phys. Rev. Lett.* **53**, 2532–2535.
- Bickerstaff, R. P., M. C. Birse, and G. A. Miller, 1985, "Dynamical Rescaling and the Size of the Pion," *Phys. Lett. B* **161**, 393–396.
- Bickerstaff, R. P., M. C. Birse, and G. A. Miller, 1986, "Partons in Nuclei," *Phys. Rev. D* **33**, 3228–3245.
- Bickerstaff, R. P., and G. A. Miller, 1986, " Q^2 Dependence of the European Muon Collaboration Effect," *Phys. Rev. D* **34**, 2890–2892.
- Bjorken, J. D., 1966, "Applications of the Chiral $U(6) \times (6)$ Algebra of Current Densities," *Phys. Rev.* **148**, 1467–1478.
- Blunden, P. G., M. Burkardt, and G. A. Miller, 1999, "Light front nuclear physics: Mean field theory for finite nuclei," *Phys. Rev. C* **60**, 055211.
- Blunden, Peter G., and Gerald A. Miller, 1996, "Quark-meson coupling model for finite nuclei," *Phys. Rev. C* **54**, 359–370.
- Bogner, S. K., R. J. Furnstahl, and A. Schwenk, 2010, "From low-momentum interactions to nuclear structure," *Prog. Part. Nucl. Phys.* **65**, 94–147.
- Bogner, S. K., A. Schwenk, R. J. Furnstahl, and A. Nogga, 2005, "Is nuclear matter perturbative with low-momentum interactions?" *Nucl. Phys. A* **763**, 59–79.
- Brockmann, R., and R. Machleidt, 1984, "Nuclear Saturation in a Relativistic Bruckner-Hartree-Fock Approach," *Phys. Lett. B* **149**, 283.
- Brown, G. E., 1967, *Unified Theory of Nuclear Models and Forces* (North-Holland Publishing Company, Amsterdam).
- Brown, G. E., and A. D. Jackson, 1976, *The Nucleon-Nucleon Interaction* (North-Holland Publishing Company, Amsterdam).
- Burkardt, M., M. R. Frank, and K. L. Mitchell, 1997, "On the calculation of hadron form-factors from Euclidean Dyson-Schwinger equations," *Phys. Rev. Lett.* **78**, 3059–3062.
- Caballero, J. A., T. W. Donnelly, E. Moya de Guerra, and J. M. Udias, 1998, "Analysis of factorization in $(e, e'p)$ reactions: A Survey of the relativistic plane wave impulse approximation," *Nucl. Phys. A* **632**, 323–362.
- Carlson, C. E., and T. J. Havens, 1983, "Quark Distributions in Nuclei," *Phys. Rev. Lett.* **51**, 261.
- Carlson, J., S. Gandolfi, F. Pederiva, Steven C. Pieper, R. Schiavilla, K. E. Schmidt, and R. B. Wiringa, 2015, "Quantum Monte Carlo methods for nuclear physics," *Rev. Mod. Phys.* **87**, 1067.
- Carlson, J., J. Jourdan, R. Schiavilla, and I. Sick, 2002, "Longitudinal and transverse quasielastic response functions of light nuclei," *Phys. Rev. C* **65**, 024002.
- Chen, Jiunn-Wei, and William Detmold, 2005, "Universality of the EMC effect," *Phys. Lett. B* **625**, 165–170.
- Chen, Jiunn-Wei, William Detmold, Joel E. Lynn, and Achim Schwenk, 2016, "Short Range Correlations and the EMC Effect in Effective Field Theory," [arXiv:1607.03065](https://arxiv.org/abs/1607.03065).
- Choi, S., J. P. Chen, and Z. E. Meziani, 2005, "Precision measurement of longitudinal and transverse response functions of quasi-elastic electron scattering in the momentum transfer range $0.55 \text{ geV}/c < q < 0.9 \text{ geV}/c$, Jefferson Lab Experiment e05-110." Ciofi degli Atti, C., 2015, "In-medium short-range dynamics of nucleons: Recent theoretical and experimental advances," *Phys. Rep.* **590**, 1.
- Ciofi degli Atti, C., L. L. Frankfurt, L. P. Kaptari, and M. I. Strikman, 2007, "On the dependence of the wave function of a bound nucleon on its momentum and the EMC effect," *Phys. Rev. C* **76**, 055206.
- Ciofi degli Atti, C., E. Pace, and G. Salme, 1980, "Realistic nucleon-nucleon interactions and the three-body electrodisintegration of H-3," *Phys. Rev. C* **21**, 805–815.
- Ciofi degli Atti, C., E. Pace, and G. Salmè, 1991, "y-scaling analysis of quasielastic electron scattering and nucleon momentum distributions in few-body systems, complex nuclei, and nuclear matter," *Phys. Rev. C* **43**, 1155–1176.
- Ciofi degli Atti, C., and S. Simula, 1996, "Realistic model of the nucleon spectral function in few- and many-nucleon systems," *Phys. Rev. C* **53**, 1689.
- Ciofi degli Atti, C., S. Simula, L. L. Frankfurt, and M. I. Strikman, 1991, "Two-nucleon correlations and the structure of the nucleon spectral function at high values of momentum and removal energy," *Phys. Rev. C* **44**, R7.
- Ciofi degli Atti, Claudio, and S. Liuti, 1989, "On the Effects of Nucleon Binding and Correlations in Deep Inelastic Electron Scattering by Nuclei," *Phys. Lett. B* **225**, 215–221.
- Cloet, I. C., W. Bentz, and A. W. Thomas, 2009, "Isovector EMC effect explains the NuTeV anomaly," *Phys. Rev. Lett.* **102**, 252301.
- Cloet, I. C., W. Bentz, and A. W. Thomas, 2012, "Parity-violating DIS and the flavour dependence of the EMC effect," *Phys. Rev. Lett.* **109**, 182301.
- Cloet, I. C., Wolfgang Bentz, and Anthony William Thomas, 2005a, "Nucleon quark distributions in a covariant quark-diquark model," *Phys. Lett. B* **621**, 246–252.
- Cloet, I. C., Wolfgang Bentz, and Anthony William Thomas, 2005b, "Spin-dependent structure functions in nuclear matter and the polarized EMC effect," *Phys. Rev. Lett.* **95**, 052302.
- Cloet, I. C., Wolfgang Bentz, and Anthony William Thomas, 2006, "EMC and polarized EMC effects in nuclei," *Phys. Lett. B* **642**, 210–217.
- Cloet, I. C., Gerald A. Miller, E. Piasezky, and G. Ron, 2009, "Neutron Properties in the Medium," *Phys. Rev. Lett.* **103**, 082301.
- Cloet, Ian C., Wolfgang Bentz, and Anthony W. Thomas, 2016, "Relativistic and Nuclear Medium Effects on the Coulomb Sum Rule," *Phys. Rev. Lett.* **116**, 032701.
- Cloet, Ian C., and Craig D. Roberts, 2014, "Explanation and Prediction of Observables using Continuum Strong QCD," *Prog. Part. Nucl. Phys.* **77**, 1–69.
- Close, F. E., 1979, *An Introduction to Quarks and Partons* (Academic Press, London).
- Close, F. E., R. G. Roberts, and Graham G. Ross, 1983, "The Effect of Confinement Size on Nuclear Structure Functions," *Phys. Lett. B* **129**, 346–350.
- Colle, C., *et al.*, 2015, "Extracting the mass dependence and quantum numbers of short-range correlated pairs from $a(e, e'p)$ and $a(e, e'pp)$ scattering," *Phys. Rev. C* **92**, 024604.
- Colle, Camille, Wim Cosyn, Jan Ryckebusch, and Maarten Vanhalst, 2014, "Factorization of exclusive electron-induced two-nucleon knockout," *Phys. Rev. C* **89**, 024603.
- Collins, John, 2013, *Foundations of perturbative QCD* (Cambridge University Press, Cambridge, England).
- Cosyn, Wim, Wally Melnitchouk, and Misak Sargsian, 2014, "Final-state interactions in inclusive deep-inelastic scattering from the deuteron," *Phys. Rev. C* **89**, 014612.

- Cosyn, Wim, and Misak Sargsian, 2011, “Final-state interactions in semi-inclusive deep inelastic scattering off the Deuteron,” *Phys. Rev. C* **84**, 014601.
- Cosyn, Wim, and Misak M. Sargsian, 2016, “High x Structure Function of the Virtually Free Neutron,” *Phys. Rev. C* **93**, 055205.
- Day, D. B., J. S. McCarthy, T. W. Donnelly, and I. Sick, 1990, *Annu. Rev. Nucl. Part. Sci.* **40**, 357.
- Day, D. B., *et al.*, 1987, “ y scaling in electron-nucleus scattering,” *Phys. Rev. Lett.* **59**, 427–430.
- De Forest, T., 1983, “Off-Shell electron Nucleon Cross-Sections. The Impulse Approximation,” *Nucl. Phys. A* **392**, 232–248.
- De Forest, Jr., T., and J. D. Walecka, 1966, “Electron scattering and nuclear structure,” *Adv. Phys.* **15**, 1–109.
- Detmold, W., G. A. Miller, and Jason Robert Smith, 2006, “Role of the nuclear vector potential in deep inelastic scattering,” *Phys. Rev. C* **73**, 015204.
- Diakonov, Dmitri, V. Petrov, P. Pobylitsa, Maxim V. Polyakov, and C. Weiss, 1996, “Nucleon parton distributions at low normalization point in the large $N(c)$ limit,” *Nucl. Phys. B* **480**, 341–380.
- Dieperink, A. E. L., and G. A. Miller, 1991, “Nucleon binding corrections to lepton nucleus deep inelastic scattering: Use of a realistic spectral function,” *Phys. Rev. C* **44**, 866–869.
- Dieterich, S., *et al.*, 2001, “Polarization transfer in the He-4(polarized-e, e-prime polarized-p)H-3 reaction,” *Phys. Lett. B* **500**, 47–52.
- Do Dang, G., M. L’Huillier, Nguyen Van Giai, and J. Wallace Van Orden, 1987, “Coulomb sum rules in the relativistic Fermi gas model,” *Phys. Rev. C* **35**, 1637–1645.
- Dulat, Sayipjamal, Tie-Jiun Hou, Jun Gao, Marco Guzzi, Joey Huston, Pavel Nadolsky, Jon Pumplin, Carl Schmidt, Daniel Stump, and C. P. Yuan, 2016, “New parton distribution functions from a global analysis of quantum chromodynamics,” *Phys. Rev. D* **93**, 033006.
- Dutta, D., K. Hafidi, and M. Strikman, 2013, “Color Transparency: past, present and future,” *Prog. Part. Nucl. Phys.* **69**, 1–27.
- Egiyan, K., *et al.* (CLAS Collaboration), 2003, “Observation of nuclear scaling in the $a(e, e')$ reaction at x_b greater than 1,” *Phys. Rev. C* **68**, 014313.
- Egiyan, K., *et al.* (CLAS Collaboration), 2006, “Measurement of 2- and 3-nucleon short range correlation probabilities in nuclei,” *Phys. Rev. Lett.* **96**, 082501.
- Epelbaum, Evgeny, Hans-Werner Hammer, and Ulf-G. Meissner, 2009, “Modern Theory of Nuclear Forces,” *Rev. Mod. Phys.* **81**, 1773–1825.
- Ericson, Magda, and Anthony William Thomas, 1983, “Pionic Corrections and the EMC Enhancement of the Sea in Iron,” *Phys. Lett. B* **128**, 112–116.
- Ericson, Magda, and Anthony William Thomas, 1984, “Evidence for an Enhanced Nuclear Sea From the Proton—Nucleus Drell-Yan Process,” *Phys. Lett. B* **148**, 191–193.
- Fanchiotti, Huner, Carlos A. García Canal, Tatiana Tarutina, and Vicente Vento, 2014, “Medium effects in dis from polarized nuclear targets,” *Eur. Phys. J. A* **50**, 116.
- Farrar, Glennys R., and Darrell R. Jackson, 1975, “Pion and nucleon structure functions near $x = 1$,” *Phys. Rev. Lett.* **35**, 1416–1419.
- Farrar, Glennys R., Huan Liu, Leonid L. Frankfurt, and Mark I. Strikman, 1988, “Transparency in nuclear quasiexclusive processes with large momentum transfer,” *Phys. Rev. Lett.* **61**, 686–689.
- Feldmeier, H., W. Horiuchi, T. Neff, and Y. Suzuki, 2011, “Universality of short-range nucleon-nucleon correlations,” *Phys. Rev. C* **84**, 054003.
- Fields, L., *et al.* (MINERvA Collaboration), 2013, “Measurement of muon antineutrino quasielastic scattering on a hydrocarbon target at $E_\nu \sim 3.5$ GeV,” *Phys. Rev. Lett.* **111**, 022501.
- Fiorentini, G. A., *et al.* (MINERvA Collaboration), 2013, “Measurement of Muon Neutrino Quasielastic Scattering on a Hydrocarbon Target at $E_\nu \sim 3.5$ GeV,” *Phys. Rev. Lett.* **111**, 022502.
- Fissum, K. G., *et al.* (Jefferson Lab Hall A Collaboration), 2004, “The Dynamics of the quasielastic O-16(e, e-prime p) reaction at $Q^2 = 0.8$ (GeV/c) 2 ,” *Phys. Rev. C* **70**, 034606.
- Fomin, N., *et al.*, 2012, “New measurements of high-momentum nucleons and short-range structures in nuclei,” *Phys. Rev. Lett.* **108**, 092502.
- Frank, M. R., B. K. Jennings, and G. A. Miller, 1996, “The Role of color neutrality in nuclear physics: Modifications of nucleonic wave functions,” *Phys. Rev. C* **54**, 920–935.
- Frankfurt, L., V. Guzey, and M. Strikman, 2012, “Leading Twist Nuclear Shadowing Phenomena in Hard Processes with Nuclei,” *Phys. Rep.* **512**, 255–393.
- Frankfurt, L., M. Strikman, and M. Zhalov, 2001, “Single particle strength restoration and nuclear transparency in high Q^2 exclusive (e, e-prime p) reactions,” *Phys. Lett. B* **503**, 73–80.
- Frankfurt, L. L., G. A. Miller, and M. Strikman, 1994, “The Geometrical color optics of coherent high-energy processes,” *Annu. Rev. Nucl. Part. Sci.* **44**, 501–560.
- Frankfurt, L. L., M. M. Sargsian, and M. I. Strikman, 1997, “Feynman graphs and Gribov-Glauber approach to high-energy knockout processes,” *Phys. Rev. C* **56**, 1124–1137.
- Frankfurt, L. L., and M. I. Strikman, 1981, “High-Energy Phenomena, Short-Range Nuclear Structure and QCD,” *Phys. Rep.* **76**, 215–347.
- Frankfurt, L. L., and M. I. Strikman, 1985, “Point-like configurations in hadrons and nuclei and deep inelastic reactions with leptons: EMC and EMC like effects,” *Nucl. Phys. B* **250**, 143–176.
- Frankfurt, L. L., and M. I. Strikman, 1987, “On the Normalization of Nucleus Spectral Function and the EMC Effect,” *Phys. Lett. B* **183**, 254.
- Frankfurt, L. L., and M. I. Strikman, 1988, “Hard Nuclear Processes and Microscopic Nuclear Structure,” *Phys. Rep.* **160**, 235–427.
- Frankfurt, L. L., M. I. Strikman, D. B. Day, and M. Sargsyan, 1993, “Evidence for short-range correlations from high q^2 (e,e’) reactions,” *Phys. Rev. C* **48**, 2451.
- Frankfurt, Leonid, Misak Sargsian, and Mark Strikman, 2008, “Recent observation of short range nucleon correlations in nuclei and their implications for the structure of nuclei and neutron stars,” *Int. J. Mod. Phys. A* **23**, 2991–3055.
- Frankfurt, Leonid, and Mark Strikman, 2012, “QCD and QED dynamics in the EMC effect,” *Int. J. Mod. Phys. E* **21**, 1230002.
- Freese, Adam J, Misak M. Sargsian, and Mark I. Strikman, 2015, “Probing superfast quarks in nuclei through dijet production at the LHC,” *Eur. Phys. J. C* **75**, 534.
- Frullani, S., and J. Mougey, 1984, “Single particle properties of nuclei through (e, e’p) reactions,” *Adv. Nucl. Phys.* **14**, 1.
- Gao, J., *et al.*, 2000, “Dynamical relativistic effects in quasielastic 1p-shell proton knockout from ^{16}O ,” *Phys. Rev. Lett.* **84**, 3265.
- Gayou, O., *et al.* (Jefferson Lab Hall A Collaboration), 2002, “Measurement of $G(\text{Ep})/G(\text{Mp})$ in polarized-e p \rightarrow e polarized-p to $Q^2 = 5.6$ -GeV 2 ,” *Phys. Rev. Lett.* **88**, 092301.
- Geesaman, D. F., K. Saito, and A. W. Thomas, 1995, “The Nuclear EMC Effect,” *Annu. Rev. Nucl. Part. Sci.* **45**, 337.
- Gezerlis, A., I. Tews, E. Epelbaum, M. Freunek, S. Gandolfi, K. Hebeler, A. Nogga, and A. Schwenk, 2014, “Local chiral effective field theory interactions and quantum Monte Carlo applications,” *Phys. Rev. C* **90**, 054323.

- Golak, J., H. Kamada, H. Witala, W. Glockle, and S. Ishikawa, 1995, "Electron induced pd and ppn breakup of ^3He with full inclusion of final-state interactions," *Phys. Rev. C* **51**, 1638–1647.
- Gomes, L. C., J. D. Walecka, and V. F. Weisskopf, 1958, "Properties of nuclear matter," *Ann. Phys. (N.Y.)* **3**, 241–274.
- Gomez, J., *et al.*, 1994, "Measurement of the a dependence of deep-inelastic electron scattering," *Phys. Rev. D* **49**, 4348.
- Gribov, V. N., B. L. Ioffe, and I. Ya. Pomeranchuk, 1966, "What is the range of interactions at high-energies," *Sov. J. Nucl. Phys.* **2**, 549.
- Griffioen, K. A., *et al.*, 2015, "Measurement of the EMC Effect in the Deuteron," *Phys. Rev. C* **92**, 015211.
- Gross, Franz, and D. O. Riska, 1987, "Current Conservation and Interaction Currents in Relativistic Meson Theories," *Phys. Rev. C* **36**, 1928.
- Guichon, Pierre A. M., 1988, "A Possible Quark Mechanism for the Saturation of Nuclear Matter," *Phys. Lett. B* **200**, 235–240.
- Guichon, Pierre A. M., and Gerald A. Miller, 1984, "Quarks and the Deuteron Asymptotic D State," *Phys. Lett. B* **134**, 15–20.
- Guichon, Pierre A. M., Koichi Saito, Evgenii N. Rodionov, and Anthony William Thomas, 1996, "The Role of nucleon structure in finite nuclei," *Nucl. Phys. A* **601**, 349–379.
- Haftel, Michael I., and Frank Tabakin, 1970, "Nuclear Saturation and the Smoothness of Nucleon-Nucleon Potentials," *Nucl. Phys. A* **158**, 1–42.
- Hagen, G., *et al.*, 2015, "Neutron and weak-charge distributions of the ^{48}Ca nucleus," *Nat. Phys.* **12**, 186–190.
- Halzen, F., and Alan D. Martin, 1984, *Quarks and Leptons: An Introductory Course in Modern Particle Physics* (Wiley, New York).
- Haxel, Otto, J. Hans D. Jensen, and Hans E. Suess, 1949, "On the "magic numbers" in nuclear structure," *Phys. Rev.* **75**, 1766–1766.
- Haxton, W. C., B. F. Gibson, and E. M. Henley, 1980, "Parity Nonconservation in F-18, F-19, and NE-21," *Phys. Rev. Lett.* **45**, 1677–1681.
- Hen, O., A. Accardi, W. Melnitchouk, and E. Piassetzky, 2011, "Constraints on the large- x d/u ratio from electron-nucleus scattering at $x > 1$," *Phys. Rev. D* **84**, 117501.
- Hen, O., E. Piassetzky, and L. B. Weinstein, 2012, "New data strengthen the connection between short range correlations and the emc effect," *Phys. Rev. C* **85**, 047301.
- Hen, O., A. W. Steiner, E. Piassetzky, and L. B. Weinstein, 2016, "Analysis of Neutron Stars Observations Using a Correlated Fermi Gas Model," [arXiv:1608.00487](https://arxiv.org/abs/1608.00487).
- Hen, O., L. B. Weinstein, E. Cohen, and D. W. Higinbotham, 2016, "The CaFe Experiment: Short-Range Pairing Mechanisms in Heavy Nuclei, Jefferson Lab Proposal E12-16-004."
- Hen, O., L. B. Weinstein, S. Gilad, and W. Boeglin, 2014, "Proton and Neutron Momentum Distributions in $A = 3$ Asymmetric Nuclei, Jefferson Lab Experiment E12-14-011," [arXiv:1410.4451](https://arxiv.org/abs/1410.4451).
- Hen, O., L. B. Weinstein, E. Piassetzky, G. A. Miller, M. M. Sargsian, and Y. Sagi, 2015, "Correlated fermions in nuclei and ultracold atomic gases," *Phys. Rev. C* **92**, 045205.
- Hen, O., L. B. Weinstein, E. I. Piassetzky, and H. Hakobyan, 2014, "In Medium Proton Structure Functions, SRC, and the EMC effect, Jefferson Lab experiment E12-11-003A."
- Hen, O., L. B. Weinstein, S. A. Wood, and S. Gilad, 2011, "In Medium Nucleon Structure Functions, SRC, and the EMC effect, Jefferson Lab experiment E12-11-107."
- Hen, O., *et al.* (CLAS Collaboration), 2014, "Momentum sharing in imbalanced Fermi systems," *Science* **346**, 614–617.
- Hen, Or, D. W. Higinbotham, Gerald A. Miller, Eli Piassetzky, and Lawrence B. Weinstein, 2013, "The EMC Effect and High Momentum Nucleons in Nuclei," *Int. J. Mod. Phys. E* **22**, 1330017.
- Hen, Or, Bao-An Li, Wen-Jun Guo, L. B. Weinstein, and Eli Piassetzky, 2015, "Symmetry energy of nucleonic matter with tensor correlations," *Phys. Rev. C* **91**, 025803.
- Hobbs, T. J., Mary Alberg, and Gerald A. Miller, 2016, "A Euclidean bridge to the relativistic constituent quark model," [arXiv:1608.07319](https://arxiv.org/abs/1608.07319).
- Holt, Jeremy W., Norbert Kaiser, and Wolfram Weise, 2013, "Nuclear chiral dynamics and thermodynamics," *Prog. Part. Nucl. Phys.* **73**, 35–83.
- Holt, Roy J., 2013, "Large x physics: recent results and future plans," in *Proceedings, 43rd International Symposium on Multiparticle Dynamics (ISMD 13)*, [arXiv:1311.1527](https://arxiv.org/abs/1311.1527).
- Holt, Roy J., and Craig D. Roberts, 2010, "Nucleon and pion distribution functions in the valence region," *Rev. Mod. Phys.* **82**, 2991–3044.
- Horikawa, T., and W. Bentz, 2005, "Medium modifications of nucleon electromagnetic form-factors," *Nucl. Phys. A* **762**, 102–128.
- Horowitz, C. J., 1985, "Relativistic Love-Franey model: Covariant representation of the NN interaction for N-nucleus scattering," *Phys. Rev. C* **31**, 1340–1348.
- Hugenholtz, N. M., and L. van Hove, 1958, "A theorem on the single particle energy in a Fermi gas with interaction," *Physica (Utrecht)* **24**, 363–376.
- Ioffe, B. L., 1969, "Space-time picture of photon and neutrino scattering and electroproduction cross-section asymptotics," *Phys. Lett. B* **30**, 123–125.
- Jaffe, R. L., 1983, "Quark Distributions in Nuclei," *Phys. Rev. Lett.* **50**, 228.
- Ji, Xiangdong, 2013, "Parton Physics on a Euclidean Lattice," *Phys. Rev. Lett.* **110**, 262002.
- Jones, M. K., *et al.* (Jefferson Lab Hall A Collaboration), 2000, "G(E(p)) / G(M(p)) ratio by polarization transfer in polarized $e p \rightarrow e$ polarized p," *Phys. Rev. Lett.* **84**, 1398–1402.
- Jourdan, J., 1995, "Longitudinal response functions: The Coulomb sum revisited," *Phys. Lett. B* **353**, 189–195.
- Jourdan, J., 1996, "Quasielastic response functions: The Coulomb sum revisited," *Nucl. Phys. A* **603**, 117–160.
- Jung, H., and G. A. Miller, 1988, "Nucleonic Contribution to Lepton Nucleus Deep Inelastic Scattering," *Phys. Lett. B* **200**, 351–356.
- Jung, H., and G. A. Miller, 1990, "Pionic contributions to deep inelastic nuclear structure functions," *Phys. Rev. C* **41**, 659–664.
- Kelly, J. J., 1996, "Nucleon knockout by intermediate energy electrons," *Adv. Nucl. Phys.* **23**, 75.
- Kelly, J. J., and Stephen J. Wallace, 1994, "Comparison between relativistic and nonrelativistic models of the nucleon-nucleon effective interaction. 1: Normal parity isoscalar transitions," *Phys. Rev. C* **49**, 1315–1336.
- Kelly, James J., 1999, "Effects of spinor distortion and density-dependent form factors upon quasifree $^{16}\text{O}(\vec{e}, e' \vec{p})$."
- Kim, K. S., B. G. Yu, and M. K. Cheoun, 2006, "Coulomb sum rule in quasielastic region," *Phys. Rev. C* **74**, 067601.
- Klimenko, A. V., *et al.* (CLAS Collaboration), 2006, "Electron scattering from high-momentum neutrons in deuterium," *Phys. Rev. C* **73**, 035212.
- Koch, V., and G. A. Miller, 1985, "Six Quark Cluster Effects and Binding Energy Differences Between Mirror Nuclei," *Phys. Rev. C* **31**, 602–612; **32**, 1106(E) (1985).
- Konrad, P., H. Lenske, and U. Mosel, 2005, "Short range correlations and spectral functions in asymmetric nuclear matter," *Nucl. Phys. A* **756**, 192–212.
- Korover, I., *et al.*, 2014, "Probing the Repulsive Core of the Nucleon-Nucleon Interaction via the $^4\text{He}(e, e' p N)$ Triple-Coincidence Reaction," *Phys. Rev. Lett.* **113**, 022501.

- Kramer, G. J., H. P. Blok, and L. Lapikas, 2001, "A consistent analysis of (e,ep) and (d,3he) experiments," *Nucl. Phys. A* **679**, 267–286.
- Kuhn, S. E., and W. K. Brooks, 2014, "Jefferson lab experiment e12-14-001: The emc effect in spin structure functions."
- Kulagin, S. A., and R. Petti, 2006, "Global study of nuclear structure functions," *Nucl. Phys. A* **765**, 126–187.
- Kulagin, S. A., and R. Petti, 2010, "Structure functions for light nuclei," *Phys. Rev. C* **82**, 054614.
- Kulagin, S. A., and R. Petti, 2014, "Nuclear parton distributions and the Drell-Yan process," *Phys. Rev. C* **90**, 045204.
- Lacombe, M., B. Loiseau, R. Vinh Mau, J. Ct, P. Pirs, and R. de Tournell, 1981, "Parametrization of the deuteron wave function of the paris nn potential," *Phys. Lett. B* **101**, 139–140.
- Lapikas, L., 1993, "Quasi-elastic electron scattering off nuclei," *Nucl. Phys. A* **553**, 297–308.
- Lapikas, Louk, G. van der Steenhoven, L. Frankfurt, M. Strikman, and M. Zhalov, 2000, "The Transparency of C-12 for protons," *Phys. Rev. C* **61**, 064325.
- Lehr, J., M. Effenberger, H. Lenske, S. Leupold, and U. Mosel, 2000, "Transport theoretical approach to the nucleon spectral function in nuclear matter," *Phys. Lett. B* **483**, 324–330.
- Lehr, J., H. Lenske, S. Leupold, and U. Mosel, 2002, "Nuclear matter spectral functions by transport theory," *Nucl. Phys. A* **703**, 393.
- Lin, Huey-Wen, Jiunn-Wei Chen, Saul D. Cohen, and Xiangdong Ji, 2015, "Flavor Structure of the Nucleon Sea from Lattice QCD," *Phys. Rev. D* **91**, 054510.
- Liyanage, N., *et al.* (The Jefferson Lab Hall A Collaboration), 2001, "Dynamics of the $^{16}\text{O}(e, e'p)$ reaction at high missing energies," *Phys. Rev. Lett.* **86**, 5670–5674.
- Llewellyn Smith, C. H., 1983, "A Possible Explanation of the Difference Between the Structure Functions of Iron and Deuterium," *Phys. Lett. B* **128**, 107–111.
- Lovato, A., S. Gandolfi, Ralph Butler, J. Carlson, Ewing Lusk, Steven C. Pieper, and R. Schiavilla, 2013, "Charge Form Factor and Sum Rules of Electromagnetic Response Functions in ^{12}C ," *Phys. Rev. Lett.* **111**, 092501.
- Lovato, A., S. Gandolfi, J. Carlson, Steven C. Pieper, and R. Schiavilla, 2016, "Electromagnetic response of ^{12}C : a first-principles calculation," [arXiv:1605.00248](https://arxiv.org/abs/1605.00248).
- Lu, Ding-Hui, Kazuo Tsushima, Anthony William Thomas, Anthony Gordon Williams, and K. Saito, 1999, "Electromagnetic form-factors of the bound nucleon," *Phys. Rev. C* **60**, 068201.
- Macfarlane, M. H., and J. B. French, 1960, "Stripping reactions and the structure of light and intermediate nuclei," *Rev. Mod. Phys.* **32**, 567–691.
- Machleidt, R., 1989, "The Meson theory of nuclear forces and nuclear structure," *Adv. Nucl. Phys.* **19**, 189–376.
- Machleidt, R., and D. R. Entem, 2011, "Chiral effective field theory and nuclear forces," *Phys. Rep.* **503**, 1–75.
- Machleidt, R., K. Holinde, and C. Elster, 1987, "The Bonn Meson Exchange Model for the Nucleon Nucleon Interaction," *Phys. Rep.* **149**, 1–89.
- Makek, M., *et al.*, 2016, "Differential cross section measurement of the $^{12}\text{C}(e, epp)^{10}\text{Be}_{g.s.}$ reaction," *Eur. Phys. J. A* **52**, 298.
- Malace, S. P., *et al.*, 2011, "A precise extraction of the induced polarization in the $4\text{He}(e, e'p)3\text{H}$ reaction," *Phys. Rev. Lett.* **106**, 052501.
- Malace, Simona, David Gaskell, Douglas W. Higinbotham, and Ian C. Clot, 2014, "The challenge of the emc effect: Existing data and future directions," *Int. J. Mod. Phys. E* **23**, 1430013.
- Marco, E., E. Oset, and P. Fernandez de Cordoba, 1996, "Mesonic and binding contributions to the EMC effect in a relativistic many body approach," *Nucl. Phys. A* **611**, 484–513.
- Mayer, M., *et al.* (CLAS Collaboration), 2017, "Beam-target double-spin asymmetry in quasielastic electron scattering off the deuteron with CLAS," *Phys. Rev. C* **95**, 024005.
- Mayer, Maria Goeppert, 1950, "Nuclear configurations in the spin-orbit coupling model. i. empirical evidence," *Phys. Rev.* **78**, 16–21.
- McVoy, K. W., and L. Van Hove, 1962, "Inelastic Electron-Nucleus Scattering and Nucleon-Nucleon Correlations," *Phys. Rev.* **125**, 1034–1043.
- Melnitchouk, W., Andreas W. Schreiber, and Anthony William Thomas, 1994a, "Deep inelastic scattering from off-shell nucleons," *Phys. Rev. D* **49**, 1183–1198.
- Melnitchouk, W., Andreas W. Schreiber, and Anthony William Thomas, 1994b, "Relativistic deuteron structure function," *Phys. Lett. B* **335**, 11–16.
- Melnitchouk, W., and A. W. Thomas, 1996, "Neutron proton structure function ratio at large x," *Phys. Lett. B* **377**, 11–17.
- Meziani, Z. E., *et al.*, 1984, "Coulomb Sum Rule for Ca-40, Ca-48, and Fe-56 for $|q(\text{Vector})| \leq 550\text{-MeV}/c$," *Phys. Rev. Lett.* **52**, 2130–2133.
- Mihaila, Bogdan, and Jochen Heisenberg, 2000, "Microscopic calculation of the inclusive electron scattering structure function in O-16," *Phys. Rev. Lett.* **84**, 1403–1406.
- Mihovilovic, M., *et al.* (Jefferson Lab Hall A Collaboration), 2014, "Measurement of double-polarization asymmetries in the quasi-elastic $^3\text{He}(\vec{e}, e'd)$ process," *Phys. Rev. Lett.* **113**, 232505.
- Miller, G. A., 1984, "Six Quark Cluster Components of Nuclear Wave Functions and the Pion Nucleus Double Charge Exchange Reaction," *Phys. Rev. Lett.* **53**, 2008–2011.
- Miller, G. A., and R. Machleidt, 1999a, "Infinite nuclear matter on the light front: Nucleon-nucleon correlations," *Phys. Rev. C* **60**, 035202.
- Miller, G. A., and R. Machleidt, 1999b, "Light front theory of nuclear matter," *Phys. Lett. B* **455**, 19–24.
- Miller, Gerald A., 1984, "Building the Nucleus From Quarks: The Cloudy Bag Model and the Quark Description of the Nucleon-nucleon Wave Function," *Int. Rev. Nucl. Phys.* **1**, 189–323.
- Miller, Gerald A., 1988, "Nuclear Wave Functions in Deep Inelastic Scattering and Drell-Yan Processes," in *Workshop on Nuclear and Particle Physics on the Light Cone Los Alamos, New Mexico* (World Scientific, Singapore), pp. 0042–64.
- Miller, Gerald A., 2000, "Light front quantization: A Technique for relativistic and realistic nuclear physics," *Prog. Part. Nucl. Phys.* **45**, 83–155.
- Miller, Gerald A., 2014, "Pionic and Hidden-Color, Six-Quark Contributions to the Deuteron b1 Structure Function," *Phys. Rev. C* **89**, 045203.
- Miller, Gerald A., and Leonard S. Kisslinger, 1983, "Quark Contributions to the $pp \leftrightarrow d\pi^+$ Reaction," *Phys. Rev. C* **27**, 1669.
- Miller, Gerald A., Matthew D. Sievert, and Raju Venugopalan, 2016, "Probing short-range nucleon-nucleon interactions with an Electron-Ion Collider," *Phys. Rev. C* **93**, 045202.
- Miller, Gerald A., and Jason Robert Smith, 2002, "Return of the EMC effect," *Phys. Rev. C* **65**, 015211; **66**, 049903 (2002).
- Miller, Gerald A., and James E. Spencer, 1976, "A Survey of Pion Charge-Exchange Reactions with Nuclei," *Ann. Phys. (N.Y.)* **100**, 562.
- Mineo, H., Wolfgang Bentz, N. Ishii, Anthony William Thomas, and K. Yazaki, 2004, "Quark distributions in nuclear matter and the EMC effect," *Nucl. Phys. A* **735**, 482–514.

- Monaghan, P., *et al.*, 2014, “Measurement of the $^{12}\text{C}(e, e'p)^{11}\text{B}$ two-body breakup reaction at high missing momentum,” *J. Phys. G* **41**, 105109.
- Morgenstern, J., and Z. E. Meziani, 2001, “Is the Coulomb sum rule violated in nuclei?,” *Phys. Lett. B* **515**, 269–275.
- Mulders, P. J., 1990, “Modifications of Nucleons in Nuclei and Other Consequences of the Quark Substructure,” *Phys. Rep.* **185**, 83–169.
- Murdock, D. P., and C. J. Horowitz, 1987, “Microscopic Relativistic Description of Proton—Nucleus Scattering,” *Phys. Rev. C* **35**, 1442–1462.
- Neff, Thomas, Hans Feldmeier, and Wataru Horiuchi, 2015, “Short-range correlations in nuclei with similarity renormalization group transformations,” *Phys. Rev. C* **92**, 024003.
- Negele, John W., 1999, “Instantons, the QCD vacuum, and hadronic physics,” *Nucl. Phys. B, Proc. Suppl.* **73**, 92–104.
- Noble, J. V., 1981, “Modification of the nucleon’s properties in nuclear matter,” *Phys. Rev. Lett.* **46**, 412–415.
- Norton, P. R., 2003, “The EMC Effect,” *Rep. Prog. Phys.* **66**, 1253.
- Olive, K. A., *et al.* (Particle Data Group), 2014, “Review of Particle Physics,” *Chin. Phys. C* **38**, 090001.
- Owens, J. F., A. Accardi, and W. Melnitchouk, 2013, “Global parton distributions with nuclear and finite- Q^2 corrections,” *Phys. Rev. D* **87**, 094012.
- Palli, V., C. Ciofi degli Atti, L. P. Kaptari, C. B. Mezzetti, and M. Alvioli, 2009, “Slow Proton Production in Semi-Inclusive Deep Inelastic Scattering off Deuteron and Complex Nuclei: Hadronization and Final State Interaction Effects,” *Phys. Rev. C* **80**, 054610.
- Paolone, M., *et al.*, 2010, “Polarization Transfer in the $4\text{He}(e, e'p)3\text{H}$ Reaction at $Q_2 = 0.8$ and 1.3 (GeV/c) 2 ,” *Phys. Rev. Lett.* **105**, 072001.
- Passchier, I., *et al.*, 2002, “Spin momentum correlations in quasielastic electron scattering from deuterium,” *Phys. Rev. Lett.* **88**, 102302.
- Perdrisat, C. F., V. Punjabi, and M. Vanderhaeghen, 2007, “Nucleon Electromagnetic Form Factors,” *Prog. Part. Nucl. Phys.* **59**, 694–764.
- Petratos, G. G., J. Gomez, R. J. Holt, and R. D. Ransome, 2010, “Measurement of the F_2n/F_2p , d/u Ratios and $A = 3$ EMC Effect in Deep Inelastic Electron Scattering Off the Tritium and Helium Mirror Nuclei, Jefferson Lab Experiment E12-10-103.”
- Piasetzky, E., M. Sargsian, L. Frankfurt, M. Strikman, and J. W. Watson, 2006, “Evidence for the strong dominance of proton-neutron correlations in nuclei,” *Phys. Rev. Lett.* **97**, 162504.
- Picklesimer, A., and J. W. Van Orden, 1989, “Polarization response functions and the (polarized- e, e' polarized- p) reaction,” *Phys. Rev. C* **40**, 290.
- Picklesimer, A., J. W. Van Orden, and S. J. Wallace, 1985, “Final state interactions and relativistic effects in the (polarized- e, e') reaction,” *Phys. Rev. C* **32**, 1312.
- Piller, Gunther, and Wolfram Weise, 2000, “Nuclear deep inelastic lepton scattering and coherence phenomena,” *Phys. Rep.* **330**, 1–94.
- Pirner, Hans J., and James P. Vary, 1981, “Deep Inelastic electron Scattering and the Quark Structure of He-3,” *Phys. Rev. Lett.* **46**, 1376–1379.
- Polls, A., A. Ramos, J. Ventura, S. Amari, and W. H. Dickhoff, 1994, “Energy weighted sum rules for spectral functions in nuclear matter,” *Phys. Rev. C* **49**, 3050–3054.
- Punjabi, V., *et al.*, 2005, “Proton elastic form-factor ratios to $Q^2 = 3.5$ GeV 2 by polarization transfer,” *Phys. Rev. C* **71**, 055202; **71**, 069902(E) (2005).
- Riordan, S., R. Beminiwatha, and A. Arrington, 2016, “the emc pvdis experiment, a constraint on isovector-dependent nuclear modification effects using parity-violating deep inelastic scattering, proposal pr12-16-006.”
- Rios, A., A. Polls, and W. H. Dickhoff, 2014, “Density and isospin asymmetry dependence of high-momentum components,” *Phys. Rev. C* **89**, 044303.
- Roberts, Craig D., Roy J. Holt, and Sebastian M. Schmidt, 2013, “Nucleon spin structure at very high- x ,” *Phys. Lett. B* **727**, 249–254.
- Roberts, R. G., 1994, *The Structure of the proton: Deep inelastic scattering* (Cambridge University Press, Cambridge, England).
- Ryckebusch, J., D. Debruyne, P. Lava, S. Janssen, B. Van Overmeire, and T. Van Cauteren, 2003, “Relativistic formulation of Glauber theory for $A(e, e\text{-prime } p)$ reactions,” *Nucl. Phys. A* **728**, 226–250.
- Ryckebusch, Jan, Maarten Vanhalst, and Wim Cosyn, 2015, “Stylized features of single-nucleon momentum distributions,” *J. Phys. G* **42**, 055104.
- Saito, K., Kazuo Tsushima, and Anthony William Thomas, 1999, “Effect of nucleon structure variation on the longitudinal response function,” *Phys. Lett. B* **465**, 27–35.
- Sargsian, M. M., T. V. Abrahamyan, M. I. Strikman, and L. L. Frankfurt, 2005, “Exclusive electro-disintegration of He-3 at high Q_2 . II. Decay function formalism,” *Phys. Rev. C* **71**, 044615.
- Sargsian, Misak M., 2014a, “New properties of the high-momentum distribution of nucleons in asymmetric nuclei,” *Phys. Rev. C* **89**, 034305.
- Sargsian, Misak M., 2014b, “Protons in High Density Neutron Matter,” *J. Phys. Conf. Ser.* **496**, 012007.
- Schiavilla, R., O. Benhar, A. Kievsky, L. E. Marcucci, and M. Viviani, 2005, “Polarization transfer in He-4(polarized- e, e' polarized- p) H-3: Is the ratio $G(Ep) / G(Mp)$ modified in medium?,” *Phys. Rev. Lett.* **94**, 072303.
- Schiavilla, R., R. B. Wiringa, Steven C. Pieper, and J. Carlson, 2007, “Tensor forces and the ground-state structure of nuclei,” *Phys. Rev. Lett.* **98**, 132501.
- Schlumpf, Felix, 1992, “Relativistic constituent quark model for baryons,” Ph.D. thesis (Zurich U.), [arXiv:hep-ph/9211255](https://arxiv.org/abs/hep-ph/9211255).
- Schlumpf, Felix, 1993, “Relativistic constituent quark model of electroweak properties of baryons,” *Phys. Rev. D* **47**, 4114; **49**, 6246(E) (1994).
- Seely, J., *et al.*, 2009, “New measurements of the european muon collaboration effect in very light nuclei,” *Phys. Rev. Lett.* **103**, 202301.
- Shneur, R., *et al.*, 2007, “Investigation of proton-proton short-range correlations via the $^{12}\text{C}(e, e'pp)$ reaction,” *Phys. Rev. Lett.* **99**, 072501.
- Sick, I., 1985, “How Much Do Nucleons Change in Nuclei?,” *Nucl. Phys. A* **434**, 677C–684C.
- Sloan, T., R. Voss, and G. Smadja, 1988, “The Quark Structure of the Nucleon from the CERN Muon Experiments,” *Phys. Rep.* **162**, 46.
- Smith, Jason Robert, and Gerald A. Miller, 2002, “Return of the EMC effect: Finite nuclei,” *Phys. Rev. C* **65**, 055206.
- Smith, Jason Robert, and Gerald A. Miller, 2003, “Chiral solitons in nuclei: Saturation, EMC effect and Drell-Yan experiments,” *Phys. Rev. Lett.* **91**, 212301; **98**, 099902(E) (2007).
- Smith, Jason Robert, and Gerald A. Miller, 2004, “Chiral solitons in nuclei: Electromagnetic form-factors,” *Phys. Rev. C* **70**, 065205.
- Smith, Jason Robert, and Gerald A. Miller, 2005, “Polarized quark distributions in nuclear matter,” *Phys. Rev. C* **72**, 022203.

- Solvignon-Slifer, P., and J. Arrington, 2011, "Precision measurement of the isospin dependence in the 2N and 3N short range correlation region, Jefferson Lab Experiment E12-11-112."
- Souder, P. A., 2016, "Parity Violation in Deep Inelastic Scattering with the SoLID Spectrometer at JLab," *Int. J. Mod. Phys. Conf. Ser.* **40**, 1660077.
- Stoks, V. G. J., R. A. M. Klomp, C. P. F. Terheggen, and J. J. de Swart, 1994, "Construction of high quality N N potential models," *Phys. Rev. C* **49**, 2950–2962.
- Stone, J. R., P. A. M. Guichon, P. G. Reinhard, and A. W. Thomas, 2016, "Finite Nuclei in the Quark-Meson Coupling Model," *Phys. Rev. Lett.* **116**, 092501.
- Strauch, S., *et al.* (Jefferson Lab E93-049), 2003, "Polarization transfer in the He-4 (polarized-e, e-prime polarized-p) H-3 reaction up to $Q^2 = 2.6$ -(GeV/c) 2 ," *Phys. Rev. Lett.* **91**, 052301.
- Strauch, Steffen, 2012, "Hadron medium modifications," *EPJ Web Conf.* **36**, 00016.
- Subedi, R., *et al.*, 2008, "Probing Cold Dense Nuclear Matter," *Science* **320**, 1476–1478.
- Tang, A., *et al.*, 2003, "n-p short-range correlations from (p, 2p + n) measurements," *Phys. Rev. Lett.* **90**, 042301.
- Thomas, Anthony William, and Wolfram Weise, 2001, *The Structure of the Nucleon* (Wiley-VCH, Berlin).
- Tkachenko, S., *et al.* (CLAS Collaboration), 2014, "Measurement of the structure function of the nearly free neutron using spectator tagging in inelastic $^2\text{H}(e, e' p_s)x$ scattering with clas," *Phys. Rev. C* **89**, 045206.
- Udias, J. M., J. A. Caballero, E. Moya de Guerra, J. E. Amaro, and T. W. Donnelly, 1999, "Quasielastic scattering from relativistic bound nucleons: Transverse-longitudinal response," *Phys. Rev. Lett.* **83**, 5451–5454.
- Udias, J. M., and Javier R. Vignote, 2000, "Relativistic nuclear structure effects in (e,e-prime polarized-p)," *Phys. Rev. C* **62**, 034302.
- Udias, J. M., *et al.*, 1993, "Spectroscopic factors in ^{40}Ca and ^{208}Pb from (e,e'p): Fully relativistic analysis," *Phys. Rev. C* **48**, 2731.
- Udias, J. M., *et al.*, 1995, "Relativistic versus nonrelativistic optical potentials in $A(e, e' p)B$ reactions," *Phys. Rev. C* **51**, 3246.
- Vanhalst, Maarten, Wim Cosyn, and Jan Ryckebusch, 2011, "Counting the amount of correlated pairs in a nucleus," *Phys. Rev. C* **84**, 031302.
- Vanhalst, Maarten, Jan Ryckebusch, and Wim Cosyn, 2012, "Quantifying short-range correlations in nuclei," *Phys. Rev. C* **86**, 044619.
- Vary, J. P., P. U. Sauer, and C. W. Wong, 1973, "Convergence Rate of Intermediate-State Summations in the Effective Shell-Model Interaction," *Phys. Rev. C* **7**, 1776–1785.
- Walecka, J. D., 2005, *Electron scattering for nuclear and neutron structure* (Cambridge University Press, Cambridge, England).
- Wallace, S. J., and J. A. Tjon, 2008, "Coulomb corrections in quasi-elastic scattering: Tests of the effective-momentum approximation," *Phys. Rev. C* **78**, 044604.
- Weinstein, L. B., O. Hen, and E. Piasezky, 2016, "Hammer events, neutrino energies, and nucleon-nucleon correlations," *Phys. Rev. C* **94**, 045501.
- Weinstein, L. B., E. Piasezky, D. W. Higinbotham, J. Gomez, O. Hen, and R. Shneur, 2011, "Short range correlations and the emc effect," *Phys. Rev. Lett.* **106**, 052301.
- Weiss, R., R. Cruz-Torres, N. Barnea, E. Piasezky, and O. Hen, 2016, "The nuclear contacts and short range correlations in nuclei," arXiv:1612.00923.
- Weiss, Ronen, Betzalel Bazak, and Nir Barnea, 2015, "Generalized nuclear contacts and momentum distributions," *Phys. Rev. C* **92**, 054311.
- Wiringa, R. B., R. Schiavilla, Steven C. Pieper, and J. Carlson, 2014, "Nucleon and nucleon-pair momentum distributions in $A \leq 12$ nuclei," *Phys. Rev. C* **89**, 024305.
- Wiringa, R. B., V. G. J. Stoks, and R. Schiavilla, 1995, "Accurate nucleon-nucleon potential with charge-independence breaking," *Phys. Rev. C* **51**, 38–51.
- Wong, S. S. M., 1998, "Introduction," in *Nuclear Physics* (Wiley-VCH Verlag GmbH, Weinheim), 2nd ed.
- Yaron, I., *et al.* (A1 Collaboration), 2016, "Polarization-transfer measurement to a large-virtuality bound proton in the deuteron," arXiv:1602.06104.
- Zeller, G. P., *et al.*, 2002, "Precise determination of electroweak parameters in neutrino-nucleon scattering," *Phys. Rev. Lett.* **88**, 091802; **90**, 239902(E) (2003).